Electromagnetic Wave Scattering by Randomly Buried Particles

by

Prathet Tankuranun

B.Eng., King Mongkut's Institute of Technology Ladkrabung, Thailand (1990)

Submitted to the Department of Electrical Engineering and Computer Science in partial fulfillment of the requirements for the degree of

Master of Science in Computer Science and Engineering

at the

MASSACHUSETTS INSTITUTE OF TECHNOLOGY

August 1995

Author ....
Department of Electrical Engineering and Computer Science
August 11, 1995

Certified by ....
Jin Au Kong
Professor
Thesis Supervisor

Certified by ....
Kung Hau Ding
Postdoctoral Associate
Thesis Supervisor

Accepted by ....
Frederic R. Morgenthaler
Chairman, Departmental Committee on Graduate Students

Electromagnetic Wave Scattering by Randomly Buried Particles

by

Prathet Tankuranun

Submitted to the Department of Electrical Engineering and Computer Science
on August 11, 1995, in partial fulfillment of the
requirements for the degree of
Master of Science in Computer Science and Engineering

Abstract

In this thesis, the effect of volume scattering from the buried particles in half–space random media on the radar backscattering cross section is investigated. The radar clutter from a flat desert area is modeled as spherical scatterers randomly embedded within a layered medium with flat interfaces. Three approaches are used to calculate the backscattering coefficients.

The Monte Carlo method based on Transition matrix (T-matrix) approach is first applied. The multiple scattering and the coherent wave interaction are included in this approach. The couplings between scatterers and the interface are taken into account by using the image method. The multiple scattering equation is solved using the iterative technique. The solution process repeated for many realizations and averaged to calculate the backscatter.

The Radiative Transfer theory (RT) approach is also presented. The RT theory is based on the concept of energy transport and the assumption of independent scattering. The numerical solution of the RT equation is obtained using the discrete-ordinate eigenanalysis method, which includes all orders of multiple scattering.

Finally, the First Order Analytical Approximation is applied to obtain the first order solution of the multiple scattering equations derived based on T-matrix method. The First Order Analytical Approximation assumes positions of particles to be independent. The effects of coherent wave interactions are considered in this approach. However, the multiple scattering effects are neglected. The Rayleigh scatterer is assumed for each particle. A compact analytic expression for the backscattering coefficients is obtained.

The numerical calculations from all three approaches are performed and then compared. It shows that the results using RT approach are in good agreement with those of the Monte Carlo approach in this study. The First Order Analytical Approximation always gives higher returns than the other two methods, which may be accounted for by the assumption of independent particle position. Thus, from this study, though not including coherent wave interaction, the RT approach is a good model in prediction the radar return from desert media. Some parametric studies base on RT are also performed which shows that the particle size plays an important factor in the high radar return level.

Thesis Supervisor: Jin Au Kong
Title: Professor

Thesis Supervisor: Kung Hau Ding
Title: Postdoctoral Associate

Acknowledgments

I first of all wish to sincerely thank Prof. Kong for giving me the opportunity to be a member in this superb research group and for his excellent teaching which inspired me a lot of insightful knowledges in this electromagnetic area.

Thanks to Dr. Shin for his ingenious guidance throughout the work, which made this work much simpler. Thanks to Dr. Lee for his advise, guidance, sparkling ideas, not only in the technical subjects but also aspects of ways to live a happy life, and for his explanations to all of my stupid questions, ever since I was wondering why the Green's function was not a red or blue function until now I know the Green's function better than my student ID., and for his patience to all the mistakes I have done throughout.

I am especially indebted to Dr. Ding for his help, particularly the early period of my studying, and for his kindness to my ignorance. Without his numerous explanations, comments, suggestions, corrections and hints, I wouldn't have made it this far.

I gratefully recognize all of my colleagues in the group. Thanks to Chih, Sean for answering me all those questions. Thanks to C.P., Gung, Lifang, and Kevin. Thanks to Joel for his friendliness. I really had fun at the Halloween party that night. Thanks to Jerry, especially for going with me to my driver's license road test. Thanks to Yan, who always brought many interesting discussions to me, though I couldn't answer everything. Also thanks to Kent, a good driver who drove us to all the parties and picnics. Special thanks and sincere best wish to Christina, a lively, nice and very talkative woman and one of the best friends of mine.

Thanks to Ping (if it were not for you this thesis would have been finished long before, – just kidding!) for those hard times and happy times we were and will be together.

Finally, I would like to express my gratitude to my parents whose love never failed to give me the energy to survive this very tough year at MIT. The merit of this thesis, should there be any, is dedicated to them.

Contents

List of Figures

List of Tables

Chapter 1

Introduction

1.1 Introduction

In the microwave remote sensing of earth terrain, there are two major sources which give significant contributions to the radar backscattering coefficients. One is the volume scattering. The other is the scattering from rough surfaces. In the volume scattering problem, two theoretical models have been: (1) the continuous random medium model in which scattering comes from a random fluctuation of the permittivity, and (2) the discrete random medium model where discrete scatterers are randomly imbedded in a homogeneous background medium. In the discrete random medium approach, spheres, spheroids, ellipsoids, discs and cylinders are among the most commonly used models of scatterers. The continuous random media model is described by a random permittivity consisting of a mean part and a fluctuating parts. The fluctuating part is usually described by its variance and its spatial correlation function [23].

In the active remote sensing, there have been many works on the modeling of the volume scattering [25], [14], [26], [28], [9]. These models can be categorized into two classes: (1) wave theory, and (2) radiative transfer theory (RT). In the wave theory models, the solutions are obtained directly by solving Maxwell's equations for the electromagnetic fields. Thus, the solutions by the wave theory contain phase correlations and coherent wave interaction among scatterers. Therefore such models can be used in applications which require the phase relation of backscatter such as Synthetic Aperture Radar (SAR) images simulation. On the other hand, the RT theory is not derived from Maxwell's equations; it is based on the energy transport equation. The fundamental quantities in the energy transport equation are not the electromagnetic fields but rather energies. The RT theory assumes incoherent wave interaction and ignores the phase relations between scattered waves from individual scatterers. However a major advantage of RT theory is that it can be applied in a more complicated configuration that are generally too complex to be solved by the wave theory.

In June 1993, a ground penetration radar (GPR) experiment was conducted in Yuma, Arizona [15], [16]. In this experiment, a number of SARs, including the SRI SAR covered the frequency bands 100-300 MHz, 200-400 MHz, and 300-500 MHz, and the Rail SAR covered the frequency band 250 MHz to 1 GHz, were applied to measure the backscatters from buried targets, surface targets, and the desert radar clutter. During the experiment, extensive clutter data were collected. The soil properties and samples of surface profiles were also measured.

In general, the radar clutter from the desert terrain is a function of vegetation, surface roughness, and soil inhomogeneities. From the Yuma experiment, the median backscattering coefficients were approximately -29 dB, -27 dB, and -25 dB for the 100-300 MHz, 200-400 MHz, and 300-500 MHz bands, respectively. The standard deviations were all about 6.9 dB [15], [16]. As expected, the backscatter was higher at higher depression angles. The backscattering coefficient increased approximately 6 dB over the 30-60 degree depression angle range. It was found, even in an area where the ground surface was flat and without any visible surface vegetation, that the backscatter was significantly higher than both the noise level and the level predicted by using a simple rough surface scattering model. It appeared that an appreciable amount of volume scattering due to soil inhomogeneities may contribute to the total backscatter.

In this thesis, we shall study the volume scattering due to rocks beneath the desert terrain. The wave and RT theories are used in conjunction with a discrete particle model. In the wave theory approach, the Transition Matrix (T-matrix) approach is applied and extended to calculate the multiple scattering from randomly distributed particles with different sizes [2]. The effects of particle-boundary interaction are taken into account by using the image method to approximate the scattered fields from buried objects which are further reflected at the boundary. An iterative solution technique is applied to solve the multiple scattering equation [30]. Then, the Monte Carlo simulation technique is used and the results are averaged over many realizations to obtain the backscattering coefficients. The First Order Analytical Approximation is another approach based on the wave theory. The First Order Analytical Approximation is obtained from the first order solution of the multiple scattering equation derived from the T-matrix formalism. By taking the configurational average over the first order scattering amplitude, the scattered field is obtained in a compact form. The RT approach is also presented in this work. The principal constituents of the RT equation are the phase matrix and the extinction matrix which are calculated based on the random discrete scatterer model. The RT equation is solved using the discrete ordinate-eigenanalysis numerical method [30].

These three approaches will be applied to study the volume scatttering which may be a possible cause to the high radar return from the 1993 Yuma experiment. Numerical results will be presented using typical physical parameters. The backscattering coefficients as functions of radar parameters and physical properties of the desert terrain will be presented. Results calculated using the three approaches will be compared. The appropriate conditions for the use of each approach will also be discussed. The developed volume scattering models may be applied to predict the radar clutter from desert media and to assess the possibility of locating and identifying underground targets.

1.2 Model Configuration

In this study, scattering due to surface roughness is ignored, and rocks are replaced by spherical particles. Figure 1-1 shows the geometrical model. The model consists

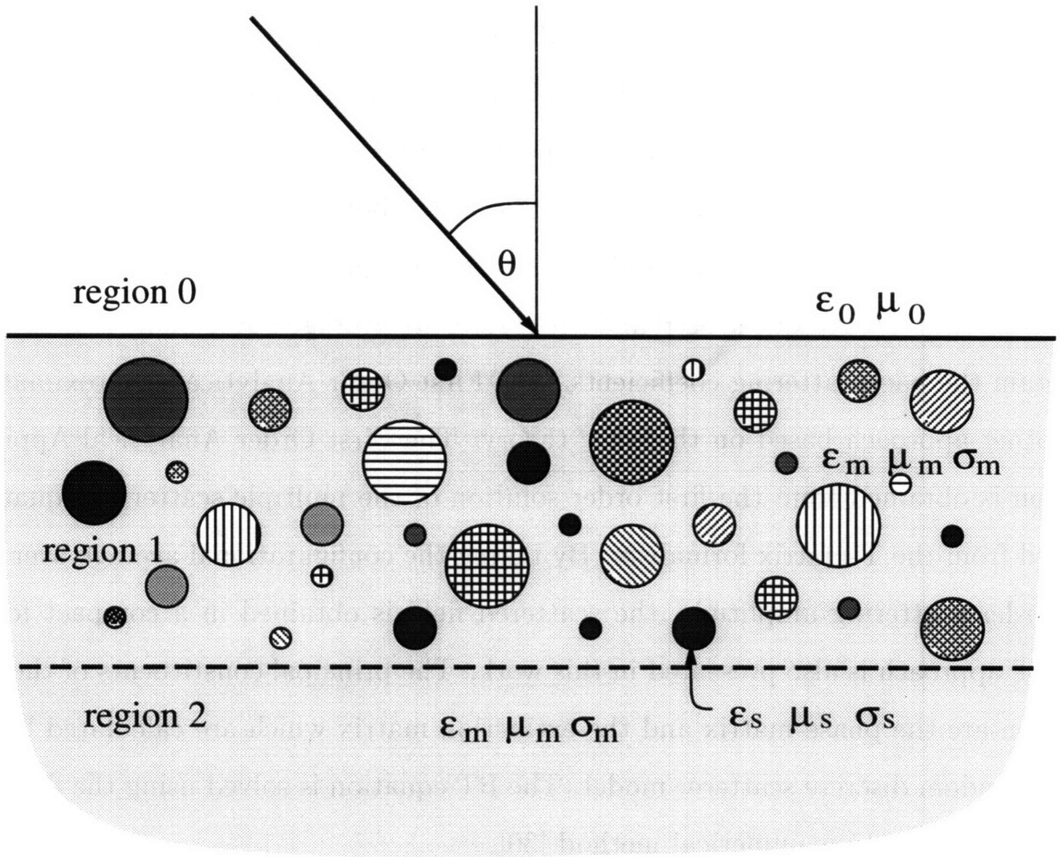

Figure 1-1: Configuration of the model

of layered media with flat interfaces. The particles are randomly embedded in region 1, and they may have different sizes and permittivities. The upper half–space is assumed to be air with permittivity ϵ_0 and permeability μ_0. The surface between air and soil is assumed to be flat. The background medium is a homogeneous half–space with permittivity ϵ_m, permeability μ_m and, conductivity σ_m. All the scatterers are assumed to be of spherical shape.

1.3 Description of The Thesis

The remaining of the thesis has five chapters. Chapter 2 gives the detailed discussion on the Transition matrix (T-matrix) approach. The derivation of T-matrix and multiple scattering equation is given. In Section 2.5, the multiple scattering equation is modified using the image particle method to take into account the particle-surface interaction when an interface is present. The iterative technique used in solving the modified multiple scattering equation is described in Section 2.6. In Chapter 3, the radiative transfer equation is presented along with its main constituents, the phase matrix and the extinction matrix and the numerical method for solving the RT equation. Chapter 4 discusses the use of analytic method in solving the first order multiple scattering equation by taking configurational average over particle positions. In Chapter 5, numerical simulation of the backscattering coefficients fir these approaches is performed using the physical parameters used in Yuma experiment. Discussions about the results from each approach are also given in this chapter. Finally, a summary and a conclusion as well as some suggested future works are given in Chapter 6.

Chapter 2

Transition Matrix

In this chapter, the Transition matrix (T-matrix, also known as the System Transfer Operator) approach is presented. The T-matrix method utilizes spherical wave expansions for both incident and scattered fields. The extended boundary condition is used to derive a system of linear equations relating the coefficients of the scattered fields to those of the incident field. The final relation between the scattered fields and the incident field is cast into a matrix form known as the transition matrix or the T-matrix. The multiple scattering equations have been established by extending the T-matrix formalism to an arbitrary number of scatterers. For a large number of particles, the multiple scattering equations can be solved using iterative technique. The Monte Carlo simulation method is then applied to calculate the scatttering from an assembly of particles by averaging over many realizations.

2.1 Solution of The Spherical Wave Equation

We begin the discussion of T-matrix approach with the derivation of the solutions of the spherical wave equation. In a linear, isotropic, homogeneous and source–free medium, an electromagnetic wave must satisfy the wave equation

$$\left(\nabla^2 + k^2\right)\left\{\begin{matrix}\overline{E}\\ \overline{H}\end{matrix}\right\} = 0 \tag{2.1}$$

where $k = \omega\sqrt{\mu\epsilon}$ is the wave number of the medium with permittivity ϵ and permeability μ.

The general solution of Equation (2.1) can be constructed from a scalar function ψ which satisfies the following scalar wave equation

$$\left(\nabla^2 + k^2\right)\psi = 0 \tag{2.2}$$

and an arbitrary constant vector $\bar{c}$. The vector wave functions $\overline{M}, \overline{N}$, and $\overline{L}$:

$$\overline{M} = \nabla \times (\bar{c}\psi) \tag{2.3}$$

$$\overline{N} = \frac{\nabla \times \overline{M}}{k} \tag{2.4}$$

$$\overline{L} = \nabla\psi \tag{2.5}$$

can be shown to satisfy the vector wave equation

$$\nabla \times \nabla \times \left\{ \begin{array}{c} \overline{M} \\ \overline{N} \end{array} \right\} - k^2 \left\{ \begin{array}{c} \overline{M} \\ \overline{N} \end{array} \right\} = 0 \tag{2.6}$$

$$\nabla(\nabla \cdot \overline{L}) + k^2\overline{L} = 0 \tag{2.7}$$

Therefore, the problem of finding solutions to the wave equation reduces to a comparatively simpler problem of finding solutions to the scalar wave equation.

Let

$$\psi = R(r)\Theta(\theta)\Phi(\phi) \tag{2.8}$$

and transform Equation (2.2) into spherical coordinate, we obtain the following differential equations for each spherical variable r, θ, and ϕ

$$r\frac{d^2}{dr^2}(rR) + \left[(kr)^2 - n(n+1)\right]R = 0 \tag{2.9}$$

$$\frac{1}{\sin\theta}\frac{d}{d\theta}\left(\sin\theta\frac{d\Theta}{d\theta}\right)+\left[n(n+1)-\frac{m^2}{\sin^2\theta}\right]\Theta=0 \tag{2.10}$$

$$\frac{d^2\Phi}{d\phi^2}+m^2\Phi=0 \tag{2.11}$$

The general solution of the Helmholtz equation in spherical coordinate system is [13]

$$Rg\psi_{mn}(kr,\theta,\phi)=j_n(kr)P_n^m(\cos\theta)e^{im\phi} \tag{2.12}$$

with $n=0,1,2,...$ and $m=0,\pm1,\pm2,...,\pm n$, j_n is the spherical Bessel function of the n th order, $P_n^m(\cos\theta)$ is the associated Legendre polynomials, and Rg stands for *Regular* which denotes that the solution is finite at the origin. The outgoing wave solution, which is used to describe the scattered fields, has the following form

$$\psi_{mn}(kr,\theta,\phi)=h_n(kr)P_n^m(\cos\theta)e^{im\phi} \tag{2.13}$$

where the spherical Bessel function j_n has been replaced by the spherical Hankel function of the first kind h_n. Then we use the relations (2.3) and (2.4) to construct the regular vector spherical wave functions $Rg\overline{M}$, and $Rg\overline{N}$ as [30]

$$Rg\overline{M}_{mn}(kr,\theta,\phi)=\gamma_{mn}\nabla\times(\overline{r}Rg\psi_{mn}(kr,\theta,\phi)) \tag{2.14}$$

$$Rg\overline{N}_{mn}(kr,\theta,\phi)=\frac{1}{k}\nabla\times(Rg\overline{M}_{mn}(kr,\theta,\phi)) \tag{2.15}$$

where

$$\gamma_{mn}=\sqrt{\frac{(2n+1)(n-m)!}{4\pi(n+1)(n+m)!}} \tag{2.16}$$

In terms of regular vector spherical wave functions, a plane wave propagates in the direction $\hat{k}_i$ can be expressed as [30]

$$\overline{E}_i=(E_{vi}\hat{v}_i+E_{hi}\hat{h}_i)e^{i\hat{k}_i\cdot\hat{r}}$$

$$= \sum_{mn} \left[a_{mn}^{(M)} Rg\overline{M}_{mn}(kr,\theta,\phi) + a_{mn}^{(N)} Rg\overline{N}_{mn}(kr,\theta,\phi) \right] \tag{2.17}$$

where $a_{mn}^{(M)}$ and $a_{mn}^{(N)}$ are the expansion coefficients

$$a_{mn}^{(M)} = (-1)^m \frac{1}{\gamma_{mn}} \frac{(2n+1)}{n(n+1)} i^n \left[\overline{E}_{vi} \left(\hat{\theta}_i \cdot \overline{C}_{-mn}(\theta_i,\phi_i) \right) + \overline{E}_{hi} \left(\hat{\phi}_i \cdot \overline{C}_{-mn}(\theta_i,\phi_i) \right) \right] \tag{2.18}$$

$$a_{mn}^{(N)} = (-1)^m \frac{1}{\gamma_{mn}} \frac{(2n+1)}{n(n+1)} i^n \left[\overline{E}_{vi} \left(\hat{\theta}_i \cdot (-i\overline{B}_{-mn}(\theta_i,\phi_i)) \right) + \overline{E}_{hi} \left(\hat{\phi}_i \cdot (-i\overline{B}_{-mn}(\theta_i,\phi_i)) \right) \right] \tag{2.19}$$

and

$$\hat{k}_i = \sin\theta_i \cos\phi_i \hat{x} + \sin\theta_i \sin\phi_i \hat{y} + \cos\theta_i \hat{z} \tag{2.20}$$

$$\hat{v}_i = \cos\theta_i \cos\phi_i \hat{x} + \cos\theta_i \sin\phi_i \hat{y} - \sin\theta_i \hat{z} \tag{2.21}$$

$$\hat{h}_i = -\sin\phi_i \hat{x} + \cos\phi_i \hat{y} \tag{2.22}$$

with $\hat{v}_i$ and $\hat{h}_i$ begin the incident vertical and horizontal polarization vectors respectively. The vector spherical harmonics $\overline{B}(\theta,\phi)$ and $\overline{C}(\theta,\phi)$ in (2.18) and (2.19) are defined as [30]

$$\overline{B}_{mn}(\theta,\phi) = \left(\hat{\theta} \frac{dP_n^m(\cos\theta)}{d\theta} + \hat{\phi} \frac{im}{\sin\theta} P_n^m(\cos\theta) \right) e^{im\phi} \qquad (n = 1,2,3,...) \tag{2.23}$$

$$\overline{C}_{mn}(\theta,\phi) = \left(\hat{\theta} \frac{im}{\sin\theta} - \hat{\phi} \frac{dP_n^m(\cos\theta)}{d\theta} P_n^m(\cos\theta) \right) e^{im\phi} \qquad (n = 1,2,3,...) \tag{2.24}$$

The vector spherical waves $\overline{M}_{mn}(kr,\theta,\phi)$ and $\overline{N}_{mn}(kr,\theta,\phi)$ which will be used to describe the scattered field from a particle can be obtained from (2.14) and (2.15) by replacing the spherical Bessel functions with the spherical Hankel functions. The asymptotic far-field expressions of $\overline{M}_{mn}(kr,\theta,\phi)$ and $\overline{N}_{mn}(kr,\theta,\phi)$, for $kr \to \infty$, are

$$\lim_{kr\to\infty} \overline{M}_{mn}(kr,\theta,\phi) = \gamma_{mn} \overline{C}_{mn}(\theta,\phi) i^{-n-1} \frac{1}{kr} e^{ikr} \tag{2.25}$$

$$\lim_{kr\to\infty} \overline{N}_{mn}(kr,\theta,\phi) = \gamma_{mn} \overline{B}_{mn}(\theta,\phi) i^{-n-1} \frac{1}{kr} e^{ikr} \tag{2.26}$$

2.2 Definition of T-matrix

The T-matrix which characterizes the scattering properties of the object is defined as

$$\overline{E}^S(\overline{r}) = \overline{\overline{T}}\,\overline{E}^E(\overline{r}) \tag{2.27}$$

where $\overline{E}^E(\overline{r})$ and $\overline{E}^S(\overline{r})$ are the exciting and scattered fields for a particle respectively.

Consider an incident wave $\overline{E}^{inc}(\overline{r})$ impinges on a particle which is characterized by permittivity ϵ_s, Figure 2-1, it gives rise to a scattered wave $\overline{E}^S(\overline{r})$. We can express $\overline{E}^{inc}(\overline{r})$ and $\overline{E}^S(\overline{r})$ in terms of vector spherical waves as

$$\overline{E}^E(\overline{r}) = \overline{E}^{inc}(\overline{r}) = \sum_{mn} \left[a_{mn}^{E(M)} Rg\overline{M}_{mn}(k\overline{r}) + a_{mn}^{E(N)} Rg\overline{N}_{mn}(k\overline{r})\right] \tag{2.28}$$

$$\overline{E}^S(\overline{r}) = \sum_{mn} \left[a_{mn}^{S(M)} \overline{M}_{mn}(k\overline{r}) + a_{mn}^{S(N)} \overline{N}_{mn}(k\overline{r})\right] \tag{2.29}$$

with a_{mn}^E and a_{mn}^S being the expansion coefficients for the exciting and scattered fields respectively.

The T-matrix is then used to describe the linear relation between scattered field coefficients a_{mn}^S and the exciting filed coefficients a_{mn}^E

$$a_{mn}^{S(M)} = \sum_{m'n'} \left[\overline{\overline{T}}_{mnm'n'}^{(11)} a_{m'n'}^{E(M)} + \overline{\overline{T}}_{mnm'n'}^{(12)} a_{m'n'}^{E(N)}\right] \tag{2.30}$$

$$a_{mn}^{S(N)} = \sum_{m'n'} \left[\overline{\overline{T}}_{mnm'n'}^{(21)} a_{m'n'}^{E(M)} + \overline{\overline{T}}_{mnm'n'}^{(22)} a_{m'n'}^{E(N)}\right] \tag{2.31}$$

The summations in (2.30) and (2.31) are usually truncated with a finite terms at $n = N_{max}$. A combined index l is used to represent the two indices n and m as follows [30]:

$$l = n(n+1) + m \tag{2.32}$$

Thus, the corresponding L_{max} is

$$L_{max} = N_{max}(N_{max} + 2) \tag{2.33}$$

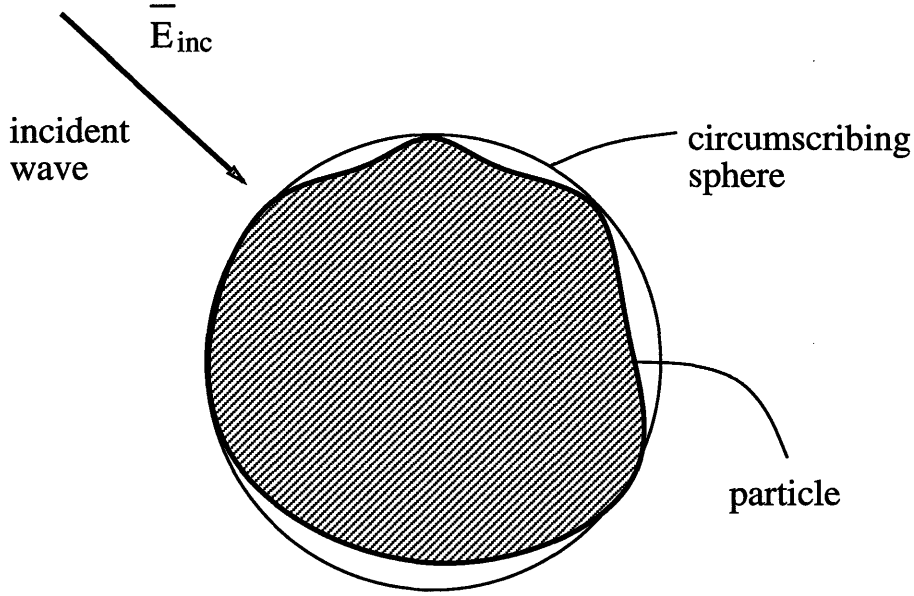

Figure 2-1: Incident wave on a particle with a circumscribing sphere.

Upon using the new combined index l, the relations (2.30) and (2.31) can be rewritten as

$$\begin{bmatrix} \overline{a}^{S(M)} \\ \overline{a}^{S(N)} \end{bmatrix} = \begin{bmatrix} \overline{\overline{T}}^{(11)} \overline{\overline{T}}^{(12)} \\ \overline{\overline{T}}^{(21)} \overline{\overline{T}}^{(22)} \end{bmatrix} \begin{bmatrix} \overline{a}^{E(M)} \\ \overline{a}^{E(N)} \end{bmatrix} \tag{2.34}$$

where $\overline{a}^{E(M)}$ and $\overline{a}^{E(N)}$ are column matrices of dimensions $L_{max} \times 1$ representing the coefficients $a_l^{E(M)}$ and $a_l^{E(N)}$ respectively, and $\overline{a}^{S(M)}$ and $\overline{a}^{S(N)}$ are column matrices of coefficients $a_l^{S(M)}$ and $a_l^{S(N)}$, respectively. We further let

$$\overline{a}^S = \begin{bmatrix} \overline{a}^{S(M)} \\ \overline{a}^{S(N)} \end{bmatrix}; \quad \overline{a}^E = \begin{bmatrix} \overline{a}^{E(M)} \\ \overline{a}^{E(N)} \end{bmatrix}; \quad \overline{\overline{T}} = \begin{bmatrix} \overline{\overline{T}}^{(11)} \overline{\overline{T}}^{(12)} \\ \overline{\overline{T}}^{(21)} \overline{\overline{T}}^{(22)} \end{bmatrix} \tag{2.35}$$

Equation (2.34) becomes

$$\overline{a}^S = \overline{\overline{T}} \overline{a}^E \tag{2.36}$$

where $\overline{\overline{T}}$ is of dimension $2L_{max} \times 2L_{max}$. Thus, Equation (2.36) implies that once the T-matrix of an object is obtained, the scattered field may be calculated from a knowledge of the exciting field.

2.3 T-matrix for a Sphere

In the case of spherical scatterers, there is no coupling between different multipoles of the incident wave and the scattered wave, the T-matrix for a sphere is of a diagonal form [30]

$$\overline{\overline{T}} = \begin{bmatrix} \overline{\overline{T}}^{(11)} & 0 \\ 0 & \overline{\overline{T}}^{(22)} \end{bmatrix} \tag{2.37}$$

where the matrix elements are

$$T^{(11)}_{mnm'n'} = \delta_{mm'}\delta_{nn'}T^{(M)}_n \tag{2.38}$$

$$T^{(22)}_{mnm'n'} = \delta_{mm'}\delta_{nn'}T^{(N)}_n \tag{2.39}$$

and

$$T^{(M)}_n = -\frac{j_n(k_s a)[kaj_n(ka)]' - j_n(ka)[k_s a j_n(k_s a)]'}{j_n(k_s a)[kah_n(ka)]' - h_n(ka)[k_s a j_n(k_s a)]'} \tag{2.40}$$

$$T^{(N)}_n = -\frac{[k_s^2 a^2 j_n(k_s a)][kaj_n(ka)]' - [k^2a^2 j_n(ka)][k_s a j_n(k_s a)]'}{[k_s^2 a^2 j_n(k_s a)][kah_n(ka)]' - [k^2a^2 h_n(ka)][k_s a j_n(k_s a)]'} \tag{2.41}$$

For small dielectric spheres, $ka \ll 1$ and $k_s a \ll 1$, the electric dipole term $T^{(N)}_1$ dominates and is the term that needs to be retained in the T-matrix. However, in order that the optical theorem be satisfied, it is important to keep the leading term of the imaginary part and the leading term of the real part of $T^{(N)}_1$. Using (2.41), it can be shown that for $ka \ll 1$ and $k_s a \ll 1$

$$T^{(N)}_1 = T^{(N)}_{1r} + iT^{(N)}_{1i} \tag{2.42}$$

where $T^{(N)}_{1r}$ and $T^{(N)}_{1i}$ are both complex for lossy scatterers, and

$$T^{(N)}_{1i} = \frac{2}{3}(ka)^3 y \tag{2.43}$$

$$y = \frac{\epsilon_s - \epsilon}{\epsilon_s + 2\epsilon} \tag{2.44}$$

$$T_{1r} = -(T_{1i}^{(N)})^2 \tag{2.45}$$

Note that since $ka \ll 1$, we have $|T_{1r}^{(N)}| \ll |T_{1i}^{(N)}|$. The extinction cross section is

$$\sigma_e = -\frac{6\pi}{k^2}[\mathrm{Re}\, T_{1r}^{(N)} - \mathrm{Im}\, T_{1i}^{(N)}]$$

$$= \frac{4\pi}{k^2}(ka)^3[\mathrm{Im}\, y + \frac{2}{3}(ka)^3 \mathrm{Re}\, y^2] \tag{2.46}$$

The scattering cross section is

$$\sigma_s = -\frac{6\pi}{k^2}|T_{1i}^{(N)}|^2 = \frac{8\pi}{3}(ka)^6|y|^2 \tag{2.47}$$

The optical theorem is satisfied with (2.46) and (2.47) because the $T_{1r}^{(N)}$ term in (2.42) has been included in spite of the fact that it is much smaller than $T_{1i}^{(N)}$.

2.4 Multiple Scattering Equations for N Particles

In this section, we will consider the scattering from multiple particles. The multiple scattering equations can be derived by extending the T-matrix formalism to an arbitrary number of particles [30].

Consider N scatterers bounded by surfaces $S_1, S_2, ..., S_N$ occupying regions $V_1, V_2, ..., V_N$. The scatterers are centered at $\overline{r}_1, \overline{r}_2, ..., \overline{r}_N$. It is also assumed that the scatterers are enclosed by circumscribing spheres that do not overlap each other (Figure 2-2). We consider a coordinate system with origin 0 outside the particles. Let the background region be denoted by V_0. The i th scatterer has permittivity equal to ϵ_i, wavenumber k_i, and permeability μ. For an incident plane wave, the multiple scattering equations of the system of scatterers (Figure 2-2) can be expressed in terms of T-matrix as [30]

$$\overline{a}^{E(\alpha)} = \sum_{\substack{\beta=1 \\ \beta\neq\alpha}}^{N} \left\{ \overline{\overline{\sigma}}(k\overline{r}_\alpha \overline{r}_\beta) \overline{\overline{T}}^{(\beta)} \overline{a}^{E(\beta)} \right\} + e^{i(\overline{k}_i \cdot \overline{r}_\alpha)} \overline{a}_{inc} \tag{2.48}$$

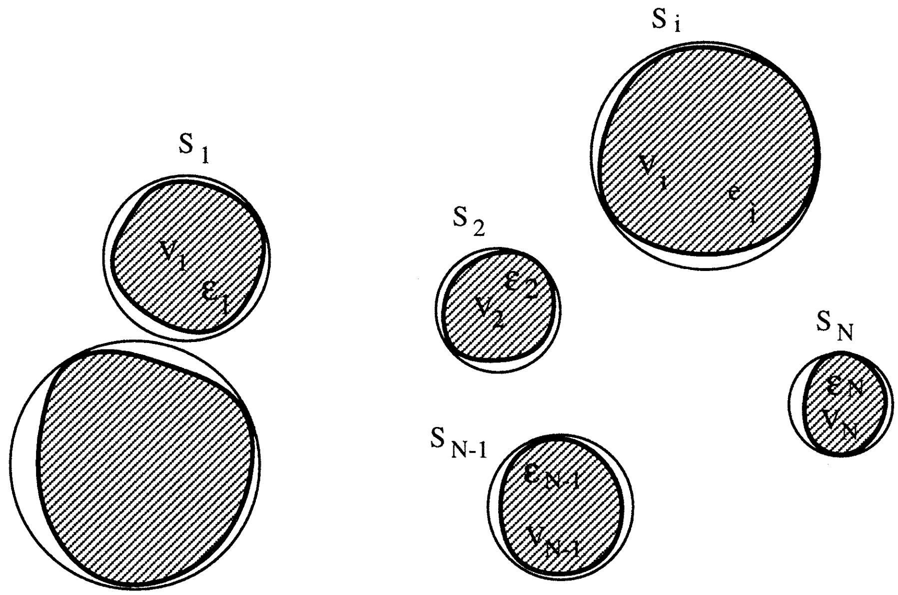

Figure 2-2: Particles $1, 2, ..., N$ occupying regions $V_1, V_2, ..., V_N$. and bounded by surfaces $S_1, S_2, ..., S_N$, respectively. They are enclosed by non-overlapping circumscribing spheres.

with $\alpha = 1, 2, 3, ..., N$. Equation (2.48) is known as the multiple scattering equation using T-matrix. In Equation (2.48), $\overline{a}^{E(\alpha)}$ is a column vector that represents the final exiting field of the scatterer α, $\overline{a}_{inc}$ is a column vector that contains the coefficients of the incident wave, $\overline{\overline{T}}^{(\beta)}$ is the T-matrix that describes scattering from the scatterer β, and $\overline{\overline{\sigma}}(k\overline{r_\alpha r_\beta})$ is a transformation matrix that transforms the vector spherical waves centered at $\overline{r}_{(\beta)}$ to the spherical waves centered at $\overline{r}_{(\alpha)}$. The physical interpretation of Equation (2.48) is that the final exciting field at the scatterer α is the sum of the incident field and the scattered fields from all other particles except itself. Note that in Equation (2.48), the exciting field $\overline{a}^{E(\alpha)}$ depends on the exciting field $\overline{a}^{E(\beta)}$ on the right hand side. Equation (2.48) includes multiple-scattering effect among particles. The near-, intermediate-, and far-field interactions are all included too. Equation (2.48) is a system of N equations for N unknowns $\overline{a}^{E(\alpha)}$ and in principle it can be solved.

After the exciting field $\overline{a}^{E(\alpha)}$ is solved, the scattered field $\overline{a}^{S(\alpha)}$ of particle α is calculated from

$$\overline{a}^{S(\alpha)} = \overline{\overline{T}}^{(\alpha)} \overline{a}^{E(\alpha)} \tag{2.49}$$

The total scattered field from all particles in the direction $\hat{k}_s$,

$$\hat{k}_s = \hat{x} \sin\theta_s \cos\phi_s + \hat{y} \sin\theta_s \sin\phi_s + \hat{z} \cos\theta_s \tag{2.50}$$

at an observation point R, for $kR \to \infty$, is

$$\overline{E}_S = \frac{e^{i(kR)}}{kR} \sum_{mn} \gamma_{mn} \left[a_{mn}^{S(M)} \overline{C}_{mn}(\theta_s, \phi_s) i^{-n-1} + a_{mn}^{S(N)} \overline{B}_{mn}(\theta_s, \phi_s) i^{-n} \right] \tag{2.51}$$

where k is the wave number of the background medium,$\overline{B}_{mn}$ and $\overline{C}_{mn}$ are vector spherical wave functions, and γ_{mn} is a coefficient given in (2.16).

We can combine Equations (2.48) and (2.49) to calculate directly the multiply scattered field coefficients $\overline{a}^{S(\alpha)}$

$$\overline{a}^{S(\alpha)} = \sum_{\substack{\beta=1 \\ \beta\neq\alpha}}^{N} \left\{ \overline{\overline{T}}^{(\alpha)} \overline{\overline{\sigma}}(k\overline{r_\alpha r_\beta}) \overline{a}^{S(\beta)} \right\} + e^{i(\overline{k}_i \cdot \overline{r}_\alpha)} \overline{\overline{T}}^{(\alpha)} \overline{a}_{inc} \tag{2.52}$$

The equation (2.52) describes the relationship between the scattered fields from the α particle and the β particle.

2.5 Multiple Scattering Equations for Buried Particles

In this section, we shall derive the multiple scattering equations for buried scatterers. Due to the presence of boundary surface, we have to consider the interaction between scatterer and boundary. However, if we want to obtain the rigorous solution for this case, we have to express the half–space Green's function in terms of vector spherical wave functions to construct the multiple scattering equation. In order to simplify the model, we apply the method of image [15] to account for the coupling between

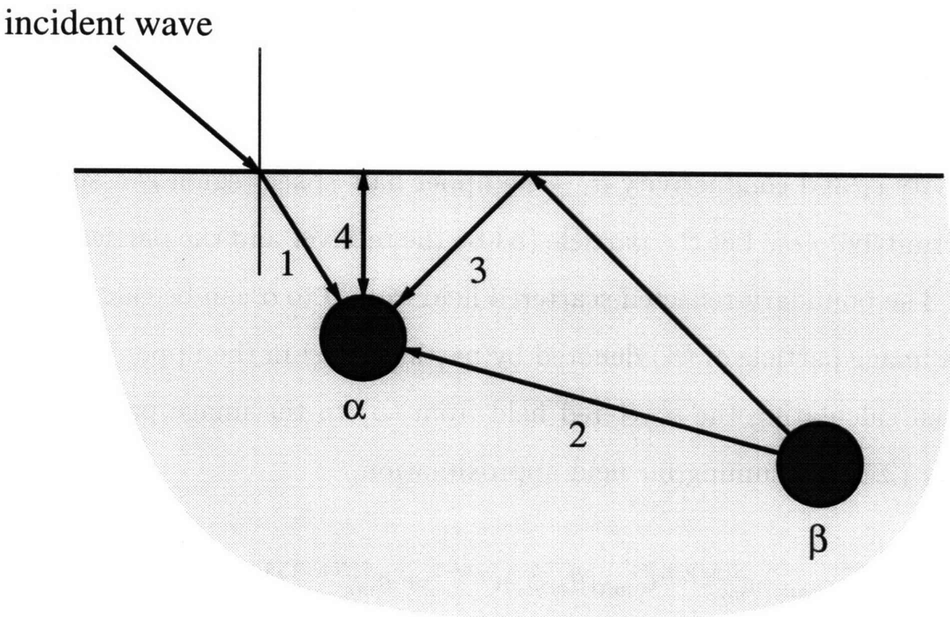

Figure 2-3: Wave contributions on a particle.

particles and interface, and then add this new contribution into the multiple scattering Equation (2.52).

The total contributions to the exciting field of particle α may be separated into four terms as illustrated in figure 2-3. The first term is the contribution from the incident wave. The second term is the direct scattering from other particles. The third contribution is from the scattering from other particles which are further reflected by the interface. And the last term is the contribution from the boundary–particle interaction of the particle itself. The first and the second terms are already included in Equation (2.52). The third and the fourth terms will be derived based on the method of image in the following.

Consider two particles (α) and (β) buried in a homogeneous half–space medium with permittivity ϵ_1 and conductivity σ_1. The upper half–space region is assumed to be air with permittivity ϵ_0. Let the particle (α) be the receiver and the particle (β) be the scatterer. The boundary-reflected scattered field from β to α can be calculated by first putting a image particle of (α) denoted by particle ($-\alpha$) in the upper half–space region and then calculating the scattered field from (β) to the image particle ($-\alpha$) (Figure 2-4) by (2.51), assuming far field approximation,

$$\overline{E}^{(-\alpha)} = \frac{e^{i(kr^{\alpha,\beta})}}{kr^{\alpha,\beta}} \sum_{mn} \gamma_{mn} \left[a_{mn}^{S(M)(\beta)} \overline{C}_{mn}(\theta_s, \phi_s) i^{-n-1} + a_{mn}^{S(N)(\beta)} \overline{B}_{mn}(\theta_s, \phi_s) i^{-n} \right] \quad (2.53)$$

where $\overline{E}^{(-\alpha)}$ is the scattered field at the image particle ($-\alpha$) due to particle β, $r^{\alpha,\beta}$ is the of the reflected ray path from β to α; (θ_s, ϕ_s) is the direction of the scattered field from (β) to (α) (see Figure 2-4), $\overline{a}_{mn}^{S(M)(\beta)}$ and $\overline{a}_{mn}^{S(N)(\beta)}$ are the expansion coefficients of the scattered field from particle β, and k is the wave number in region 1.

The field at the image particle ($-\alpha$) can be converted to a wave impinging on the particle α by multiplying it with a reflection coefficient matrix $\overline{\overline{R}}^{(\alpha,\beta)}$, which describes the reflection of the scattered wave from the interface. Then the field exciting the particle (α) from this contribution is

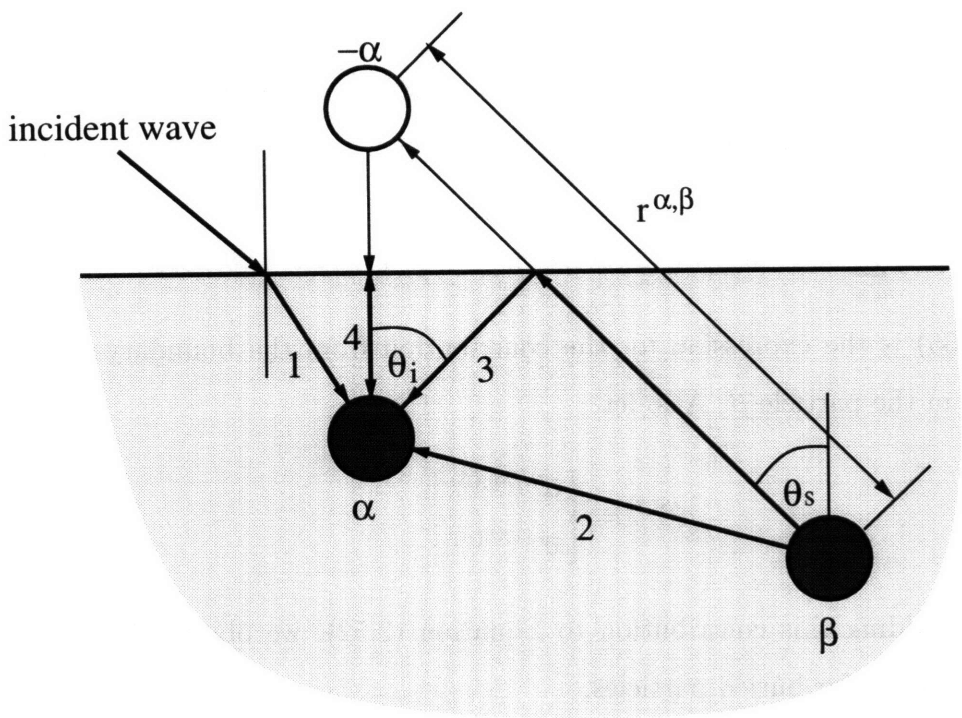

Figure 2-4: The use of Image particle $(-\alpha)$ to approximate the contribution from boundary reflectd term.

$$\overline{E}^{(\alpha)} = \frac{e^{i(kr^{\alpha,\beta})}}{kr^{\alpha,\beta}}\overline{\overline{R}}^{(\alpha,\beta)} \sum_{mn} \gamma_{mn} \left[a_{mn}^{S(M)(\beta)} \overline{C}_{mn}(\theta_s, \phi_s) i^{-n-1} + a_{mn}^{S(N)(\beta)} \overline{B}_{mn}(\theta_s, \phi_s) i^{-n} \right] \tag{2.54}$$

We can further expand this field (2.54) in terms of the regular vector spherical wave functions by taking the dot product of (2.54) with $Rg\overline{M}$ and $Rg\overline{N}$ and denote this new expansion coefficient to be $a_{mn}^{\prime S(\beta)}$

$$\left\{ \begin{array}{c} a_{mn}^{\prime S(M)(\beta)} \\ a_{mn}^{\prime S(N)(\beta)} \end{array} \right\} = (-1)^m \frac{1}{\gamma_{mn}} \frac{(2n+1)}{n(n+1)} i^n \left\{ \begin{array}{c} \hat{\theta}_i \cdot \overline{C}_{-mn}(\theta_i, \phi_i) + \hat{\phi}_i \cdot \overline{C}_{-mn}(\theta_i, \phi_i) \\ \hat{\theta}_i \cdot (-i\overline{B}_{-mn}(\theta_i, \phi_i)) + \hat{\phi}_i \cdot (-i\overline{B}_{-mn}(\theta_i, \phi_i)) \end{array} \right\}$$

$$\cdot \frac{e^{i(kr^{\alpha,\beta})}}{kr^{\alpha,\beta}} \overline{\overline{R}}^{(\alpha,\beta)} \sum_{m'n'} \gamma_{m'n'} \left[a_{m'n'}^{S(M)} \overline{C}_{m'n'}(\theta_s, \phi_s) i^{-n'-1} + a_{m'n'}^{S(N)} \overline{B}_{m'n'}(\theta_s, \phi_s) i^{-n'} \right] \tag{2.55}$$

Equation (2.55) is the expression for the contribution from the boundary-reflected scattering from the particle β. Also let

$$\overline{a}^{\prime S(\beta)} = \begin{bmatrix} \overline{a}^{\prime S(M)(\beta)} \\ \overline{a}^{\prime S(N)(\beta)} \end{bmatrix} \tag{2.56}$$

as usual. By adding this contribution to Equation (2.52), we obtain the multiple scattering equations for buried particles,

$$\overline{a}^{S(\alpha)} = \sum_{\substack{\beta=1 \\ \beta\neq\alpha}}^{N} \left\{ \overline{\overline{T}}^{(\alpha)} \overline{\overline{\sigma}}(k\overline{r_\alpha r_\beta}) \overline{a}^{S(\beta)} \right\} + e^{i(k_i r_\alpha)} \overline{\overline{T}}^{(\alpha)} \overline{a}_{inc} + \sum_{\beta=1}^{N} \overline{\overline{T}}^{(\alpha)} \overline{a}^{\prime S(\beta)} \tag{2.57}$$

Note that the summation over the new term $\overline{a}^{\prime S(\beta)}$ added starts from 1 to N which means that the contribution of the boundary-reflected scattering from the particle α itself is already included in (2.57).

2.6 Monte Carlo Simulation

In this section the Monte Carlo technique will be applied to calculate the backscattering from a layer of buried particles. The model configuration used in this approach will be specified first. Then the multiple scattering equation will be solved using an iterative technique. The solution process will be repeated for many realizations and averaged to calculate the backscattering coefficients.

2.6.1 Configuration for The T-matrix Approach

The model configuration used in this approach is shown in figure 2-5. Then, in the Monte Carlo simulation, for each realization, the model consists of finite number of particles with deterministic locations. However, the positions of particles will vary with different realizations. The locations of particles are generated using random number generators and the overlapping between particles is checked.

2.6.2 Iterative Solution

The multiple scattering equation (2.57) is solved using an iterative technique. For each iteration, the scattered field expansion coefficients are obtained from the previous calculation as

$$\overline{a}^{S(\alpha)(v+1)} = \sum_{\substack{\beta=1 \\ \beta\neq\alpha}}^{N} \left\{ \overline{\overline{T}}^{(\alpha)} \overline{\overline{\sigma}}(k\overline{r_\alpha r_\beta}) \overline{a}^{S(\beta)(v)} \right\} + e^{i(k_i r_\alpha)} \overline{\overline{T}}^{(\alpha)} \overline{a}_{inc} + \sum_{\beta=1}^{N} \overline{\overline{T}}^{(\alpha)} \overline{a}'^{S(\beta)(v)}, \quad (2.58)$$

where $\overline{a}^{S(\alpha)(v+1)}$ is the solution of the $(v+1)^{th}$ iteration, and $\overline{a}^{S(\beta)(v)}$ is the solution of the $(v)^{th}$ iteration. Once the result from the v^{th} iteration is obtained, it will be substituted back to right-hand side of the equation, where the $\overline{a}'^{S(\beta)(v)}$ represents the contribution from the reflected scattering term and can be obtained from $\overline{a}^{S(\beta)(v)}$ by using (2.56), and (2.55). Thus for the zeroth-order iteration, the contribution to $\overline{a}^{S(\beta)(1)}$ is only the incident wave $\overline{a}_{inc}$. The iterative process can be carried on up to the desired order. Then the scattered field is obtained by using (2.29) given in Section 2.2.

In the $i-th$ realization, we denote the backscattering field to be $\overline{E}^i$. Then the

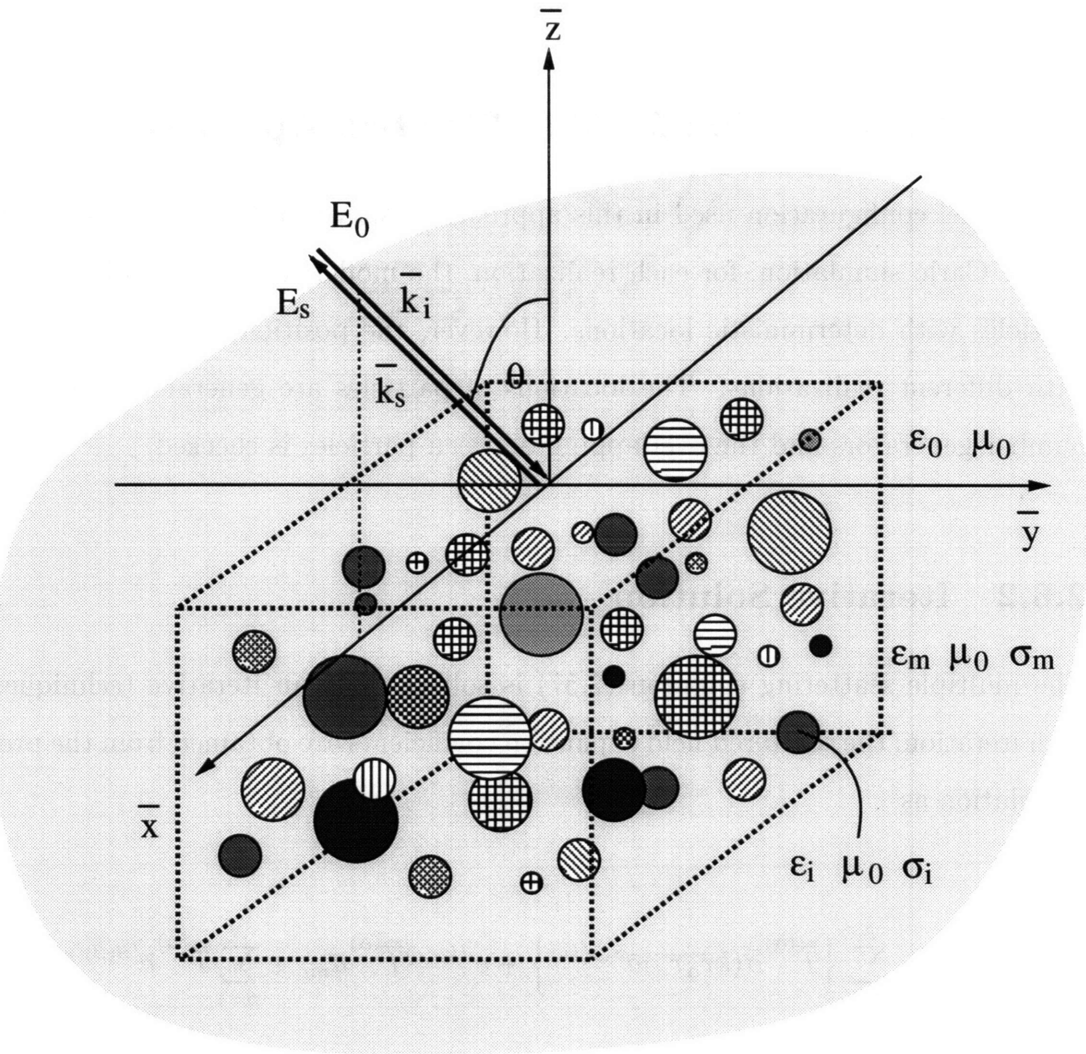

Figure 2-5: Configuration used in T-matrix approach.

backscattered intensity for the $i-th$ realization is

$$I^i = \overline{E}^i \cdot \overline{E}^{i*} \tag{2.59}$$

where the $*$ denotes the complex conjugate. The averaged field $\langle\, \overline{E}\, \rangle$ and the averaged intensity I_{coh} are obtained by averaging over M realizations,

$$\langle\, \overline{E}\, \rangle = \frac{1}{M}\sum_{i=1}^{M} \overline{E}^i \tag{2.60}$$

$$I_{coh} = \frac{1}{M}\sum_{i=1}^{M} \left(\overline{E}^i \cdot \overline{E}^{i*}\right) \tag{2.61}$$

The incoherent backscattered intensity I_{incoh} is calculated as

$$I_{incoh} = I_{coh} - |\langle\, \overline{E}\, \rangle|^2 \tag{2.62}$$

The backscattering coefficient is

$$\sigma = \lim_{r\to\infty} \frac{4\pi r^2}{A} \frac{I_{incoh}}{\overline{E}_0 \cdot \overline{E}_0^*} \tag{2.63}$$

Chapter 3

Radiative Transfer Theory

The radiative transfer theory (RT) has been used to model microwave scattering from geophysical media extensively, [7], [8], [10], [11], [19], [20], [21], [22], [27], [29], [31], [36]. Even though it deals only with the intensities of the field quantities and neglects their coherent nature, it accounts for the multiple scattering and obeys energy conservation. The propagation characteristics of the Stokes parameters are described by an integro-differential equation. Iterative and numerical (or discrete eigenanalysis) methods have been used to solve RT equations. The iterative method is convenient for the case of small albedo when the attenuation is dominated by absorption. It also gives physical insight into the multiple scattering processes since there is a one-to-one correspondence between the order of iteration and the order of multiple scattering. The discrete eigenanalysis method provides a valid solution for both small and large albedo cases. There are two principal constituents in the RT equation. The first one is the extinction matrix, which describes the attenuation of specific intensity due to absorption and scattering. The other is the phase matrix which characterizes the coupling of intensities in two different directions due to scattering. Although RT does not take into account the coherent wave interactins, it can be applied to deal with scattering problems having much more complex geometry, such as snow terrain, sea ice and vegetation canopies. Rough or flat surface boundary conditions can be imposed at each interface of the layered structure [30],[23].

In this chapter, the radiative transfer theory approach will be presented. First in

Section 3.1, the radiative transfer equation is given as well as the definition of the Stokes vector. The constituents of the RT equation and the boundary conditions are also derived in Section 3.3 and Section 3.2 respectively. Then the numerical method of solving the RT equation is given in Section 3.4 using planer surface boundary conditions.

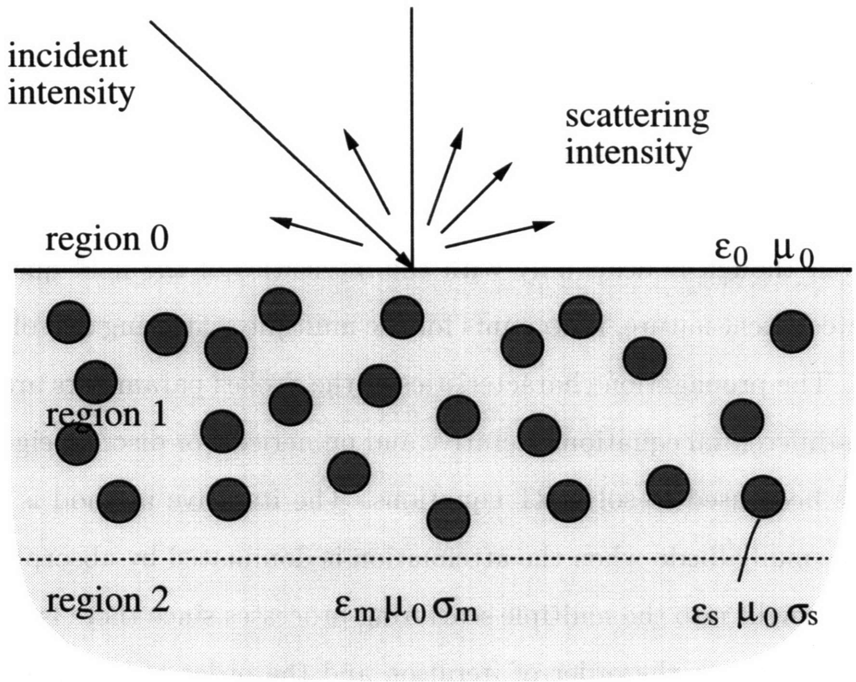

Figure 3-1: Configuration for the two-layer with discrete spherical scatterers.

The configuration used for the RT approach is shown in Figure 3-1. The model consists of a layer of discrete scatterers embedded in a homogeneous half–space medium. The discrete scatterers are characterized by their fractional volume (f), permittivity (ϵ_s) and size (a). The background medium in region 1 is described by its thickness (d) and permittivity (ϵ_1). Region 0 is assumed to be free space with permittivity ϵ_0. The region 2 is homogeneous half–space medium characterized by permittivity (ϵ_2), which may be the same as that of region 1.

3.1 Equation of Transfer

In this section, the radiative transfer equation is first introduced along with the definition of the Stokes parameters.

The Stokes vector associated with the incident wave is given by

$$\overline{I}_i = \begin{bmatrix} I_{vi} \\ I_{hi} \\ U_i \\ V_i \end{bmatrix} = \frac{1}{\eta} \begin{bmatrix} E_{vi}E_{vi}^* \\ E_{hi}E_{hi}^* \\ 2\,\mathrm{Re}\,(E_{vi}E_{hi}^*) \\ 2\,\mathrm{Im}\,(E_{vi}E_{hi}^*) \end{bmatrix} \tag{3.1}$$

Similarly, the Stokes vector associated with the spherical wave scattered from a random medium is

$$\overline{I}_s = \begin{bmatrix} I_{vs} \\ I_{hs} \\ U_s \\ V_s \end{bmatrix} = \frac{1}{\eta} \lim_{\substack{r\to\infty \\ A\to\infty}} \frac{r^2}{A\cos\theta_s} \begin{bmatrix} \langle E_{vs}E_{vs}^* \rangle \\ \langle E_{hs}E_{hs}^* \rangle \\ 2\,\mathrm{Re}\,\langle E_{vs}E_{hs}^* \rangle \\ 2\,\mathrm{Im}\,\langle E_{vs}E_{hs}^* \rangle \end{bmatrix} \tag{3.2}$$

where η is the characteristic impedance, A is the illuminated area and $\langle\rangle$ denotes ensemble average.

For a two-layer structure, the radiative transfer equation inside the particle layer can be written as [30]:

$$\begin{aligned} \cos\theta \frac{d}{dz}\overline{I}(\theta,\phi,z) &= -\overline{\overline{\kappa}}_e(\theta,\phi)\cdot\overline{I}(\theta,\phi,z) \\ &\quad + \int_{4\pi} d\Omega'\,\overline{\overline{P}}(\theta,\phi;\theta',\phi')\cdot\overline{I}(\theta',\phi',z) \end{aligned} \tag{3.3}$$

This equation is based on the energy transport and can be interpreted in the following way. As the intensities propagates through an infinitesimal length $ds =$

$dz/\cos\theta$, there is a attenuation ($\overline{\overline{\kappa}}_e$) due to the absorption loss and scattering loss, but they are also enhanced by the scattering from all other direction (θ', ϕ') into the direction of propagation (θ, ϕ). The coupling is taken into account by the phase matrix $\overline{\overline{P}}$ and the integration over solid angle 4π in Equation (3.3).

3.2 Boundary Conditions

In order to completely solve the intensities inside the layered structure, we must specify the boundary conditions at interfaces $z = 0$ and $z = -d$.

For planar surfaces, the boundary conditions have the following form [23]:
Interface 1 $(z = 0)$:

$$\overline{I}(\pi - \theta, \phi, z = 0) = \overline{\overline{T}}_{01}(\theta_0) \cdot \overline{I}_{0i}(\pi - \theta_0, \phi_0) + \overline{\overline{R}}_{10}(\theta) \cdot \overline{I}(\theta, \phi, z = 0) \tag{3.4}$$

Interface 2 $(z = -d)$:

$$\overline{I}(\theta, \phi, z = -d) = \overline{\overline{R}}_{12}(\theta) \cdot \overline{I}(\pi - \theta, \phi, z = -d) \tag{3.5}$$

where $\overline{I}_{0i}(\theta_0, \phi_0)$ is the incident source in region 0 and is given by:

$$\overline{I}_{0i}(\theta_0, \phi_0) = \overline{I}_{0i}\delta(\cos\theta_0 - \cos\theta_{0i})\delta(\phi_0 - \phi_{0i}) \tag{3.6}$$

and $\overline{\overline{R}}_{10}$, $\overline{\overline{R}}_{12}$ are the reflection matrices which relate the incident to the reflected Stokes vector in region 1 at interface 1 $(z = 0)$ and interface 2 $(z = -d)$, respectively. Similarly, $\overline{\overline{T}}_{01}$ is the transmission matrix which relates the incident Stokes vector in region 0 to the transmitted Stokes vector in region 1 at interface 1 $(z = 0)$.

These reflection and transmission matrices for planar surfaces are given in [23]. The matrices at the interface $\alpha - \beta$ have the following form:

$$\overline{\overline{R}}_{\alpha\beta}(\theta_\alpha) = \begin{bmatrix} |S_{\alpha\beta}|^2 & 0 & 0 & 0 \\ 0 & |R_{\alpha\beta}|^2 & 0 & 0 \\ 0 & 0 & \mathrm{Re}\,(S_{\alpha\beta}R^*_{\alpha\beta}) & -\mathrm{Im}\,(S_{\alpha\beta}R^*_{\alpha\beta}) \\ 0 & 0 & \mathrm{Im}\,(S_{\alpha\beta}R^*_{\alpha\beta}) & \mathrm{Re}\,(S_{\alpha\beta}R^*_{\alpha\beta}) \end{bmatrix} \tag{3.7}$$

$$\overline{\overline{T}}_{\alpha\beta}(\theta_\alpha) = \frac{\epsilon'_\beta}{\epsilon'_\alpha} \begin{bmatrix} |Y_{\alpha\beta}|^2 & 0 & 0 & 0 \\ 0 & |X_{\alpha\beta}|^2 & 0 & 0 \\ 0 & 0 & \frac{\cos(\theta_\beta)}{\cos(\theta_\alpha)}\mathrm{Re}\,(Y_{\alpha\beta}X^*_{\alpha\beta}) & -\frac{\cos(\theta_\beta)}{\cos(\theta_\alpha)}\mathrm{Im}\,(Y_{\alpha\beta}X^*_{\alpha\beta}) \\ 0 & 0 & \frac{\cos(\theta_\beta)}{\cos(\theta_\alpha)}\mathrm{Im}\,(Y_{\alpha\beta}X^*_{\alpha\beta}) & \frac{\cos(\theta_\beta)}{\cos(\theta_\alpha)}\mathrm{Re}\,(Y_{\alpha\beta}X^*_{\alpha\beta}) \end{bmatrix} \tag{3.8}$$

where

$$R_{\alpha\beta} = \frac{k_{\alpha zi} - k_{\beta zi}}{k_{\alpha zi} + k_{\beta zi}} \tag{3.9}$$

$$S_{\alpha\beta} = \frac{k_\beta^2 k_{\alpha zi} - k_\alpha^2 k_{\beta zi}}{k_\beta^2 k_{\alpha zi} + k_\alpha^2 k_{\beta zi}} \tag{3.10}$$

$$X_{\alpha\beta} = 1 + R_{\alpha\beta} \tag{3.11}$$

$$Y_{\alpha\beta} = 1 + S_{\alpha\beta} \tag{3.12}$$

and ϵ'_α and ϵ'_β are the real parts of the permittivities of the medium α and medium β respectively.

Once the solution inside region 1 is obtained, the scattered Stokes vector can be calculated by using the following boundary condition:

$$\overline{I}_{0s}(\theta_0, \phi_0, z=0) = \overline{\overline{R}}_{01}(\theta_0) \cdot \overline{I}_{0i}(\pi - \theta_0, \phi_0) + \overline{\overline{T}}_{10}(\theta) \cdot \overline{I}(\theta, \phi, z=0) \tag{3.13}$$

where ϕ and ϕ_0 are equal, and θ and θ_0 are related by Snell's law.

3.3 Phase and Extinction matrices

In this section, we shall derive the phase and extinction matrices for spheres. The Laplace equation is used to solve for the induced dipole moments in a sphere due to a plane incident wave. The radiation of the induced dipoles gives the scattered field of the object. Because of the usage of Laplace equation rather than the wave equation, the derived scattering function matrix is only valid in the low-frequency limit when the particle size is much smaller than the wavelength.

The Stokes matrix relates the Stokes parameters of the scattered wave to those of the incident wave whereas the scattering function matrix relates the scattered field to the incident field. For the case of incoherent addition of scattered waves, the phase matrix is the averaging of the Stokes matrices over orientation and size of the particles. Thus, we shall study the Stokes matrix of a single particle.

Consider an incident field $\overline{E}_i$ on a scatterer which give rise to the scattered field $\overline{E}_s$. Both fields are decomposed into two polarizations, horizontal ($\hat{h}$) and vertical ($\hat{v}$). The relation between the scattered field and the incident field is given by the scattering matrix and the following equation :

$$\begin{bmatrix} E_{vs} \\ E_{hs} \end{bmatrix} = \frac{e^{ikr}}{r} \begin{bmatrix} f_{vv} & f_{vh} \\ f_{hv} & f_{hh} \end{bmatrix} \cdot \begin{bmatrix} E_{vi} \\ E_{hi} \end{bmatrix} \tag{3.14}$$

where k is the wave number in the background medium, r is the distance from the center of the scatterer and $f_{\alpha\beta}$ are elements of the scattering matrix, which are functions of incident and scattering directions and the shape and permittivity of the scatterer.

The Stokes matrix $\overline{\overline{L}}(\theta, \phi; \theta', \phi')$ relates the Stokes vector $\overline{I}_i$ associated with the incident field to the Stokes vector $\overline{I}_s$ associated to the scattered field

$$\overline{I}_s = \frac{1}{r^2}\overline{\overline{L}}(\theta, \phi; \theta', \phi')\overline{I}_i \tag{3.15}$$

Because of the incoherent addition of Stokes parameters, the phase matrix $\overline{\overline{P}}(\theta, \phi; \theta', \phi')$ is obtained from the scattering matrix and by incoherent averaging over the types, dimensions and orientations of the scatterers. For example, the phase matrix for a mixture of ellipsoids is given by

$$\begin{aligned}\overline{\overline{P}}(\theta,\phi;\theta',\phi') &= n_o \int da \int db \int dc \int d\alpha \int d\beta \int d\gamma \\ &\cdot \mathrm{p}(a,b,c,\alpha,\beta,\gamma)\cdot \overline{\overline{L}}(\theta,\phi;\theta',\phi')\end{aligned} \tag{3.16}$$

where n_o is the number of scatterer per unit volume; a, b, c are the lengths of the ellipsoid semi-major axis; α, β, γ are the Eulerian angles which give the orientation of the ellipsoid and $\mathrm{p}(a,b,c,\alpha,\beta,\gamma)$ is the joint probability density function for the quantities $a,b,c,\alpha,\beta,\gamma$. For the case of spherical scatterers, Equation (3.16) reduces to an easy form:

$$\overline{\overline{P}}(\theta,\phi;\theta',\phi') = n_o \overline{\overline{L}}(\theta,\phi;\theta',\phi') \tag{3.17}$$

where the Stokes matrix $\overline{\overline{L}}(\theta,\phi;\theta',\phi')$ is given by :

$$\overline{\overline{L}}(\theta,\phi;\theta',\phi') = \begin{bmatrix} |f_{vv}|^2 & |f_{vh}|^2 & \mathrm{Re}\,(f_{vv}f_{vh}^*) & -\mathrm{Im}\,(f_{vv}f_{vh}^*) \\ |f_{vv}|^2 & |f_{vh}|^2 & \mathrm{Re}\,(f_{hv}f_{hh}^*) & -\mathrm{Im}\,(f_{hv}f_{hh}^*) \\ 2\ \mathrm{Re}\,(f_{vv}f_{hv}^*) & 2\ \mathrm{Re}\,(f_{vh}f_{hh}^*) & \mathrm{Re}\,(f_{vv}f_{hh}^* + f_{vh}f_{hv}^*) & -\mathrm{Im}\,(f_{vv}f_{hh}^* - f_{vh}f_{hv}^*) \\ 2\ \mathrm{Im}\,(f_{vv}f_{hv}^*) & 2\ \mathrm{Im}\,(f_{vh}f_{hh}^*) & \mathrm{Im}\,(f_{vv}f_{hh}^* + f_{vh}f_{hv}^*) & \mathrm{Re}\,(f_{vv}f_{hh}^* - f_{vh}f_{hv}^*) \end{bmatrix} \tag{3.18}$$

The other component of th RT equation is the extinction matrix. For spherical particles the extinction matrix is simply diagonal

$$\overline{\overline{\kappa}}_e = \begin{bmatrix} \kappa_e & 0 & 0 & 0 \\ 0 & \kappa_e & 0 & 0 \\ 0 & 0 & \kappa_e & 0 \\ 0 & 0 & 0 & \kappa_e \end{bmatrix} \tag{3.19}$$

where κ_e is the extinction coefficient whihc is equal to the summation of the scattering coefficient κ_s and the absorption coefficient κ_a.

The phase matrix $\overline{\overline{P}}(\theta, \phi; \theta', \phi')$, the scattering coefficient κ_s, and the absorption coefficient κ_a for a small spherical dielectric particle are given in the following.

The scattered field from a Rayleigh sphere is given by

$$\overline{E}_s = \frac{k^2 e^{ikr}}{4\pi r} 3v_0 y(\overline{\overline{I}} - \hat{k}_s\hat{k}_s) \cdot \hat{e}_i \overline{E}_0 \tag{3.20}$$

and

$$y = \frac{\epsilon_s - \epsilon}{\epsilon_s + 2\epsilon} \tag{3.21}$$

where $v_0 = 4\pi a^3/3$ and ϵ_s and ϵ are the permittivities for the particle and the background medium respecitvely. Hence, the scattering function matrix is

$$\overline{\overline{F}}(\theta_s, \phi_s; \theta_i, \phi_i) = k^2 \frac{3v_0 y}{4\pi} (\overline{\overline{I}} - \hat{k}_s\hat{k}_s) \cdot (\overline{\overline{I}} - \hat{k}_i\hat{k}_i) \tag{3.22}$$

From the scattering function matrix $\overline{\overline{F}}$, we can calculate the Stokes matrix $\overline{\overline{L}}$ and the phase matrix $\overline{\overline{P}}$. For spherical scatterers , the phase matrix is obtained as

$$\overline{\overline{P}}(\theta, \phi, \theta', \phi') = \begin{bmatrix} P_{11} & P_{12} & P_{13} & 0 \\ P_{21} & P_{22} & P_{23} & 0 \\ P_{31} & P_{32} & P_{33} & 0 \\ 0 & 0 & 0 & P_{44} \end{bmatrix} \tag{3.23}$$

where

$$P_{11} = \omega[\sin^2\theta \sin^2\theta' + 2\sin\theta \sin\theta' \cos\theta \cos\theta' \cos(\phi - \phi') + \cos^2\theta \cos^2\theta' \cos^2(\phi - \phi')] \tag{3.24}$$

$$P_{12} = \omega \cos^2\theta \sin^2(\phi - \phi') \tag{3.25}$$

$$P_{13} = \omega[\cos\theta \sin\theta \sin\theta' \sin(\phi - \phi') + \cos^2\theta \cos\theta' \sin(\phi - \phi') \cos(\phi - \phi')] \tag{3.26}$$

$$P_{21} = \omega \cos^2\theta' \sin^2(\phi - \phi') \tag{3.27}$$

$$P_{22} = \omega \cos^2(\phi - \phi') \tag{3.28}$$

$$P_{23} = -\omega \cos\theta' \sin(\phi - \phi') \cos(\phi - \phi') \tag{3.29}$$

$$P_{31} = \omega[-2\sin\theta \sin\theta' \cos\theta' \sin(\phi - \phi') - 2\cos\theta \cos^2\theta' \cos(\phi - \phi') \sin(\phi - \phi')] \tag{3.30}$$

$$P_{32} = 2\omega \cos\theta \sin(\phi - \phi') \cos(\phi - \phi') \tag{3.31}$$

$$P_{33} = \omega[\sin\theta \sin\theta' \cos(\phi - \phi') + \cos\theta \cos\theta'(\cos^2(\phi - \phi') - \sin^2(\phi - \phi'))] \tag{3.32}$$

$$P_{44} = \omega[\sin\theta \sin\theta' \cos(\phi - \phi') + \cos\theta \cos\theta'] \tag{3.33}$$

$$\omega = \frac{3}{8\pi}\kappa_s \tag{3.34}$$

and κ_s is the scattering coefficient

$$\kappa_s = \frac{8\pi}{3} n_0 k^4 a^6 |y|^2 = 2fk^4 a^3 |y|^2 \tag{3.35}$$

where $f = n_0 v_0$ is the fractional volume occupied by the particles. The internal power absorption due to one single scatterer is

$$\int dv \omega \epsilon_s'' \frac{\left|\overline{E}^{int}(\overline{r})\right|^2}{2} = v_0 \omega \epsilon_s'' \left|\frac{3\epsilon}{(\epsilon_s + 2\epsilon)}\right|^2 \frac{|E_0|^2}{2} \tag{3.36}$$

where the ϵ_s'' is the imaginary part of the permittivity of the particle. The absorption cross section σ_a, hence, is

$$\sigma_a = v_0 \omega \epsilon_s'' \eta \left|\frac{3\epsilon}{(\epsilon_s + 2\epsilon)}\right|^2 \tag{3.37}$$

The absorption coefficient due to the scatterer is $n_0\sigma_a$. Therefore, the absorption coefficient is

$$\kappa_a = fk\frac{\epsilon_s''}{\epsilon}\left|\frac{3\epsilon}{(\epsilon_s + 2\epsilon)}\right|^2 \tag{3.38}$$

Extinction coefficient κ_e is the sum of κ_s and κ_a. The extinction matrix is diagonal with each element equal to κ_e.

3.4 Numerical solution

In the this section, the RT equation is solved using the discrete ordinate-eigenanalysis method [30],[23], or so-called numerical RT. All orders of multiple scattering effects are included in this numerical solution.

First, the RT equation is expanded into Fourier series of the azimuthal angle ϕ. Thus the ϕ dependence in the radiative transfer equation is eliminated. Then, the set of all integrals over ϕ are carried out analytically. The resulting RT equation is solved using the Gaussian quadrature method by discretizing the angular variable θ for each harmonic of ϕ. Thus, the RT equation is transformed into a set of coupled first-order differential equations with constant coefficients. This set of equations is solved using the eigenanalysis method by obtaining the eigenvalues and eigenvectors and by matching the boundary conditions to determine the unknown coefficients. The detail of this method is described in [23], the main steps of numerical procedure are given in this section.

3.4.1 Fourier Series Expansion in Azimuthal Direction

Starting with the radiative transfer equation, we first expand the Stokes vector and the phase matrix into a Fourier series of $(\phi - \phi')$:

$$\begin{aligned} \overline{\overline{P}}(\theta,\phi;\theta',\phi') &= \sum_{m=0}^{\infty} \frac{1}{(1+\delta_{m0})\pi} \\ &\quad \left[\overline{\overline{P}}^{mc}(\theta,\theta')\cos m(\phi-\phi') + \overline{\overline{P}}^{ms}(\theta,\theta')\sin m(\phi-\phi')\right] \end{aligned} \tag{3.39}$$

$$\overline{I}(\theta,\phi,z) = \sum_{m=0}^{\infty} \left[\overline{I}^{mc}(\theta,z)\cos m(\phi-\phi') + \overline{I}^{ms}(\theta,z)\sin m(\phi-\phi')\right] \quad (3.40)$$

The incident Stokes vector can be written as:

$$\begin{aligned}
\overline{I}_{0i}(\pi-\theta_0,\phi_0) &= \overline{I}_{0i}\ \delta(\cos\theta_0-\cos\theta_{0i})\ \delta(\phi_0-\phi_{0i}) \\
&= \overline{I}_{0i}\ \delta(\cos\theta_0-\cos\theta_{0i}) \sum_{m=0}^{\infty} \frac{1}{(1+\delta_{m0})\pi}\cos m(\phi_0-\phi_{0i}) \quad (3.41)
\end{aligned}$$

where m is the order of harmonics in the azimuthal direction, and the superscripts c and s indicate the cosine and sine dependence. The δ_{ij} is the Kronecker delta function and is defined as:

$$\delta_{ij} = \begin{cases} 1 & \text{if} \quad i=j \\ 0 & \text{if} \quad i \neq j \end{cases} \quad (3.42)$$

Also note that the zeroth-order sine dependence terms are zero.

$$\overline{I}^{0s}(\theta,z) = 0 \quad (3.43)$$

$$\overline{\overline{P}}^{0s}(\theta,z) = 0 \quad (3.44)$$

Substituting (3.39)-(3.40) into the radiative transfer equation and carrying out the integration over ϕ' leads to the following RT equations.

For m = 0, 1, 2, 3, ...

$$\begin{aligned}
\cos\theta\frac{d}{dz}\overline{I}^{mc}(\theta,z) &= -\overline{\overline{\kappa}}_e(\theta)\cdot\overline{I}^{mc}(\theta,z) + \int_0^{\pi} d\theta'\sin\theta' \\
&\quad \times\left[\overline{\overline{P}}^{mc}(\theta,\theta')\cdot\overline{I}^{mc}(\theta',z) - \overline{\overline{P}}^{ms}(\theta,\theta')\cdot\overline{I}^{ms}(\theta',z)\right] \quad (3.45) \\
\cos\theta\frac{d}{dz}\overline{I}^{ms}(\theta,z) &= -\overline{\overline{\kappa}}_e(\theta)\cdot\overline{I}^{ms}(\theta,z) + \int_0^{\pi} d\theta'\sin\theta' \\
&\quad \times\left[\overline{\overline{P}}^{ms}(\theta,\theta')\cdot\overline{I}^{mc}(\theta',z) + \overline{\overline{P}}^{mc}(\theta,\theta')\cdot\overline{I}^{ms}(\theta',z)\right] \quad (3.46)
\end{aligned}$$

One should note that these two equations are coupled. Next, we will define the even and odd modes in order to decouple the above two equations.

The general form of the phase matrix for an azimuthally isotropic medium is [23]:

$$\overline{\overline{P}}^{mc}(\theta, \theta') = \begin{bmatrix} p_{11}^{mc} & p_{12}^{mc} & 0 & 0 \\ p_{21}^{mc} & p_{22}^{mc} & 0 & 0 \\ 0 & 0 & p_{33}^{mc} & p_{34}^{mc} \\ 0 & 0 & p_{43}^{mc} & p_{44}^{mc} \end{bmatrix} \tag{3.47}$$

$$\overline{\overline{P}}^{ms}(\theta, \theta') = \begin{bmatrix} 0 & 0 & p_{13}^{ms} & p_{14}^{ms} \\ 0 & 0 & p_{23}^{ms} & p_{24}^{ms} \\ p_{31}^{ms} & p_{32}^{ms} & 0 & 0 \\ p_{41}^{ms} & p_{42}^{ms} & 0 & 0 \end{bmatrix} \tag{3.48}$$

Using this symmetry, we can decouple Equations (3.45),(3.46) into

$$\begin{aligned} \cos\theta \frac{d}{dz}\overline{I}^{m\alpha}(\theta, z) &= -\overline{\overline{\kappa}}_e(\theta) \cdot \overline{I}^{m\alpha}(\theta, z) \\ &\quad + \int_0^\pi d\theta' \sin\theta' \overline{\overline{P}}^{m\alpha}(\theta, \theta') \cdot \overline{I}^{m\alpha}(\theta', z) \end{aligned} \tag{3.49}$$

where $\alpha = e$ or o (even and odd modes) and

$$\overline{I}^{me}(\theta, z) = \begin{bmatrix} I_v^{mc}(\theta, z) \\ I_h^{mc}(\theta, z) \\ U^{ms}(\theta, z) \\ V^{ms}(\theta, z) \end{bmatrix} \tag{3.50}$$

$$\overline{I}^{mo}(\theta, z) = \begin{bmatrix} I_v^{ms}(\theta, z) \\ I_h^{ms}(\theta, z) \\ U^{mc}(\theta, z) \\ V^{mc}(\theta, z) \end{bmatrix} \tag{3.51}$$

$$\overline{\overline{P}}^{me}(\theta,\theta') = \begin{bmatrix} p_{11}^{mc} & p_{12}^{mc} & -p_{13}^{ms} & -p_{14}^{ms} \\ p_{21}^{mc} & p_{22}^{mc} & -p_{23}^{ms} & -p_{24}^{ms} \\ p_{31}^{ms} & p_{32}^{ms} & p_{33}^{mc} & p_{34}^{mc} \\ p_{41}^{ms} & p_{42}^{ms} & p_{43}^{mc} & p_{44}^{mc} \end{bmatrix} \tag{3.52}$$

$$\overline{\overline{P}}^{mo}(\theta,\theta') = \begin{bmatrix} p_{11}^{mc} & p_{12}^{mc} & p_{13}^{ms} & p_{14}^{ms} \\ p_{21}^{mc} & p_{22}^{mc} & p_{23}^{ms} & p_{24}^{ms} \\ p_{31}^{ms} & p_{32}^{ms} & p_{33}^{mc} & p_{34}^{mc} \\ p_{41}^{ms} & p_{42}^{ms} & p_{43}^{mc} & p_{44}^{mc} \end{bmatrix} \tag{3.53}$$

In this formulation the boundary conditions become

$$\overline{I}^{m\alpha}(\pi-\theta, z=0) = \overline{\overline{T}}_{01}(\theta_0)\cdot\overline{I}_{0i}(\pi-\theta_0) + \overline{\overline{R}}_{10}(\theta)\cdot\overline{I}^{m\alpha}(\theta, z=0) \tag{3.54}$$

$$\overline{I}^{m\alpha}(\theta, z=-d) = \overline{\overline{R}}_{12}(\theta)\cdot\overline{I}^{m\alpha}(\pi-\theta, z=-d) \tag{3.55}$$

where $\overline{\overline{R}}_{\beta\gamma}$ and $\overline{\overline{T}}_{\beta\gamma}$ are the coherent reflection and transmission matrices, respectively, for planar surface given in Section 3.2. The scattered Stokes vector in region 0 can be obtained by using

$$\overline{I}_{0s}(\theta_0) = \overline{\overline{T}}_{10}(\theta)\cdot\overline{I}^{m\alpha}(\theta, z=0) + \overline{\overline{R}}_{01}(\theta_0)\cdot\overline{I}_{0i}^{m\alpha}(\pi-\theta_0) \tag{3.56}$$

where θ_0 is related to θ by Snell's law and

$$\overline{I}_{0i}^{me}(\pi-\theta_0) = \begin{bmatrix} I_{v0i} \\ I_{h0i} \\ 0 \\ 0 \end{bmatrix} \tag{3.57}$$

$$\overline{I}_{0i}^{mo}(\pi - \theta_0) = \begin{bmatrix} 0 \\ 0 \\ U_{0i} \\ V_{0i} \end{bmatrix} \tag{3.58}$$

It should be noted that the superscripts me and mo will be dropped from now on, since the procedure for obtaining the solution is the same for all the harmonics m and all the modes e, o.

3.4.2 Upward and Downward Propagating Intensities

First, the following matrices are defined:

$$\overline{I}_1(\theta, z) = \begin{bmatrix} I_v(\theta, z) \\ I_h(\theta, z) \end{bmatrix} \tag{3.59}$$

$$\overline{I}_2(\theta, z) = \begin{bmatrix} U(\theta, z) \\ V(\theta, z) \end{bmatrix} \tag{3.60}$$

$$\overline{\overline{\kappa}}_{e1}(\theta) = \begin{bmatrix} \kappa_{e11}(\theta) & 0 \\ 0 & \kappa_{e22}(\theta) \end{bmatrix} \tag{3.61}$$

$$\overline{\overline{\kappa}}_{e2}(\theta) = \begin{bmatrix} \kappa_{e33}(\theta) & \kappa_{e34}(\theta) \\ \kappa_{e43}(\theta) & \kappa_{e44}(\theta) \end{bmatrix} \tag{3.62}$$

$$\overline{\overline{P}}_{11}(\theta, \theta') = \begin{bmatrix} p_{11}(\theta, \theta') & p_{12}(\theta, \theta') \\ p_{21}(\theta, \theta') & p_{22}(\theta, \theta') \end{bmatrix} \tag{3.63}$$

$$\overline{\overline{P}}_{12}(\theta, \theta') = \begin{bmatrix} p_{13}(\theta, \theta') & p_{14}(\theta, \theta') \\ p_{23}(\theta, \theta') & p_{24}(\theta, \theta') \end{bmatrix} \tag{3.64}$$

$$\overline{\overline{P}}_{21}(\theta, \theta') = \begin{bmatrix} p_{31}(\theta, \theta') & p_{32}(\theta, \theta') \\ p_{41}(\theta, \theta') & p_{42}(\theta, \theta') \end{bmatrix} \tag{3.65}$$

$$\overline{\overline{P}}_{22}(\theta,\theta') = \begin{bmatrix} p_{33}(\theta,\theta') & p_{34}(\theta,\theta') \\ p_{43}(\theta,\theta') & p_{44}(\theta,\theta') \end{bmatrix} \tag{3.66}$$

where only six elements are needed in the extinction matrix due to azimuthal symmetry.

Using these definitions, Equation (3.49) can be rewritten as:

$$\cos\theta \frac{d}{dz}\overline{I}_1(\theta,z) = -\overline{\overline{\kappa}}_{e1}(\theta)\cdot\overline{I}_1(\theta,z) + \int_0^{\pi} d\theta' \sin\theta' \left[\overline{\overline{P}}_{11}(\theta,\theta')\cdot\overline{I}_1(\theta',z) + \overline{\overline{P}}_{12}(\theta,\theta')\cdot\overline{I}_2(\theta',z)\right] \tag{3.67}$$

$$\cos\theta \frac{d}{dz}\overline{I}_2(\theta,z) = -\overline{\overline{\kappa}}_{e2}(\theta)\cdot\overline{I}_2(\theta,z) + \int_0^{\pi} d\theta' \sin\theta' \left[\overline{\overline{P}}_{21}(\theta,\theta')\cdot\overline{I}_1(\theta',z) + \overline{\overline{P}}_{22}(\theta,\theta')\cdot\overline{I}_2(\theta',z)\right] \tag{3.68}$$

Furthermore, each of these equations can be broken into upward (θ, z) and downward $(\pi-\theta, z)$ propagating intensities, which gives:

$$\begin{aligned} \cos\theta \frac{d}{dz}\overline{I}_1(\theta,z) = {} & -\overline{\overline{\kappa}}_{e1}(\theta)\cdot\overline{I}_1(\theta,z) + \int_0^{\pi/2} d\theta' \sin\theta' \\ & \left[\overline{\overline{P}}_{11}(\theta,\theta')\cdot\overline{I}_1(\theta',z) + \overline{\overline{P}}_{11}(\theta,\pi-\theta')\cdot\overline{I}_1(\pi-\theta',z)\right. \\ & \left. + \overline{\overline{P}}_{12}(\theta,\theta')\cdot\overline{I}_2(\theta',z) + \overline{\overline{P}}_{12}(\theta,\pi-\theta')\cdot\overline{I}_2(\pi-\theta',z)\right] \end{aligned} \tag{3.69}$$

$$\begin{aligned} -\cos\theta \frac{d}{dz}\overline{I}_1(\pi-\theta,z) = {} & -\overline{\overline{\kappa}}_{e1}(\theta)\cdot\overline{I}_1(\pi-\theta,z) + \int_0^{\pi/2} d\theta' \sin\theta' \\ & \left[\overline{\overline{P}}_{11}(\theta,\pi-\theta')\cdot\overline{I}_1(\theta',z) + \overline{\overline{P}}_{11}(\theta,\theta')\cdot\overline{I}_1(\pi-\theta',z)\right. \\ & \left. - \overline{\overline{P}}_{12}(\theta,\pi-\theta')\cdot\overline{I}_2(\theta',z) - \overline{\overline{P}}_{12}(\theta,\theta')\cdot\overline{I}_2(\pi-\theta',z)\right] \end{aligned} \tag{3.70}$$

$$\cos\theta \frac{d}{dz}\overline{I}_2(\theta,z) = -\overline{\overline{\kappa}}_{e2}(\theta)\cdot\overline{I}_2(\theta,z) + \int_0^{\pi/2} d\theta' \sin\theta'$$

$$\left[\overline{\overline{P}}_{21}(\theta,\theta')\cdot\overline{I}_1(\theta',z)+\overline{\overline{P}}_{21}(\theta,\pi-\theta')\cdot\overline{I}_1(\pi-\theta',z)\right.$$
$$\left.+\,\overline{\overline{P}}_{22}(\theta,\theta')\cdot\overline{I}_2(\theta',z)+\overline{\overline{P}}_{22}(\theta,\pi-\theta')\cdot\overline{I}_2(\pi-\theta',z)\right] \tag{3.71}$$

$$-\cos\theta\,\frac{d}{dz}\overline{I}_2(\pi-\theta,z) = -\overline{\overline{\kappa}}_{e2}(\theta)\cdot\overline{I}_2(\pi-\theta,z)+\int_0^{\pi/2}d\theta'\sin\theta'$$
$$\left[-\overline{\overline{P}}_{21}(\theta,\pi-\theta')\cdot\overline{I}_1(\theta',z)-\overline{\overline{P}}_{21}(\theta,\theta')\cdot\overline{I}_1(\pi-\theta',z)\right.$$
$$\left.+\,\overline{\overline{P}}_{22}(\theta,\pi-\theta')\cdot\overline{I}_2(\theta',z)+\overline{\overline{P}}_{22}(\theta,\theta')\cdot\overline{I}_2(\pi-\theta',z)\right] \tag{3.72}$$

where the following reciprocity relations have been used for α, $\beta = 1$ or 2.

$$\overline{\overline{\kappa}}_{e\alpha}(\theta) = \overline{\overline{\kappa}}_{e\alpha}(\pi-\theta) \tag{3.73}$$

$$\overline{\overline{P}}_{\alpha\beta}(\pi-\theta,\pi-\theta') = (-1)^{\alpha+\beta}\,\overline{\overline{P}}_{\alpha\beta}(\theta,\theta') \tag{3.74}$$

$$\overline{\overline{P}}_{\alpha\beta}(\pi-\theta,\theta') = (-1)^{\alpha+\beta}\,\overline{\overline{P}}_{\alpha\beta}(\theta,\pi-\theta') \tag{3.75}$$

3.4.3 Gaussian Quadrature Method

The set of decoupled radiative transfer equations without the azimuthal dependence for each harmonic can be solved numerically using the Gaussian quadrature method.

Consider an integral

$$L = \int_{-1}^{1} d\mu f(\mu) \tag{3.76}$$

over the interval -1 to 1. Then the integral can be approximated by

$$L = \sum_{j=-n}^{n} a_j\, f(\mu_j) \tag{3.77}$$

where the summation j is carried over $j = \pm1, \pm2, \pm3, ..., \pm n$, μ_j are the zeroes of the even-order Legendre polynomial $P_{2n}(\mu)$, and a_j are the Christoffel weighting functions which can be found in [1]. The μ_j and a_j obey the relations

$$a_j = a_{-j} \tag{3.78}$$

$$\mu_j = -\mu_{-j} \tag{3.79}$$

By letting $\mu = \cos\theta$, the integral over $d\theta$ can be approximated by a quadrature formula as follows

$$\int_0^{\pi} d\theta \sin\theta f(\cos\theta) \approx \sum_{-n}^{n} a_j f(\mu_j) \tag{3.80}$$

This Gaussian quadrature is used to discretize Equations (3.69)-(3.72). Then, Equations (3.69)-(3.72) become :

$$\overline{\overline{\mu}}' \cdot \frac{d}{dz}\overline{I}_1^+ = -\overline{\overline{\kappa}}_{e1} \cdot \overline{I}_1^+ + \overline{\overline{F}}_{11} \cdot \overline{\overline{a}}' \cdot \overline{I}_1^+ + \overline{\overline{B}}_{11} \cdot \overline{\overline{a}}' \cdot \overline{I}_1^- + \overline{\overline{F}}_{12} \cdot \overline{\overline{a}}' \cdot \overline{I}_2^+ + \overline{\overline{B}}_{12} \cdot \overline{\overline{a}}' \cdot \overline{I}_2^- \tag{3.81}$$

$$-\overline{\overline{\mu}}' \cdot \frac{d}{dz}\overline{I}_1^- = -\overline{\overline{\kappa}}_{e1} \cdot \overline{I}_1^- + \overline{\overline{B}}_{11} \cdot \overline{\overline{a}}' \cdot \overline{I}_1^+ + \overline{\overline{F}}_{11} \cdot \overline{\overline{a}}' \cdot \overline{I}_1^- - \overline{\overline{B}}_{12} \cdot \overline{\overline{a}}' \cdot \overline{I}_2^+ - \overline{\overline{F}}_{12} \cdot \overline{\overline{a}}' \cdot \overline{I}_2^- \tag{3.82}$$

$$\overline{\overline{\mu}}' \cdot \frac{d}{dz}\overline{I}_2^+ = -\overline{\overline{\kappa}}_{e2} \cdot \overline{I}_2^+ + \overline{\overline{F}}_{21} \cdot \overline{\overline{a}}' \cdot \overline{I}_1^+ + \overline{\overline{B}}_{21} \cdot \overline{\overline{a}}' \cdot \overline{I}_1^- + \overline{\overline{F}}_{22} \cdot \overline{\overline{a}}' \cdot \overline{I}_2^+ + \overline{\overline{B}}_{22} \cdot \overline{\overline{a}}' \cdot \overline{I}_2^- \tag{3.83}$$

$$-\overline{\overline{\mu}}' \cdot \frac{d}{dz}\overline{I}_2^- = -\overline{\overline{\kappa}}_{e2} \cdot \overline{I}_2^- - \overline{\overline{B}}_{21} \cdot \overline{\overline{a}}' \cdot \overline{I}_1^+ - \overline{\overline{F}}_{21} \cdot \overline{\overline{a}}' \cdot \overline{I}_1^- + \overline{\overline{B}}_{22} \cdot \overline{\overline{a}}' \cdot \overline{I}_2^+ + \overline{\overline{F}}_{22} \cdot \overline{\overline{a}}' \cdot \overline{I}_2^- \tag{3.84}$$

where $\overline{I}_1^{\pm}$ and $\overline{I}_2^{\pm}$ are $2n \times 1$ vectors

$$\overline{I}_1^{\pm} = \begin{bmatrix} I_v(\pm\mu_1, z) \\ \vdots \\ I_v(\pm\mu_n, z) \\ I_h(\pm\mu_1, z) \\ \vdots \\ I_h(\pm\mu_n, z) \end{bmatrix} \quad \overline{I}_2^{\pm} = \begin{bmatrix} U(\pm\mu_1, z) \\ \vdots \\ U(\pm\mu_n, z) \\ V(\pm\mu_1, z) \\ \vdots \\ V(\pm\mu_n, z) \end{bmatrix} \tag{3.85}$$

and $\overline{\overline{F}}_{\alpha\beta}$ and $\overline{\overline{B}}_{\alpha\beta}$ are $2n \times 2n$ matrices

$$\overline{\overline{F}}_{\alpha\beta} = \begin{bmatrix} P_{\alpha\beta_{11}}(\mu_1, \mu_1) & \cdots & P_{\alpha\beta_{11}}(\mu_1, \mu_n) & P_{\alpha\beta_{12}}(\mu_1, \mu_1) & \cdots & P_{\alpha\beta_{12}}(\mu_1, \mu_n) \\ \vdots & \vdots & \vdots & \vdots & \vdots & \vdots \\ P_{\alpha\beta_{11}}(\mu_n, \mu_1) & \cdots & P_{\alpha\beta_{11}}(\mu_n, \mu_n) & P_{\alpha\beta_{12}}(\mu_n, \mu_1) & \cdots & P_{\alpha\beta_{12}}(\mu_n, \mu_n) \\ P_{\alpha\beta_{21}}(\mu_1, \mu_1) & \cdots & P_{\alpha\beta_{21}}(\mu_1, \mu_n) & P_{\alpha\beta_{22}}(\mu_1, \mu_1) & \cdots & P_{\alpha\beta_{22}}(\mu_1, \mu_n) \\ \vdots & \vdots & \vdots & \vdots & \vdots & \vdots \\ P_{\alpha\beta_{21}}(\mu_n, \mu_1) & \cdots & P_{\alpha\beta_{21}}(\mu_n, \mu_n) & P_{\alpha\beta_{22}}(\mu_n, \mu_1) & \cdots & P_{\alpha\beta_{22}}(\mu_n, \mu_n) \end{bmatrix} \tag{3.86}$$

$$\overline{\overline{B}}_{\alpha\beta} = \begin{bmatrix} P_{\alpha\beta_{11}}(\mu_1, -\mu_1) & \cdots & P_{\alpha\beta_{11}}(\mu_1, -\mu_n) & P_{\alpha\beta_{12}}(\mu_1, -\mu_1) & \cdots & P_{\alpha\beta_{12}}(\mu_1, -\mu_n) \\ \vdots & \vdots & \vdots & \vdots & \vdots & \vdots \\ P_{\alpha\beta_{11}}(\mu_n, -\mu_1) & \cdots & P_{\alpha\beta_{11}}(\mu_n, -\mu_n) & P_{\alpha\beta_{12}}(\mu_n, -\mu_1) & \cdots & P_{\alpha\beta_{12}}(\mu_n, -\mu_n) \\ P_{\alpha\beta_{21}}(\mu_1, -\mu_1) & \cdots & P_{\alpha\beta_{21}}(\mu_1, -\mu_n) & P_{\alpha\beta_{22}}(\mu_1, -\mu_1) & \cdots & P_{\alpha\beta_{22}}(\mu_1, -\mu_n) \\ \vdots & \vdots & \vdots & \vdots & \vdots & \vdots \\ P_{\alpha\beta_{21}}(\mu_n, -\mu_1) & \cdots & P_{\alpha\beta_{21}}(\mu_n, -\mu_n) & P_{\alpha\beta_{22}}(\mu_n, -\mu_1) & \cdots & P_{\alpha\beta_{22}}(\mu_n, -\mu_n) \end{bmatrix} \tag{3.87}$$

and $\overline{\overline{\mu}}'$ and $\overline{\overline{a}}'$ are $2n \times 2n$ diagonal matrices

$$\overline{\overline{\mu}}' = \operatorname{diag}[\mu_1, \cdots, \mu_n, \mu_1, \cdots, \mu_n] \tag{3.88}$$

$$\overline{\overline{a}}' = \mathrm{diag}\,[a_1, \cdots, a_n, a_1, \cdots, a_n] \tag{3.89}$$

The system of $8n$ first-order differential equations, (3.81)-(3.84), can be put into more compact form by defining two $4n \times 1$ vectors

$$\overline{I}_a = \begin{bmatrix} \overline{I}_1^+ + \overline{I}_1^- \\ \overline{I}_2^+ - \overline{I}_2^- \end{bmatrix} \quad \overline{I}_s = \begin{bmatrix} \overline{I}_1^+ - \overline{I}_1^- \\ \overline{I}_2^+ + \overline{I}_2^- \end{bmatrix} \tag{3.90}$$

such that the upward propagating intensity $\overline{I}^+$ is given by

$$\overline{I}^+ \equiv \begin{bmatrix} \overline{I}_1^+ \\ \overline{I}_2^+ \end{bmatrix} = \frac{1}{2}[\overline{I}_a + \overline{I}_s] \tag{3.91}$$

Using (3.90), Equations (3.81)-(3.84) become

$$\overline{\overline{\mu}} \cdot \frac{d}{dz}\overline{I}_a = \overline{\overline{W}} \cdot \overline{I}_s \tag{3.92}$$

$$\overline{\overline{\mu}} \cdot \frac{d}{dz}\overline{I}_s = \overline{\overline{A}} \cdot \overline{I}_a \tag{3.93}$$

where $\overline{\overline{W}}$ and $\overline{\overline{A}}$ are the $4n \times 4n$ matrices

$$\overline{\overline{W}} = -\begin{bmatrix} \overline{\overline{\kappa}}_{e1} & 0 \\ 0 & \overline{\overline{\kappa}}_{e2} \end{bmatrix} + \begin{bmatrix} (\overline{\overline{F}}_{11} - \overline{\overline{B}}_{11}) & (\overline{\overline{F}}_{12} + \overline{\overline{B}}_{12}) \\ (\overline{\overline{F}}_{21} - \overline{\overline{B}}_{21}) & (\overline{\overline{F}}_{22} + \overline{\overline{B}}_{22}) \end{bmatrix} \cdot \overline{\overline{a}} \tag{3.94}$$

$$\overline{\overline{A}} = -\begin{bmatrix} \overline{\overline{\kappa}}_{e1} & 0 \\ 0 & \overline{\overline{\kappa}}_{e2} \end{bmatrix} + \begin{bmatrix} (\overline{\overline{F}}_{11} + \overline{\overline{B}}_{11}) & (\overline{\overline{F}}_{12} - \overline{\overline{B}}_{12}) \\ (\overline{\overline{F}}_{21} + \overline{\overline{B}}_{21}) & (\overline{\overline{F}}_{22} - \overline{\overline{B}}_{22}) \end{bmatrix} \cdot \overline{\overline{a}} \tag{3.95}$$

The matrices $\overline{\overline{F}}_{\alpha\beta}$ and $\overline{\overline{B}}_{\alpha\beta}$, $\alpha, \beta = 1, 2$, are given in (3.86) and (3.87), and $\overline{\overline{\mu}}$ and $\overline{\overline{a}}$ are $4n \times 4n$ diagonal matrices

$$\overline{\overline{\mu}} = \mathrm{diag}\,[\mu_1, \cdots, \mu_n, \mu_1, \cdots, \mu_n, \mu_1, \cdots, \mu_n, \mu_1, \cdots, \mu_n] \tag{3.96}$$

$$\overline{\overline{a}} = \mathrm{diag}\,[a_1, \cdots, a_n, a_1, \cdots, a_n, a_1, \cdots, a_n, a_1, \cdots, a_n] \tag{3.97}$$

3.4.4 Eigenanalysis Solution

The homogeneous solutions for Equations (3.92) and (3.93) have the following form:

$$\overline{I}_a = \overline{I}_{ao} e^{\alpha z} \tag{3.98}$$

$$\overline{I}_s = \overline{I}_{so} e^{\alpha z} \tag{3.99}$$

and $\overline{I}_{ao}$ and $\overline{I}_{so}$ satisfy the following eigenvalue equations

$$\left(\overline{\overline{\mu}}^{-1} \cdot \overline{\overline{W}} \cdot \overline{\overline{\mu}}^{-1} \cdot \overline{\overline{A}} - \alpha^2 \overline{\overline{I}}\right) \cdot \overline{I}_{ao} = 0 \tag{3.100}$$

$$\overline{I}_{so} = \alpha^{-1} \cdot \overline{\overline{\mu}}^{-1} \cdot \overline{\overline{A}} \cdot \overline{I}_{ao} \tag{3.101}$$

where $\overline{\overline{I}}$ is an identity matrix. The above system of equations has $4n$ eigenvalues corresponding to $\pm\alpha_i$. The eigenvectors $\overline{I}_{ai}$ associated to the eigenvalue α_i can be regrouped in the matrix $\overline{\overline{E}}$ which is a $4n \times 4n$ matrix. Therefore, the solution can be written as

$$\overline{I}_a = \overline{\overline{E}} \cdot \overline{\overline{D}}(z) \cdot \frac{\overline{x}}{2} + \overline{\overline{E}} \cdot \overline{\overline{U}}(z+d) \cdot \frac{\overline{y}}{2} \tag{3.102}$$

$$\overline{I}_s = \overline{\overline{Q}} \cdot \overline{\overline{D}}(z) \cdot \frac{\overline{x}}{2} - \overline{\overline{Q}} \cdot \overline{\overline{U}}(z+d) \cdot \frac{\overline{y}}{2} \tag{3.103}$$

where Equation (3.101) has been used to obtain $\overline{I}_s$, and

$$\overline{\overline{Q}} = \overline{\overline{\mu}}^{-1} \cdot \overline{\overline{A}} \cdot \overline{\overline{E}} \cdot \overline{\overline{\alpha}}^{-1} \tag{3.104}$$

$$\overline{\overline{D}}(z) = \mathrm{diag}\left[e^{\alpha_1 z}, \cdots, e^{\alpha_{4n} z}\right] \tag{3.105}$$

$$\overline{\overline{U}}(z) = \mathrm{diag}\left[e^{-\alpha_1 z}, \cdots, e^{-\alpha_{4n} z}\right] \tag{3.106}$$

$$\overline{\overline{\alpha}} = \mathrm{diag}\left[\alpha_1, \cdots, \alpha_{4n}\right] \tag{3.107}$$

where $\overline{x}$ and $\overline{y}$ are $4n \times 1$ unknown vectors which will be solved by matching the boundary conditions. Using Equation (3.90) the solution for the upward and downward propagating Stokes vectors can be recovered

$$\overline{I}^{+}(z) = (\overline{\overline{E}} + \overline{\overline{Q}}) \cdot \overline{\overline{D}}(z) \cdot \overline{x} + (\overline{\overline{E}} - \overline{\overline{Q}}) \cdot \overline{\overline{U}}(z+d) \cdot \overline{y} \tag{3.108}$$

$$\overline{I}^{-}(z) = (\overline{\overline{E}}' + \overline{\overline{Q}}') \cdot \overline{\overline{D}}(z) \cdot \overline{x} + (\overline{\overline{E}}' - \overline{\overline{Q}}') \cdot \overline{\overline{U}}(z+d) \cdot \overline{y} \tag{3.109}$$

where

$$\overline{\overline{E}}' = \overline{\overline{\mu}}^{-1} \cdot \overline{\overline{W}}' \cdot \overline{\overline{Q}} \cdot \overline{\overline{\alpha}}^{-1} \tag{3.110}$$

$$\overline{\overline{Q}}' = \overline{\overline{\mu}}^{-1} \cdot \overline{\overline{A}}' \cdot \overline{\overline{E}} \cdot \overline{\overline{\alpha}}^{-1} \tag{3.111}$$

and

$$\overline{\overline{W}}' = -\begin{bmatrix} \overline{\overline{\kappa}}_{e1} & 0 \\ 0 & -\overline{\overline{\kappa}}_{e2} \end{bmatrix} + \begin{bmatrix} (\overline{\overline{F}}_{11} - \overline{\overline{B}}_{11}) & (\overline{\overline{F}}_{12} + \overline{\overline{B}}_{12}) \\ -(\overline{\overline{F}}_{21} - \overline{\overline{B}}_{21}) & -(\overline{\overline{F}}_{22} + \overline{\overline{B}}_{22}) \end{bmatrix} \cdot \overline{\overline{a}} \tag{3.112}$$

$$\overline{\overline{A}}' = -\begin{bmatrix} -\overline{\overline{\kappa}}_{e1} & 0 \\ 0 & \overline{\overline{\kappa}}_{e2} \end{bmatrix} + \begin{bmatrix} -(\overline{\overline{F}}_{11} + \overline{\overline{B}}_{11}) & -(\overline{\overline{F}}_{12} - \overline{\overline{B}}_{12}) \\ (\overline{\overline{F}}_{21} + \overline{\overline{B}}_{21}) & (\overline{\overline{F}}_{22} - \overline{\overline{B}}_{22}) \end{bmatrix} \cdot \overline{\overline{a}} \tag{3.113}$$

Finally, using the boundary conditions (3.54) and (3.55) which can be put in the following form

$$\overline{I}^{+}(z=-d) = \overline{\overline{R}}_{12} \cdot \overline{I}^{-}(z=-d) \tag{3.114}$$

$$\overline{I}^{-}(z=0) = \overline{\overline{R}}_{10} \cdot \overline{I}^{+}(z=0) + \overline{\overline{T}}_{01} \cdot \overline{I}_{0i}^{-} \tag{3.115}$$

where

$$\left[\overline{I}_{0i}^{-}\right]_j = \left[\overline{I}_{0i}\right]_j \frac{\delta_{jk}\epsilon_0 \cos\theta_{0k}}{a_j \epsilon_1' \cos\theta_k} \tag{3.116}$$

which takes into account the discretization of the delta function [50], and ϵ_1' is the real part of ϵ_1, θ_k and θ_{0k} are related by the Snell's law. Combining (3.108),(3.109) and (3.114),(3.115) leads to the following system of $8n \times 8n$ equations

$$\begin{bmatrix} (\overline{\overline{E}}' + \overline{\overline{Q}}') - \overline{\overline{R}}_{10} \cdot (\overline{\overline{E}} + \overline{\overline{Q}}) & \left\{ (\overline{\overline{E}}' - \overline{\overline{Q}}') - \overline{\overline{R}}_{10} \cdot (\overline{\overline{E}} - \overline{\overline{Q}}) \right\} \overline{\overline{D}}(-d) \\ \left\{ (\overline{\overline{E}} + \overline{\overline{Q}}) - \overline{\overline{R}}_{12} \cdot (\overline{\overline{E}}' + \overline{\overline{Q}}') \right\} \overline{\overline{D}}(-d) & (\overline{\overline{E}} - \overline{\overline{Q}}) - \overline{\overline{R}}_{12} \cdot (\overline{\overline{E}}' - \overline{\overline{Q}}') \end{bmatrix}$$

$$\cdot \begin{bmatrix} \overline{x} \\ \overline{y} \end{bmatrix} = \begin{bmatrix} \overline{\overline{T}}_{01} \cdot \overline{I}_{0i}^{-} \\ 0 \end{bmatrix} \tag{3.117}$$

Once the solution to this set of equations is obtained, $\overline{x}$ and $\overline{y}$ can be inserted into the boundary condition (3.56) to obtain the scattered Stokes vector in region 0,

$$\overline{I}_{0s} = \overline{\overline{T}}_{10} \cdot \overline{I}^{+}(z=0) + \overline{\overline{R}}_{01} \cdot \overline{I}_{0i}^{-} \tag{3.118}$$

where $\overline{I}^{+}(z=0)$ is obtained using (3.108). The total solution can be obtained by reconstructing the Fourier series for the odd and even modes. The backscattering coefficient $\sigma_{\alpha\beta}$ can be determined from the scattered Stokes vector $\overline{I}_{os}$

$$\sigma_{\alpha\beta} = \lim_{\substack{r\to\infty \\ A\to\infty}} \frac{4\pi r^2}{A} \frac{\langle\, E_{\alpha s} E_{\alpha s}^{*} \,\rangle}{E_{\beta i} E_{\beta i}^{*}} \tag{3.119}$$

where $\alpha, \beta = v$ or h and A is the illumination area.

Chapter 4

First Order Analytical Approximation

In this chapter, we shall derive the First Order Analytical Approximation solution for the scattering from multiple spheres. The First Order Analytical Approximation solution is obtained by taking the configurational average over the first order scattering solution of the multiple scattering equations derived in chapter 2. In this method, the statistics of the positions of particles will be applied. Since we use the probability density function of the particle positions, there is no need to calculate the average over many realizations as in the Monte Carlo technique,which makes this approach much more computationally efficient than the T-matrix–Monte Carlo simulation approach.

It will be shown later that this simple solution gives a reasonable approximation in cases when the fractional volume is small. The simple analytical solution gives a good approximation and has advantages in terms of the computational time and the complexity of the governing equation for the calculation of scattering. Also the First Order Analytical Approximation approach includes the effects of coherent wave interactions. However, the multiple scattering is neglected in this approach, which is the trade-off for its simplicity. In the derivation, we assume all the particles to have independent position, which means the pair distribution function is equal to one. This assumption is not valid when the medium is dense. Thus this analytical approximation is valid in the limit of small fractional volume only. The better approximations of the pair distribution can be found in [30].

4.1 Scattering from a Single Particle

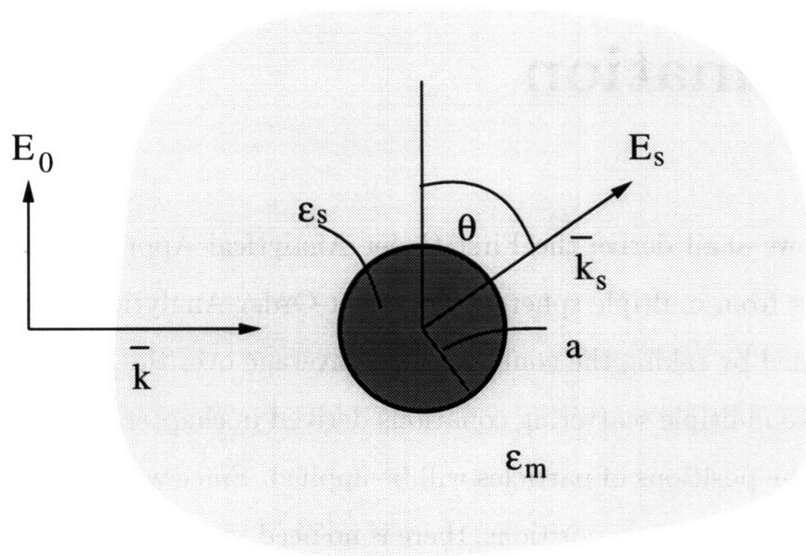

Figure 4-1: Incident plane wave E_0 on a small particle gives rise to scattering wave E_s.

We assume that all the particles have sizes which are small enough to be in the Rayleigh scattering regime. The scattered electric field E_s resulted from the incident field E_0 (Figure 4-1) for a small particle of radius a centered at origin is given by [13]:

$$E_s = -\left(\frac{\epsilon_s - \epsilon_m}{\epsilon_s + 2\epsilon_m}\right) k^2 a^3 \frac{e^{ikr}}{r} E_0 \sin\theta \tag{4.1}$$

where ϵ_s is the permittivity of the particle, ϵ_m is the permittivity of the background medium and $k = \omega\sqrt{\mu_0 \epsilon_m}$. If the scatterer is located at $\bar{r}'$, and applying the far field approximation on the term $|\bar{r} - \bar{r}'|$, the scattered field then becomes

$$E_s = -\left(\frac{\epsilon_s - \epsilon_m}{\epsilon_s + 2\epsilon_m}\right) k^2 a^3 \frac{e^{ikr}}{r} e^{-i\bar{k}_s \cdot \bar{r}'} E_0 e^{i\bar{k}\cdot\bar{r}'} \sin\theta \tag{4.2}$$

where $\bar{k}$ is the k vector of the incident wave and the $\bar{k}_s$ is the k vector of the scattered wave. If we are interested in the backscattering direction only, then

$$-\bar{k}_s = \bar{k}_i, \quad \sin\theta = 1$$

and the backscattered field is

$$E_s = -\left(\frac{\epsilon_s - \epsilon_m}{\epsilon_s + 2\epsilon_m}\right) k^2 a^3 e^{2i\bar{k}_i \cdot \bar{r}'} E_0 \frac{e^{ikr}}{r} \tag{4.3}$$

4.2 Scattering from Multiple Particles

Equation (4.3) is the scattered field in the backscattering direction from a single small particle centered at $\bar{r}'$ based on Rayleigh's formulation. In this section, we consider the scattering from multiple particles as shown in Figure 4-2. It is assumed that all the particles have the same size a and permittivity ϵ_s. The background medium is homogeneous with permittivity ϵ_m. In this section, the background medium is assumed to be lossless.

The backscattered field from a particle i centered at $\bar{r}_i$ is given by:

$$E_{si} = -\left(\frac{\epsilon_s - \epsilon_m}{\epsilon_s + 2\epsilon_m}\right) k^2 a^3 e^{2i\bar{k}\cdot\bar{r}_i} E_0 \frac{e^{ikr}}{r} \tag{4.4}$$

The total backscattered field from all particles is just the sum of scattered field from each particle

$$E_s = -\left(\frac{\epsilon_s - \epsilon_m}{\epsilon_s + 2\epsilon_m}\right) k^2 a^3 E_0 \frac{e^{ikr}}{r} \sum_{i=1}^{N} e^{2i\bar{k}\cdot\bar{r}_i} \tag{4.5}$$

where N is the total number of particles in the interested region. We note that Equation (4.5) is the first order solution of the multiple scattering equation derived

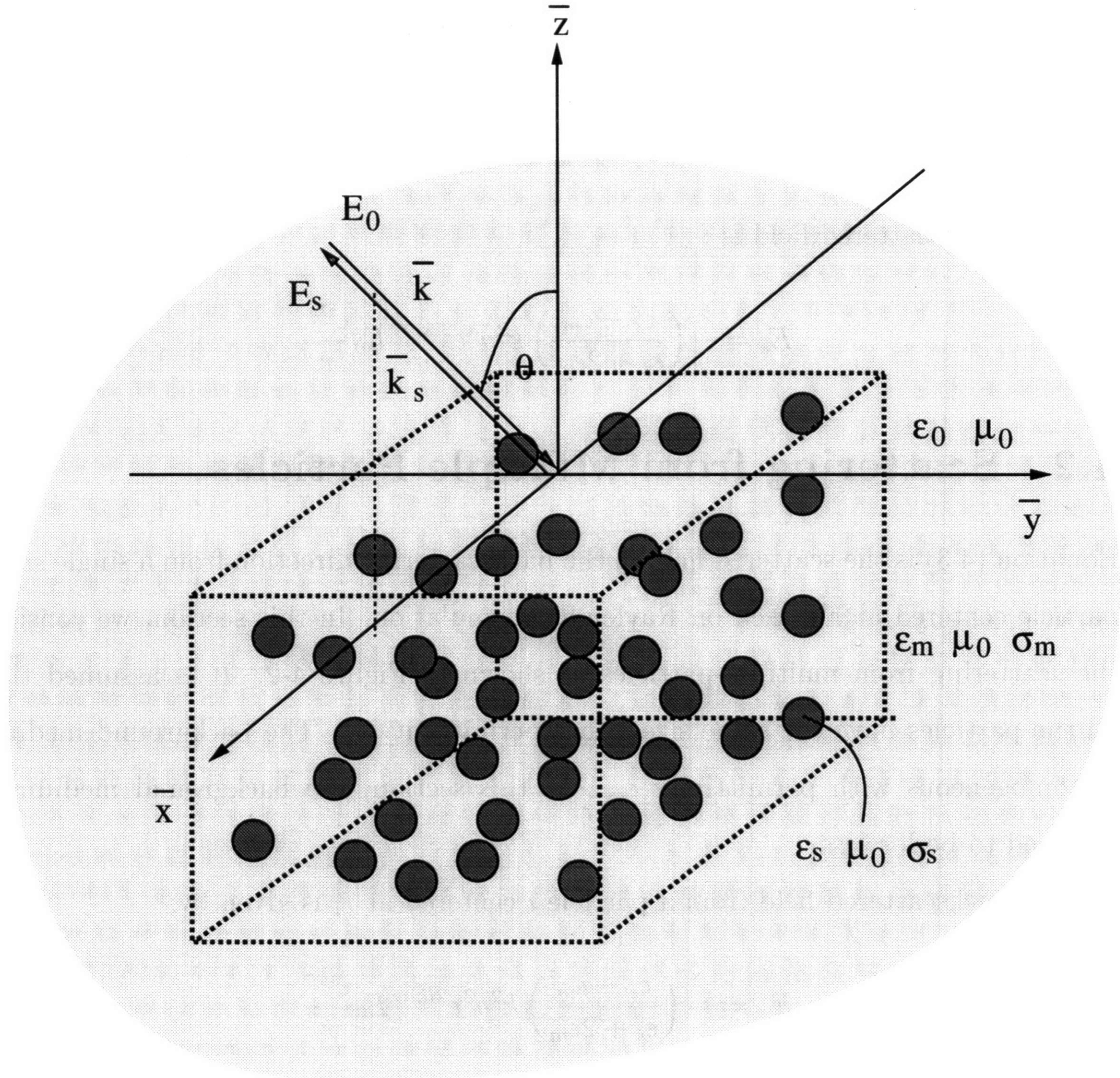

Figure 4-2: Configuration for First Order Analytical Approximation: Multiple particles confined in a rectangular box in an unbounded homogeneous medium

in Chapter 2, which means we ignore the higher order multiple scattering effects and consider only the contribution from the incident wave impinged on that particle.

From (4.5), we can see that the random position of $\bar{r}_i$ gives random phase fluctuation. Taking the configurational average of (4.5) gives

$$\langle\, E_s \,\rangle = -\left(\frac{\epsilon_s - \epsilon_m}{\epsilon_s + 2\epsilon_m}\right) k^2 a^3 E_0 \frac{e^{ikr}}{r} N \int_V d\bar{r}_i \, p(\bar{r}_i) e^{2i\bar{k}_i \cdot \bar{r}_i} \tag{4.6}$$

where V is the volume containg the particles. The angular bracket $\langle\ \rangle$ denotes the configurational average.

We also assume the single particle probability density $p(\bar{r}_i)$ to be

$$p(\bar{r}_i) = \frac{1}{V} \tag{4.7}$$

For a rectangular volume $V = L \times L \times D$, the Equation (4.6) becomes

$$\langle\, E_s \,\rangle = -\left(\frac{\epsilon_s - \epsilon_m}{\epsilon_s + 2\epsilon_m}\right) k^2 a^3 E_0 \frac{e^{ikr}}{r} \frac{N}{L^2 D} \int_{-\frac{L}{2}}^{\frac{L}{2}} dx_i \, e^{2ik_x x_i} \int_{-\frac{L}{2}}^{\frac{L}{2}} dy_i \, e^{2ik_y y_i} \int_{-\frac{D}{2}}^{\frac{D}{2}} dz_i \, e^{2ik_z z_i} \tag{4.8}$$

Performing the integration, we obtain the equation for the average total scattered field

$$\langle\, E_s \,\rangle = -\left(\frac{\epsilon_s - \epsilon_m}{\epsilon_s + 2\epsilon_m}\right) k^2 a^3 E_0 \frac{e^{ikr}}{r} N \left\{ \mathrm{sinc}(k_x L) \mathrm{sinc}(k_y L) \mathrm{sinc}(k_z L) \right\} \tag{4.9}$$

where $\mathrm{sinc}(x) = \sin(x)/x$ is the sinc function.

The incoherent scattered field $\mathcal{E}_s$ is defined as

$$\mathcal{E}_s = E_s - \langle\, E_s \,\rangle \tag{4.10}$$

The average of the incoherent scattered fields is zero, $\langle\, \mathcal{E}_s \,\rangle = 0$. However, the configurational average of the incoherent intensity is not zero

$$\langle\, \mathcal{E}_s \mathcal{E}_s^* \,\rangle = \langle\, E_s E_s^* \,\rangle - |\langle\, E_s \,\rangle|^2 \tag{4.11}$$

The intensity for the backscattered field (4.5) is

$$|E_s|^2 = \left| \left(\frac{\epsilon_s - \epsilon_m}{\epsilon_s + 2\epsilon_m} \right) k^2 a^3 \frac{E_0}{r} \right|^2 \sum_{i=1}^{N} e^{2i\bar{k}\cdot\bar{r}_i} \sum_{j=1}^{N} e^{-2i\bar{k}\cdot\bar{r}_j} \tag{4.12}$$

The double summations are separated into two terms, for $i = j$ and $i \neq j$. Thus,

$$\sum_{i=1}^{N} e^{2i\bar{k}\cdot\bar{r}_i} \sum_{j=1}^{N} e^{-2i\bar{k}\cdot\bar{r}_j} = N + \sum_{i=1}^{N} \sum_{\substack{j=1 \\ i\neq j}}^{N} e^{2i\bar{k}\cdot(\bar{r}_i - \bar{r}_j)} \tag{4.13}$$

The configurational average of (4.12) is performed with the double summation in (4.13) replaced by an average over the two-particle joint probability density function $p(\bar{r}_i, \bar{r}_j)$

$$\langle\ |E_s|^2 \rangle = \left| \left(\frac{\epsilon_s - \epsilon_m}{\epsilon_s + 2\epsilon_m} \right) k^2 a^3 \frac{E_0}{r} \right|^2 \left\{ N + N(N-1) \int_V d\bar{r}_i \int_V d\bar{r}_j p(\bar{r}_i, \bar{r}_j) e^{2i\bar{k}\cdot(\bar{r}_i - \bar{r}_j)} \right\} \tag{4.14}$$

On the assumption of independent particle positions,

$$p(\bar{r}_i, \bar{r}_j) = p(\bar{r}_i)p(\bar{r}_j) = \frac{1}{V^2} = \frac{1}{L^4 D^2} \tag{4.15}$$

and using (4.15) in (4.14), we have

$$\langle\ E_s E_s^*\ \rangle = \left| \left(\frac{\epsilon_s - \epsilon_m}{\epsilon_s + 2\epsilon_m} \right) k^2 a^3 \frac{E_0}{r} \right|^2 \left\{ N + N(N-1)\text{sinc}^2(k_x L)\text{sinc}^2(k_y L)\text{sinc}^2(k_z D) \right\} \tag{4.16}$$

Note that the first term in the curly bracket of Equation (4.16) is the conventional independent scattering result and the other term represents the correlated scattering effects. From Equations (4.9) and (4.16), we can calculate the incoherent intensity.

From Equation (4.9), we have

$$|\langle\ E_s\ \rangle|^2 = \left| \left(\frac{\epsilon_s - \epsilon_m}{\epsilon_s + 2\epsilon_m} \right) k^2 a^3 \frac{E_0}{r} \right|^2 \left[N \left\{ \text{sinc}(k_x L)\text{sinc}(k_y L)\text{sinc}(k_z D) \right\} \right]^2 \tag{4.17}$$

Substituting (4.16) and (4.17) into (4.11), the incoherent backscattered intensity is obtained as

$$\langle \mathcal{E}_s \mathcal{E}_s^* \rangle = \left| \left(\frac{\epsilon_s - \epsilon_m}{\epsilon_s + 2\epsilon_m} \right) k^2 a^3 \frac{E_0}{r} \right|^2 N \left\{ 1 - \mathrm{sinc}^2(k_x L) \mathrm{sinc}^2(k_y L) \mathrm{sinc}^2(k_z D) \right\} \quad (4.18)$$

We also note that the second term in (4.18) vanishes for large V which is identical to the result of independent scattering.

4.3 Scattering from a Layer of Particles

For the case of layered medium, we have to take into account the transmitivity of the incident wave as well as the scattered wave. We shall begin the derivation by quoting Equation (4.4) from the previous section.

$$E_{si} = -\left(\frac{\epsilon_s - \epsilon_m}{\epsilon_s + 2\epsilon_m} \right) k^2 a^3 e^{2i\bar{k}\cdot\bar{r}_i} E_0 \frac{e^{ikr}}{r} \quad (4.19)$$

In the case of particles buried in a layered medium (Figure 4-2), the exciting field for a single particle is replaced by $T_{01}\ E_0$, where T_{01} is the transmission coefficient from region 0 to region 1. The transmisstion coefficients for TM and TE modes are given as

$$T_{01}^{TE} = \frac{2k_{0z}}{k_{0z} + k_z} \quad (4.20)$$

$$T_{01}^{TM} = \sqrt{\frac{\epsilon_m}{\epsilon_0}} \left(\frac{2\epsilon_0 k_{0z}}{\epsilon_m k_{0z} + \epsilon_0 k_z} \right) \quad (4.21)$$

where $k_0 = \omega\sqrt{\mu_0\epsilon_0}$ is the wave number in the region 0, and $k = \omega\sqrt{\mu_0\epsilon_m}$ is the wave number in the region 1. The transmission coefficient from region 1 to region 0 of the radiation from a dipole source is also equal to T_{01} (see Appendix A) Then Equation (4.4) is modified for a buried particle i centered at $\bar{r}_i$ to be

$$E_{si} = -\left(\frac{\epsilon_s - \epsilon_m}{\epsilon_s + 2\epsilon_m} \right) T_{01}^2 k^2 a^3 e^{2i\bar{k}\cdot\bar{r}_i} E_0 \frac{e^{ik_0 r}}{r} \quad (4.22)$$

where the far field approximation has been used. If the medium and the scatterers are lossy, the permittivities ϵ_m, ϵ_s and the wave number k are complex numbers.

$$\epsilon_m = \epsilon_0(\epsilon_m' + i\frac{\sigma_m}{\omega\epsilon_0}) \tag{4.23}$$

$$\epsilon_s = \epsilon_0(\epsilon_s' + i\frac{\sigma_s}{\omega\epsilon_0}) \tag{4.24}$$

where the ϵ_s', ϵ_m' are the real parts of permittivities of scatterers and the medium, σ_s, σ_m are the conductivities of the scatterers and the medium. However, by the condition of phase matching with the $\bar{k}_0$ in the region 0, only the complex form of the z component of the wave vector $\bar{k}$ in the phase term of equation (4.22) will be retained

$$k_x = \mathrm{Re}\{k\} \sin\theta \cos\phi \tag{4.25}$$

$$k_y = \mathrm{Re}\{k\} \sin\theta \sin\phi \tag{4.26}$$

$$k_z = k\cos\theta = \mathrm{Re}\{k_z\} + i\mathrm{Im}\{k_z\} \tag{4.27}$$

Summation of the scattered fields from all particles is

$$E_s = -\left(\frac{\epsilon_s - \epsilon_m}{\epsilon_s + 2\epsilon_m}\right) T_{01}^2 k^2 a^3 E_0 \frac{e^{ik_0 r}}{r} \sum_{i=1}^{N} e^{2i\bar{k}\cdot\bar{r}_i} \tag{4.28}$$

Taking the configurational average of (4.28), it becomes

$$\langle\ E_s\ \rangle = -\left(\frac{\epsilon_s - \epsilon_m}{\epsilon_s + 2\epsilon_m}\right) T_{01}^2 k^2 a^3 E_0 \frac{e^{ik_0 r}}{r} N \int_V p(\bar{r}_i) d\bar{r}_i e^{2i\bar{k}\cdot\bar{r}_i} \tag{4.29}$$

Using (4.7) and carrying out the integration over a rectangular volume, we obtain the average backscattered field

$$\langle\ E_s\ \rangle = -\left(\frac{\epsilon_s - \epsilon_m}{\epsilon_s + 2\epsilon_m}\right) T_{01}^2 k^2 a^3 E_0 \frac{e^{ik_0 r}}{r} N \mathrm{sinc}(k_x L) \mathrm{sinc}(k_y L) \left(\frac{1 - e^{-2ik_z D}}{2ik_z D}\right) \tag{4.30}$$

From (4.28), the intensity of the backscattered field is

$$|E_s|^2 = \left|\left(\frac{\epsilon_s - \epsilon_m}{\epsilon_s + 2\epsilon_m}\right) T_{01}^2 k^2 a^3 E_0 \frac{e^{ik_0 r}}{r}\right|^2 \sum_{i=1}^{N} e^{2i\bar{k}\cdot\bar{r}_i} \sum_{j=1}^{N} e^{-2i\bar{k}^*\cdot\bar{r}_j} \tag{4.31}$$

Similarly, the multiplication of two summations can be separated into two terms, $i = j$ and $i \neq j$

$$\sum_{i=1}^{N} e^{2i\bar{k}\cdot\bar{r}_i} \sum_{j=1}^{N} e^{-2i\bar{k}^*\cdot\bar{r}_j} = \sum_{i=1}^{N} e^{-4\mathrm{Im}\{k_z\}z_i} + \sum_{i=1}^{N}\sum_{\substack{j=1\\ i\neq j}}^{N} e^{2i(\bar{k}\cdot\bar{r}_i - \bar{k}^*\cdot\bar{r}_j)} \tag{4.32}$$

Taking the configurational average of (4.31), the first term in Equation (4.32) gives

$$\left\langle \sum_{i=j}^{N} e^{-4\mathrm{Im}\{k_z\}r_{zi}} \right\rangle = N\int_{-D}^{0} dz_i \frac{1}{D} e^{-4\mathrm{Im}\{k_z\}z_i} = N\left(\frac{1-e^{4\mathrm{Im}\{k_z\}D}}{-4\mathrm{Im}\{k_z\}D}\right) \tag{4.33}$$

where $\mathrm{Im}k_z$ is negative since the direction of the wave impinging on the particle is downward in the medium. The average of the second term of Equation (4.32) gives

$$\left\langle \sum_{i=1}^{N}\sum_{\substack{j=1\\ i\neq j}}^{N} e^{2i(\bar{k}\cdot\bar{r}_i - \bar{k}^*\cdot\bar{r}_j)} \right\rangle = N(N-1)\iiint_V d\bar{r}_i \iiint_V d\bar{r}_j \frac{1}{V^2} e^{2i(\bar{k}\cdot\bar{r}_i - \bar{k}^*\cdot\bar{r}_j)}$$

$$= \mathrm{sinc}^2(k_xL)\mathrm{sinc}^2(k_yL)\left|\frac{(1-e^{-2ik_zD})}{2ik_zD}\right|^2 \tag{4.34}$$

Therefore, the configurational average of (4.31) becomes

$$\langle\, E_s E_s^* \,\rangle = \left|\left(\frac{\epsilon_s - \epsilon_m}{\epsilon_s + 2\epsilon_m}\right) T_{01}^2 k^2 a^3 \frac{E_0}{r}\right|^2$$

$$\times\left\{N\left(\frac{1-e^{4\mathrm{Im}\{k_z\}D}}{-4\mathrm{Im}\{k_z\}D}\right) + N(N-1)\mathrm{sinc}^2(k_xL)\mathrm{sinc}^2(k_yL)\left|\frac{(1-e^{-2ik_zD})}{2ik_zD}\right|^2\right\} \tag{4.35}$$

The intensity of the average backscattered field from (4.30) is

$$|\langle\, E_s \,\rangle|^2 = \left|\left(\frac{\epsilon_s - \epsilon_m}{\epsilon_s + 2\epsilon_m}\right) T_{01}^2 k^2 a^3 E_0 \frac{e^{ik_0 r}}{r}\right|^2 \left|N\mathrm{sinc}(k_xL)\mathrm{sinc}(k_yL)\left(\frac{1-e^{-2ik_zD}}{2ik_zD}\right)\right|^2 \tag{4.36}$$

Using Equations (4.35) and (4.36) in the relationship (4.11), we obtain the expression for the incoherent backscattered intensity for particles embeded in a layered medium

$$\langle\, \mathcal{E}_s \mathcal{E}_s^* \,\rangle = \left|\left(\frac{\epsilon_s - \epsilon_m}{\epsilon_s + 2\epsilon_m}\right) T_{01}^2 k^2 a^3 \frac{E_0}{r}\right|^2$$

$$\times N \left\{ \left(\frac{1 - e^{4\mathrm{Im}\{k_z\}D}}{-4\mathrm{Im}\{k_z\}D} \right) - \left| \mathrm{sinc}(k_x L)\mathrm{sinc}(k_y L) \left(\frac{1 - e^{-2ik_z D}}{2ik_z D} \right) \right|^2 \right\} \tag{4.37}$$

We note the second term on the right hand side of (4.37) vanishes as the volume of the medium is very large and the backscattered intensity then reduces to

$$\langle\, \mathcal{E}_s \mathcal{E}_s^* \,\rangle = \left| \left(\frac{\epsilon_s - \epsilon_m}{\epsilon_s + 2\epsilon_m} \right) T_{01}^2 k^2 a^3 \frac{E_0}{r} \right|^2 N \left(\frac{1 - e^{4\mathrm{Im}\{k_z\}D}}{-4\mathrm{Im}\{k_z\}D} \right) \tag{4.38}$$

The Equation (4.38) differs from the case of scattering from particles within lossless full–space medium in that (4.38) has the decay term resulted from the lossiness in the background medium and the two-way transmitivity. If the area of illumination and the number density of particles are kept constant, total number of particles N is proportional to the depth D. We can see that when the thickness of the particle layer becomes large, the exponential term drops very fast. This means that particles at the deeper levels contribute less to the backscattered intensity.

The backscattering coefficient is calculated from the incoherent intensity as [30]

$$\sigma = \lim_{r \to \infty} \frac{4\pi r^2}{A} \frac{\langle\, \mathcal{E}_s \mathcal{E}_s^* \,\rangle}{E_0 E_0^*} \tag{4.39}$$

Chapter 5

Results and Discussion

In this chapter, numerical results are carried out using the three approaches described in the previous chapters. Physical parameters used in the calculations are listed in Section 5.1. Backscatter calculations are shown in section 5.2. Finally, the backscatter, simulated using the RT theory versus radar parameters and physical properties of desert medium are given in Section 5.3.

5.1 Parameters Used in Simulation

Parameters	*Range*	*Typical value*	*Unit*
Frequency	0.1 - 1.0	0.5	GHz
Incident Angle	10.0 - 80.0	45.0	degree
Dielectric Constant of Medium	1.5 - 7.0	3.0	ϵ_0
Conductivity of Medium	6.0 - 20.0	10.0	$10^{-3}\mho/m$
Fractional Volume	1.0 - 10.0	5.0	%
Radius of Particles	0.5 - 5.0	2.0	cm
Dielectric Constant of Particles	2.5 - 8.0	6.0	ϵ_0

Table 5.1: Parameters used in calculation

In order to simulate the backscatter of the Yuma desert, the physical characteristics of the desert medium are needed. Unfortunately, the appropriate ground truth are not fully available. Instead, values listed in Table 5.1 are used: these values are not measured from the Yuma site. The dielectric constant of the background medium is based on the SIR-B Subsurface imaging experiment at Al Labbah Plaueau [3], Saudi Arabia conducted in October 1984. A table showing the moisture and electric properties of Al Labbah Plateau sand samples is given in Appendix B. The dielectric constant of rocks is obtained from [32], a laboratory measurement of dielectric properties for various kinds of rocks. A figure showing the ranges of dielectric constants of rocks is also given in Appendix B. The sizes of rocks in some desert terrains can be found in [24].

5.2 Comparison of Three Approaches

All calculations shown in this section are for HH polarization. Results for the VV polarization can be estimated based on the results for the HH polarization and by considering the difference between the two-way transmission coefficient of the TE and TM waves. It can be shown that the VV backscatter is about 1 dB higher than the HH backscatter at the 45° incident angle.

Although each approach can have different model configuration. For the purposed of comparison, the model configuration used in this simulation were chosen to be identical. The T-matrix–Monte Carlo method, although it has a capability of having particles with arbitrarily diverse sizes and permittivities, is implemented for one species of particle only. The backscattering coefficients calculated by T-matrix–Monte Carlo method and the First Order Analytical Approximation method both have the limitation that the medium has to be of finite volume; while in the RT approach, the medium is infinitely extended.

Another important parameter, which could give totally different results if inappropriately chosen, is the depth of the particle layer. Because of propagation loss, the backscatter contribution due to particles lying deep below the surface tends to decrease. The depth of the particle layer need not be too large; may be in the order of a penetration depth.

Figure 5-1 shows the backscattering coefficient calculated using the three different approaches as a function of particle layer thickness. The area of illumination used in

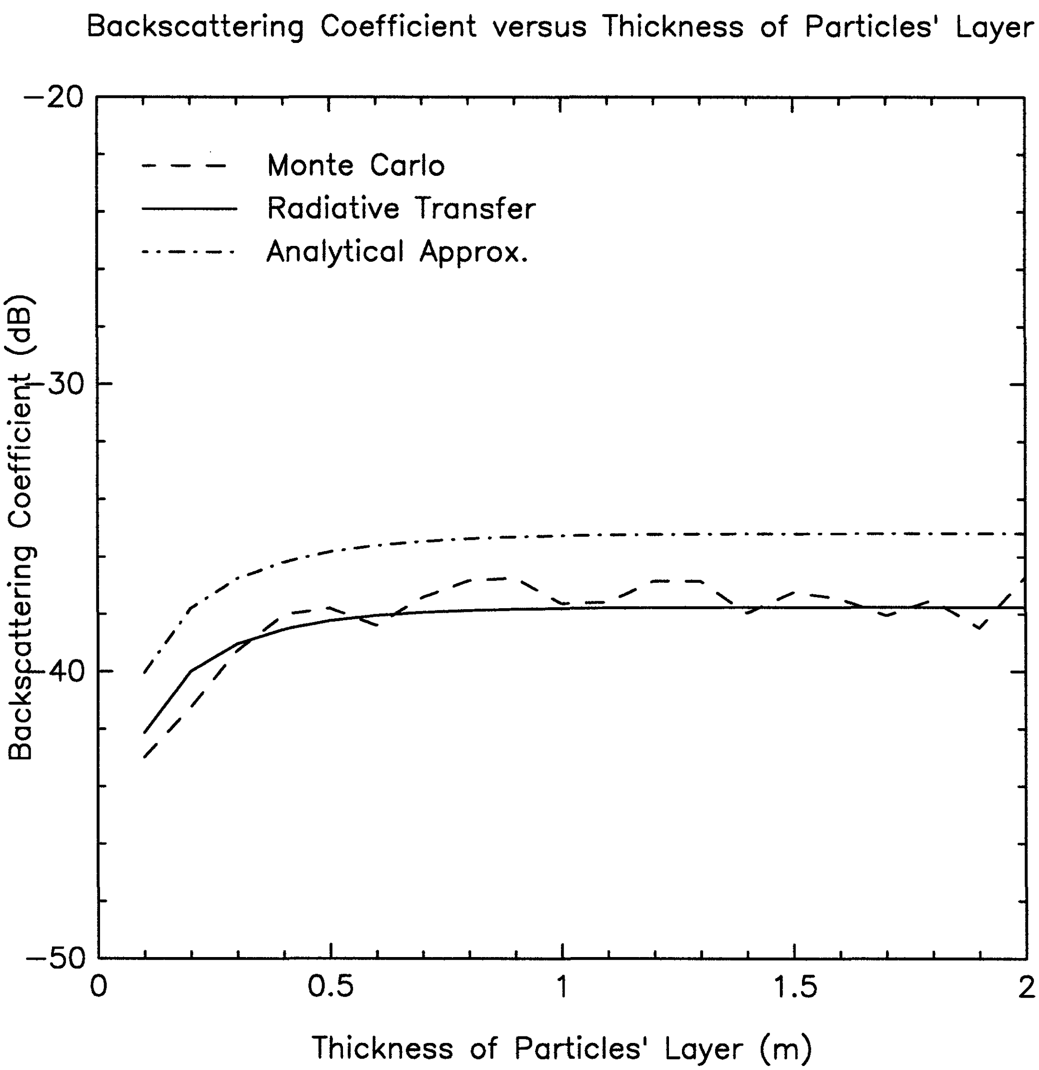

Figure 5-1: Backscattering coefficient versus thickness of particle layer.

the T-matrix–Monte Carlo simulation and the First Order Analytical Approximation is 0.5 square meter. It can be seen that, for the given set of parameters, the backscattering coefficient is almost constant after the thickness of particle layer is larger than 1 meter. This is due to the propagation loss which reduces the scattering contribution due to particles away from the interface.

Figures 5-2 to 5-8 show the simulations using the ranges of parameters shown in Section 5.1. In Figure 5-2, we plot the backscattering coefficient as a function of frequency. The backscattering coefficient increases rapidly as the frequency increases. In Rayleigh scattering, the backscattering coefficient increases as the forth power of the frequency, or approximately 12 dB when the frequency increases by the factor of 2. In the independent scattering model, the backscattering coefficient increases linearly as the fractional volume or the number of particle increase. That is, backscatter increases by 3 dB when the fractional volume doubles.

But from Figure 5-4, this approximation is not valid when the medium is dense. Since, in the case of dense medium, the probability of finding a particle in the medium is not uniform (no 2 particles can overlap the same space). This further suggests that the First Order Analytical solution method, using the independent pair distribution function, is valid for sparse medium only. However, the T-matrix–Monte Carlo simulation and RT theory method have capabilities of dealing with dense medium, as seen in Figure 5-4 that rate of increasing is not linearly dependent to the fractional volume.(Moreover, the backscattering coefficient even tends to decrease when the medium is very dense, around 60 % or higher [23]. This argument is plausible since when the fractional volume goes to 100 %, the whole medium is homogeneous, thus produces no backscatterer.)

Figure 5-3 shows the backscatter as a function of incident angle. The effect of incident angle to backscatter is due mainly to the transmitivity at the air-ground interface. This explains the higher return for the VV polarization than for the HH polarization, since the transmission coefficient of TM wave is always higher than that of TE wave. It is to be noted that due to the limitation of Gaussian quadrature method used in the numerical solution for RT, the RT approach cannot be used at

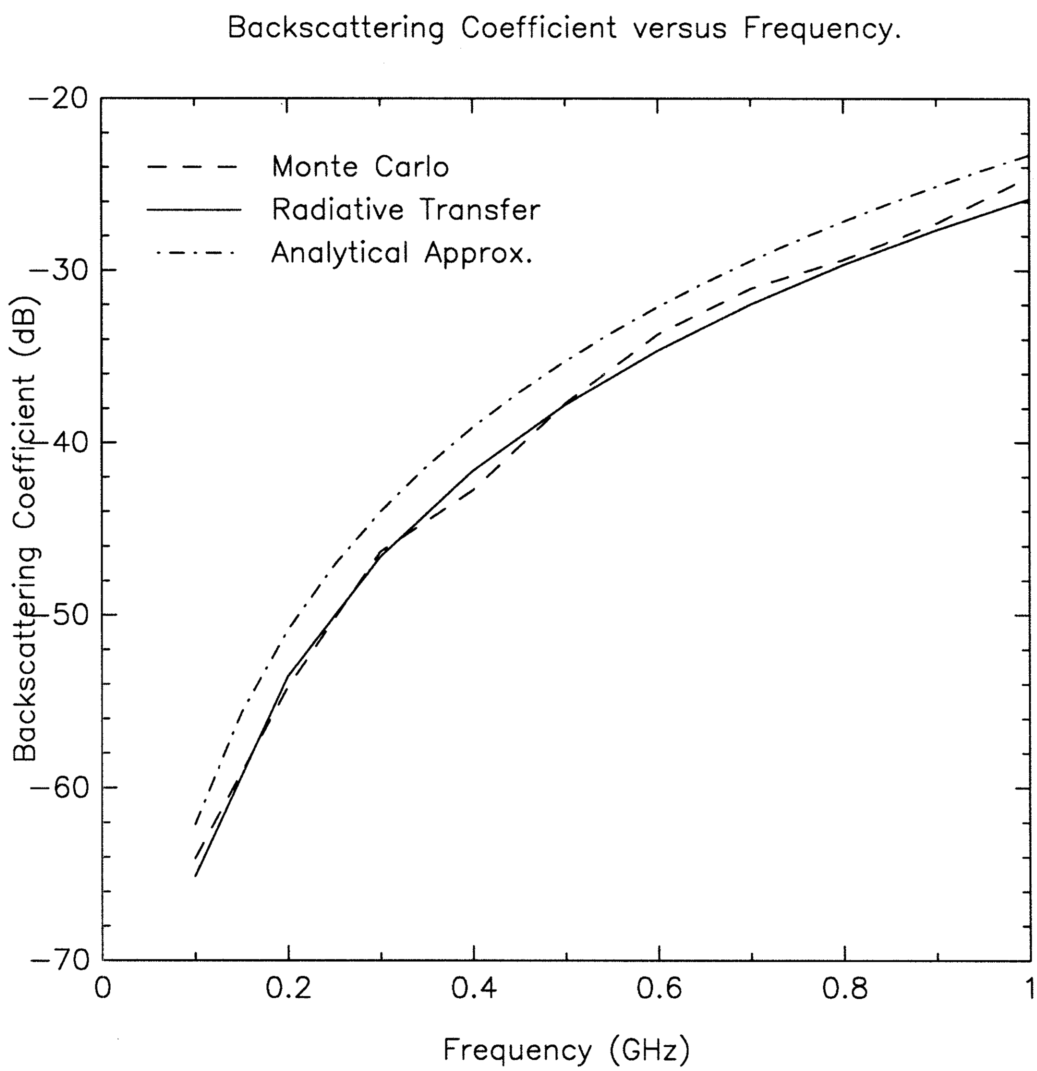

Figure 5-2: Backscattering coefficient versus frequency.

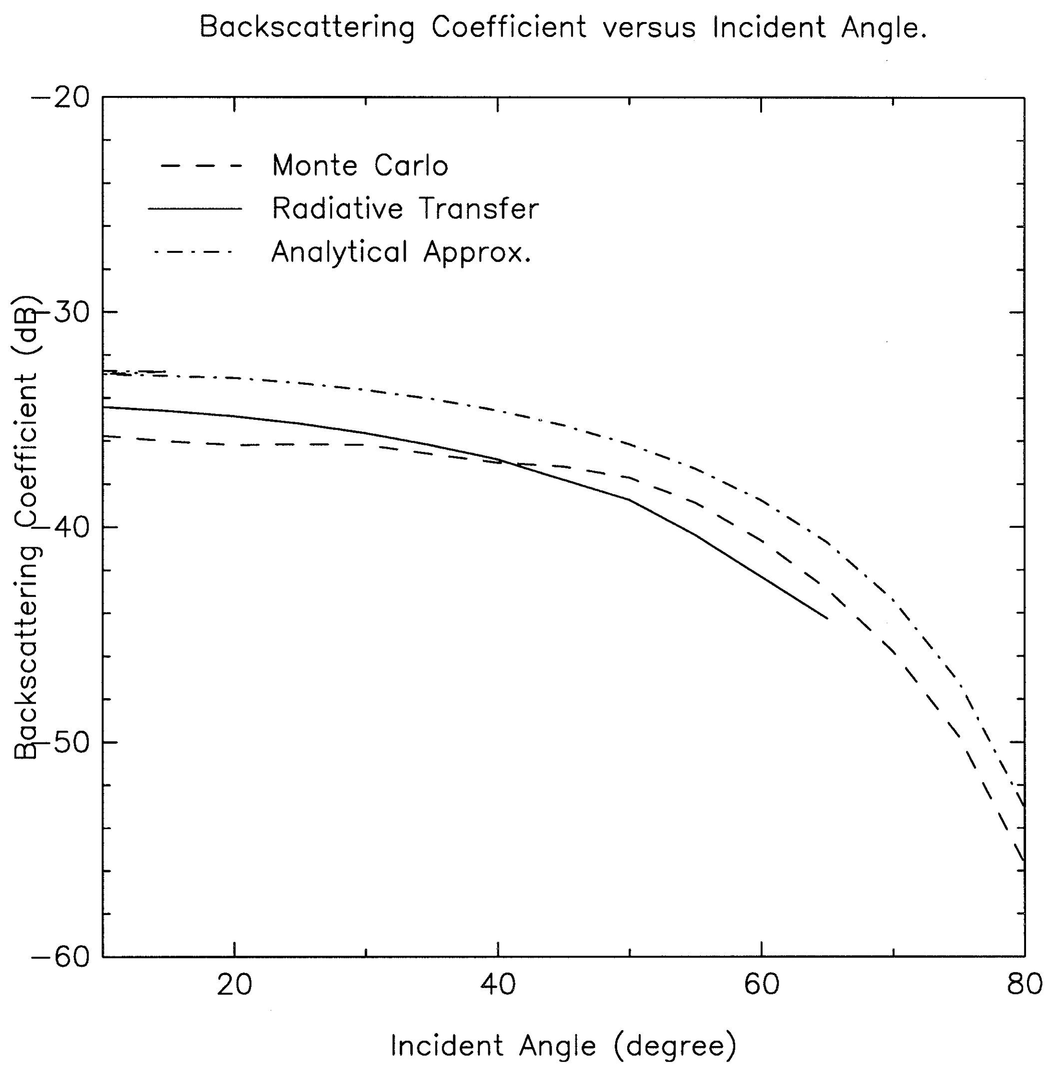

Figure 5-3: Backscattering coefficient versus incident angle.

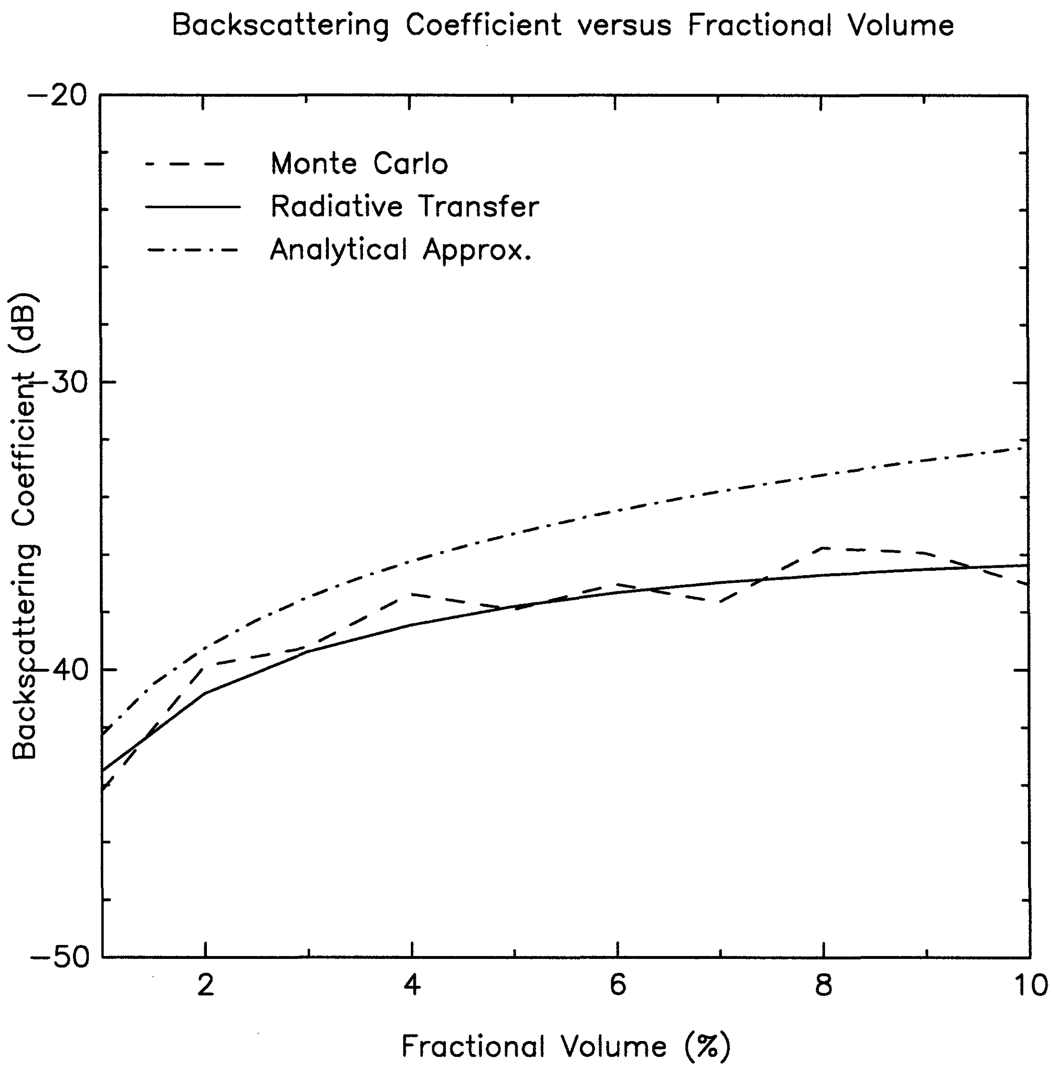

Figure 5-4: Backscattering coefficient versus fractional volume of particles.

very low depression angle region. Using the listed typical parameters, RT can be used up to no more than 70° incident angle only.

Figure 5-5 shows the backscattering coefficient versus radius of particles. Using the single scattering model, the backscattering coefficient increases to the sixth power of the radius. In our calculation, we keep the fractional volume of the particles constant, so the number of particles decreases by inverse proportion to the third power of radius of the particles. Then the backscattering coefficient in Figure 5-5 increases by only the third power of radii of particles, which is 9 dB for every two-time the radius of particles.

In Figures 5-6 and 5-7, the backscattering coefficients versus dielectric constants of the particles and the medium respectively, we can see that when the difference between dielectric constants of particles and medium is higher. the backscattering coefficient increases. And when the dielectric constant of particles and medium are the same value, the medium becomes almost homogeneous, thus producing the lowest return, as expected. The backscatterer at this point would be minus infinity if it were not for the conductivity in the medium which is the only difference between particles and medium at this point.

Figure 5-8 shows the backscattering coefficient versus the conductivity of the medium. As expected, the backscattering coefficient is lower when the conductivity is higher. The effect of conductivity on the backscattering coefficient can be easily approximated by calculating averaged round-trip loss factor of the scattered power from particles.

$$\frac{N}{D}\int_{-D}^{0} e^{4k_{iz}r_z}dr_z = N\frac{1-e^{4k_{iz}D}}{-4k_{iz}D} \tag{5.1}$$

$$k_{iz} \approx -\frac{\sigma}{2c\epsilon_0}\cos\theta_t$$

where θ_t is the incident angle in medium 1. It can be seen that when the exponential term is small, i.e. the thickness of particle layer is larger or the conductivity of the background medium is high, the loss is approximately proportional to $1/\sigma$, which means 3 dB decrease in backscattering coefficient if the conductivity doubles. This expression is also useful to predict the results for the case of different thickness of

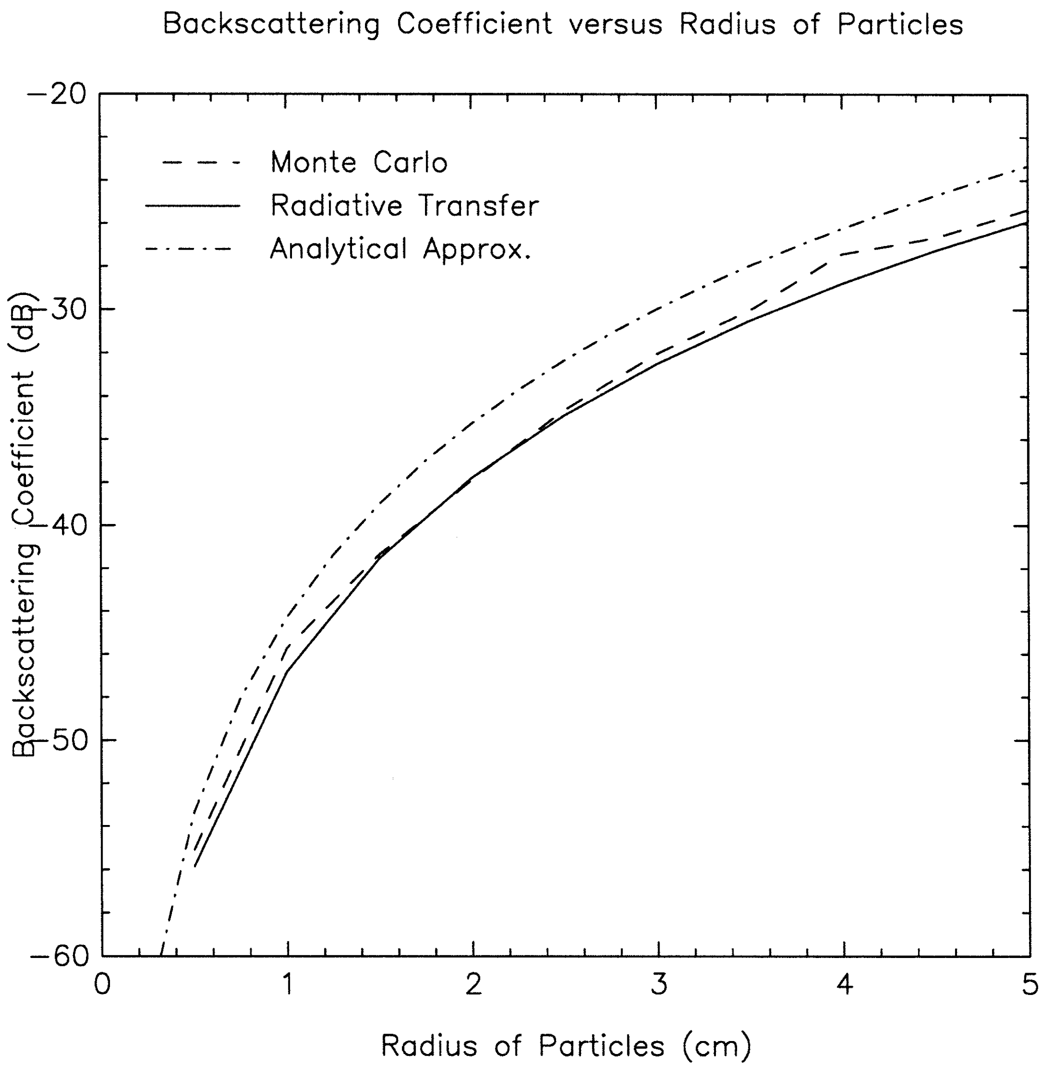

Figure 5-5: Backscattering coefficient versus radius of particles.

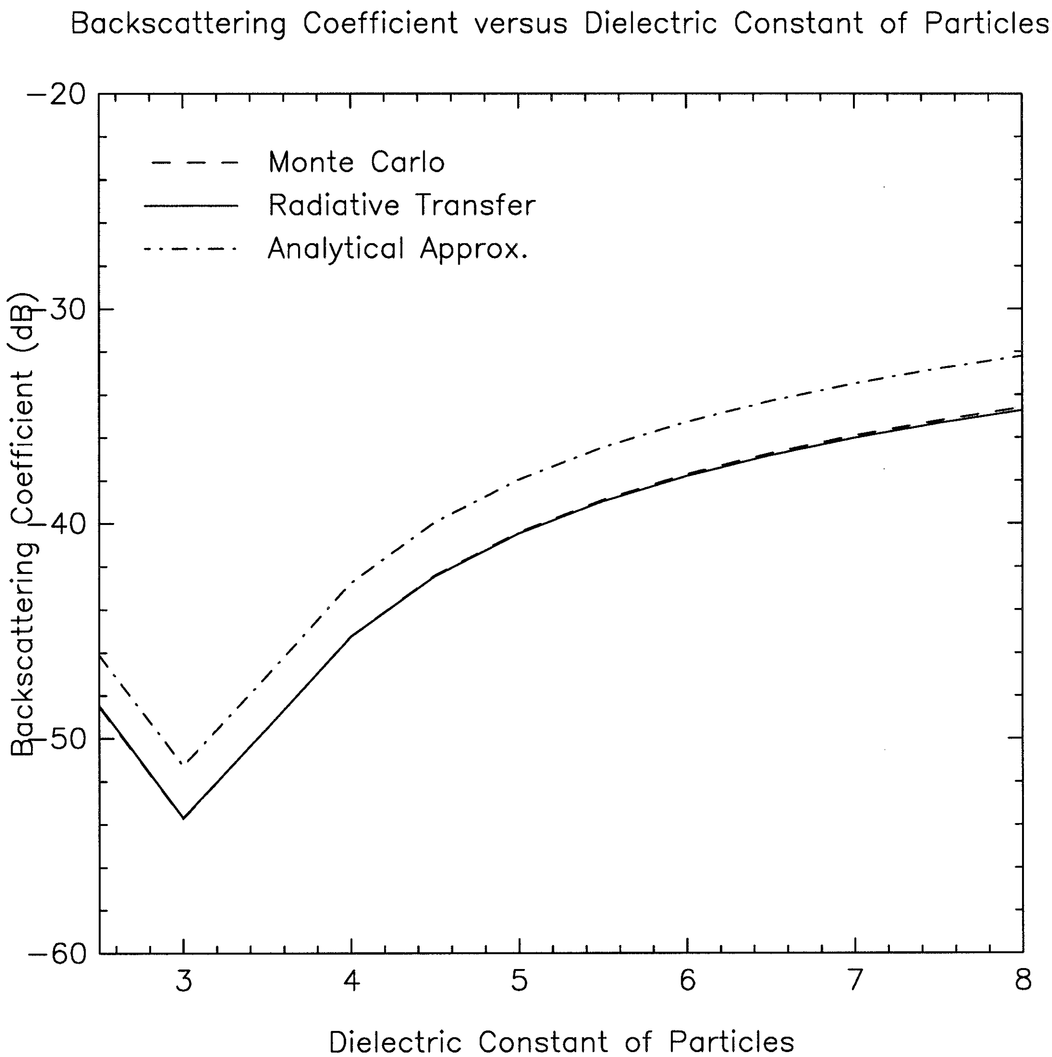

Figure 5-6: Backscattering coefficient versus dielectric constant of particles.

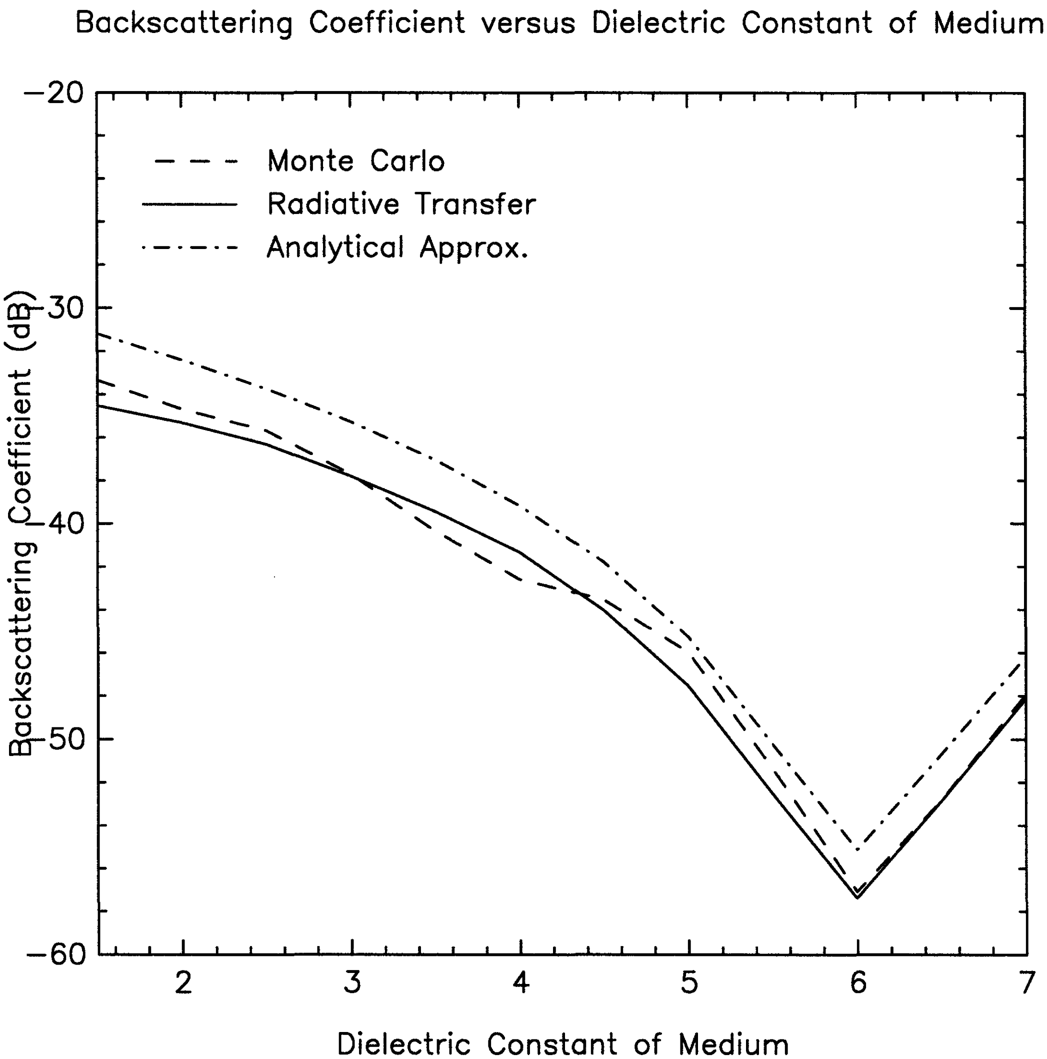

Figure 5-7: Backscattering coefficient versus dielectric constant of the background medium.

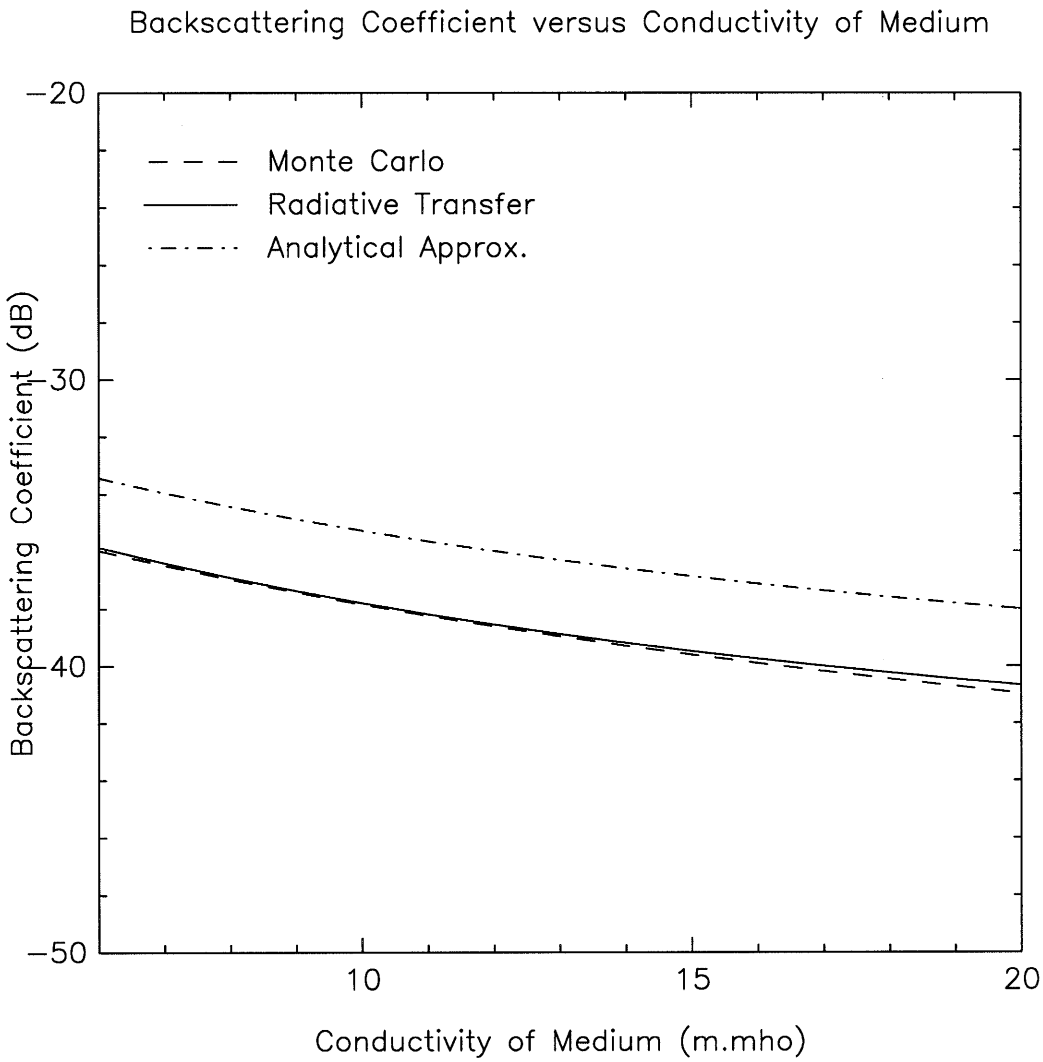

Figure 5-8: Backscattering coefficient versus conductivity of medium.

particles layer. If all properties of medium and scatterers and the area illumination are kept constant, the number of particles N is proportional to D, thus canceling the $1/D$ term. Then the backscatterer depends on the upper term of the right-hand side of (5.1), which is almost constant for large D. This is interpreted as that, for the lossy medium, the particles at the deeper distance in the medium has no effects to backscattering coefficient as seen in Figure 5-1.

From Figures 5-2 to 5-8, we can see that, results calculated using the RT theory and the T-matrix–Monte Carlo simulation agree well. The results calculated using First Order Analytical Approximation also give the same trend as those of the other two approaches, but the level of the curves is always higher. This difference may be accounted for by: 1) multiple scattering, 2) the missing absorption term in the Rayleigh's scattering equation, 3) the independent particle position assumption.

Further investigation by using T-matrix–Monte Carlo simulation to calculate the backscattering coefficient for first order and higher order iterations (Figure 5-9) shows that the effects of multiple scattering, in this set of typical parameters, is smaller. By considering the leading term of the real part of T-matrix given in Equation (2.45), section 2.3, it can be found that the effect of absorption is also very small. One can demonstrate that difference between Analytical solution approach and the other two method is due mainly to 3) by performing the Monte Carlo simulation using uniform pair distribution function without particle overlap checking. The results show that when ignoring the overlap checking in the random particle generator, Monte Carlo simulation agrees very well with the First Order Analytical Approximation. The difference from this effect is stronger when the fractional volume is larger, as it can be seen in Figure 5-4, since the assumption of independent particles' positions becomes invalid in the dense medium, thus produces larger errors. This error becomes smaller at the smaller fractional volume region, which is the valid region of the First Order Analytical Approximation approach.

Comparing results calculated using the three approaches, it can be seen that they agree well. If the computational resources required in performing the calculation of each approach is taken into account, the RT theory appears to be the best method

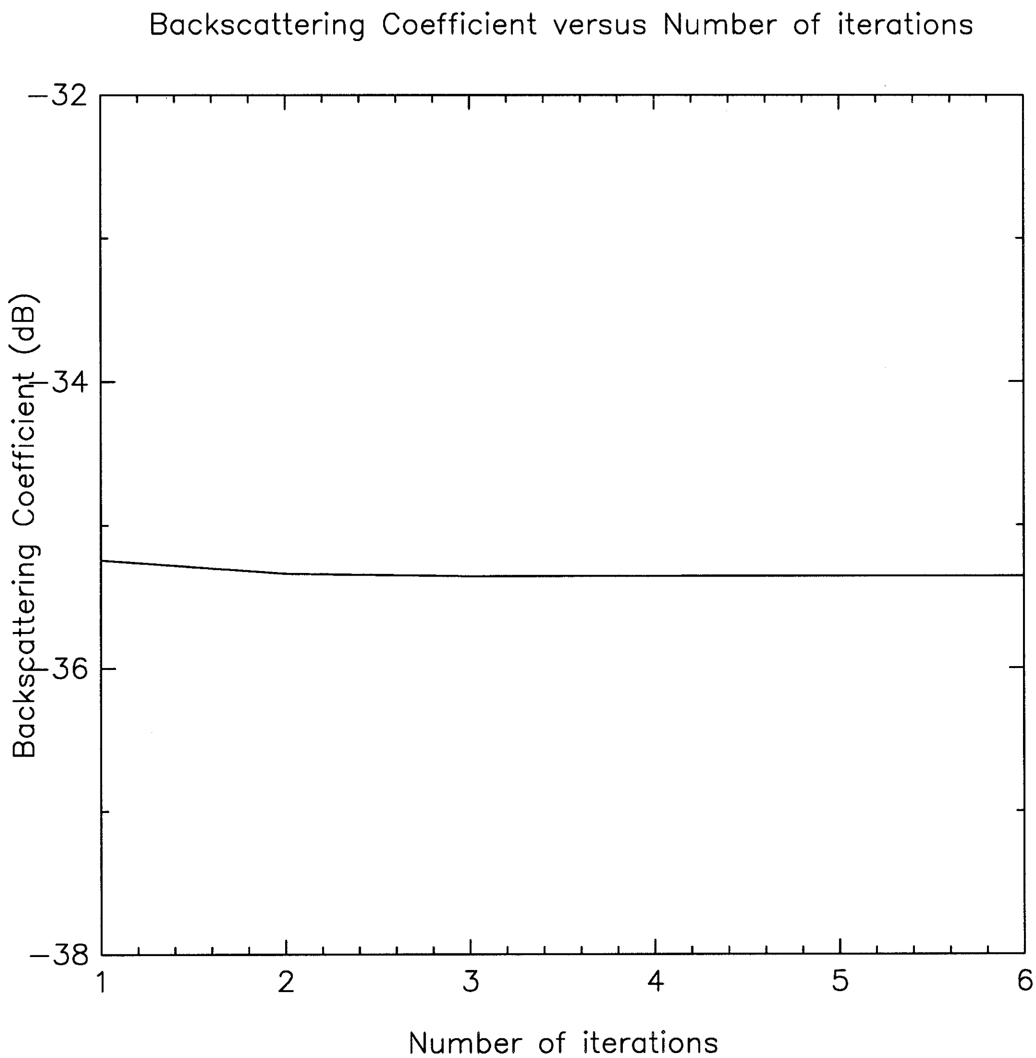

Figure 5-9: Backscattering coefficient versus number of iterations.

among the three.

5.3 Simulation Results With Particle Size Distribution

In this section, we assume that their sizes obey a Rayleigh distribution. [30]

$$n(r) = Kre^{-\frac{r^2}{2a^2}} \tag{5.2}$$

In Equation (5.2) r is the radius of the particle, and $n(r)dr$ gives the number of particles per unit volume having size between r and $r+dr$. The normalizing factor K depends on the total fractional volume f, which is the ratio of the volume occupied by particles to the bulk volume of the medium

$$f = \frac{4\pi}{3}\frac{K}{2}(2a^2)^{-(\frac{5}{2})}\Gamma\left(\frac{5}{2}\right) \tag{5.3}$$

where a is the mode radius at which $n(a)$ is a maximum in the distribution.

For a given size distribution, we can discretize the continuous size distribution into a histogram for N different sizes. Given a set of N discretized sizes r_j with number densities $n_j = 3f/4\pi r_j^3$ and the backscattering coefficient of the medium denoted by σ_j, the total backscattering coefficient of the medium with size distribution denoted by σ_t can be calculated as follow.

$$\sigma_t(a,f) = \sum_j^N \frac{n_j(r_j)}{n_{0j}(r_j)}\sigma_j(r_j) \tag{5.4}$$

where the $\sigma_j(r_j)$ is the backscattered power from the medium with the one discretized size of particle r_j, the $n_{0j}(r_j)$ is the raw number density for the of the particles with the size r_j and the n_j is the corrected number density of particles with the size r_j using the size distribution function (5.2).

Hence, from (5.4), the backscattering coefficient of the medium with size distribution can be calculated from the backscattering coefficients of N discretized sizes of particles. Figures 5-10 to 5-12 are the results calculated using the RT approach with particle size distribution mode radii from 1.0 cm to 3.0 cm.

As seen from Figures 5-10 to 5-12, all curves have the same trends as in the cases with the single size particles. If we compare the results from the previous section that uses the radius of 2 cm with the results in this section that use size distribution with mode radius of 2 cm, we can see that the backscatters from particles with size distribution produce much higher backscatter than that of cases with single size particles. This is due to the contributions from the particles with large radii. Since the backscattered power is proportional to the sixth power of the radius, the particles with large radii , even with small numbers, tend to have the significant contribution to the backscatter. With the given range of parameters, the calculated backscatters range from -20 dB to -40 dB. It is possible, therefore, that the total backscatter observed from the Yuma has a significant volume scattering component due to rocks beneath the desert surface. It may be further concluded that the volume scattering is important in GPR applications.

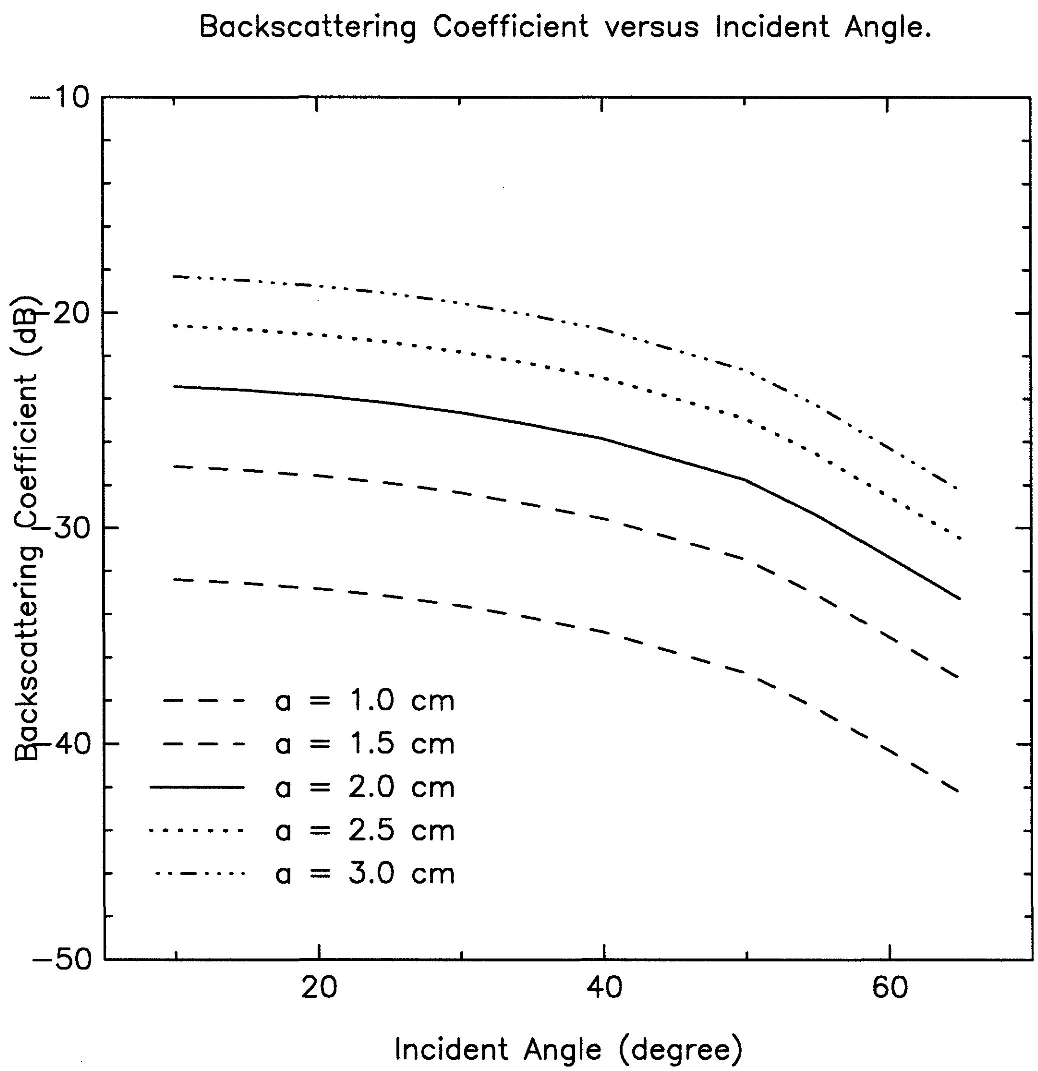

Figure 5-10: Backscattering coefficient of medium with size distribution versus incident angle

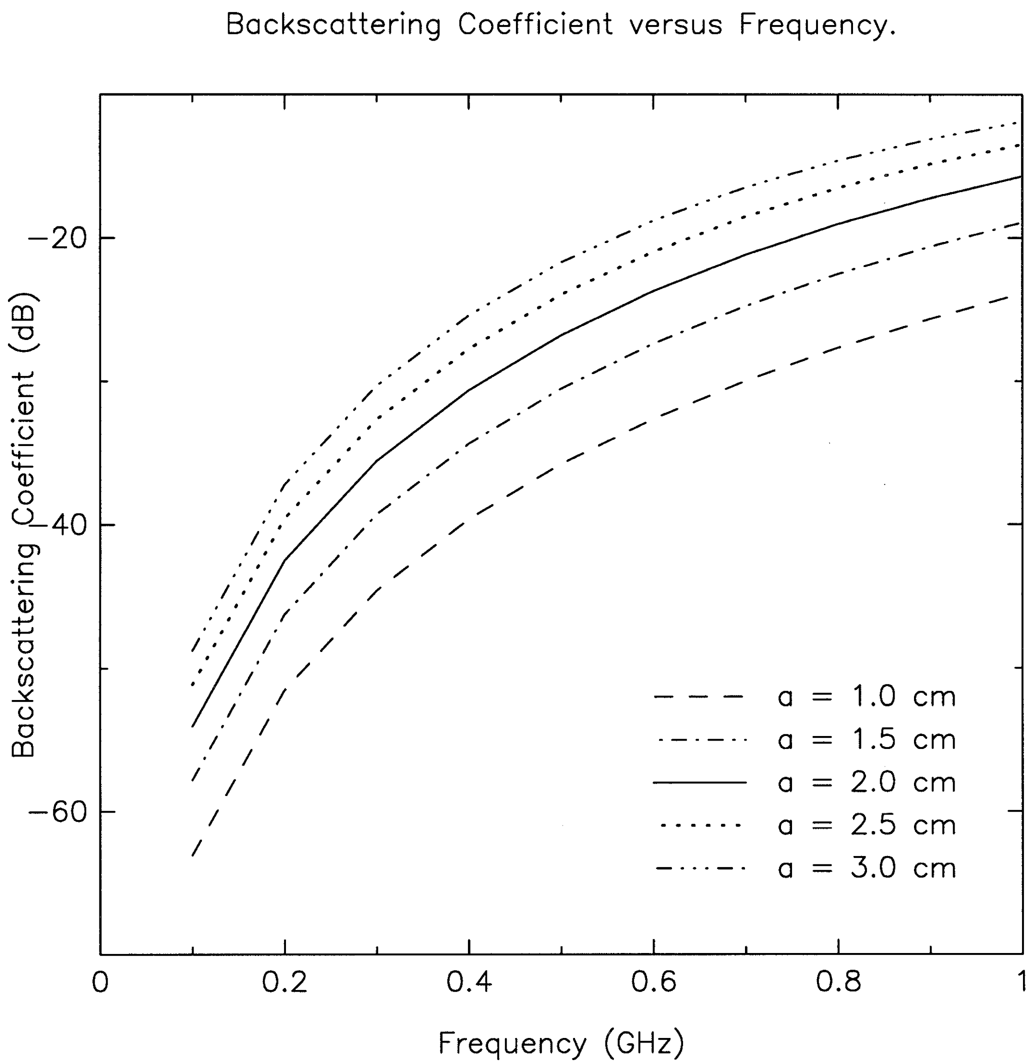

Figure 5-11: Backscattering coefficient of medium with size distribution versus frequency.

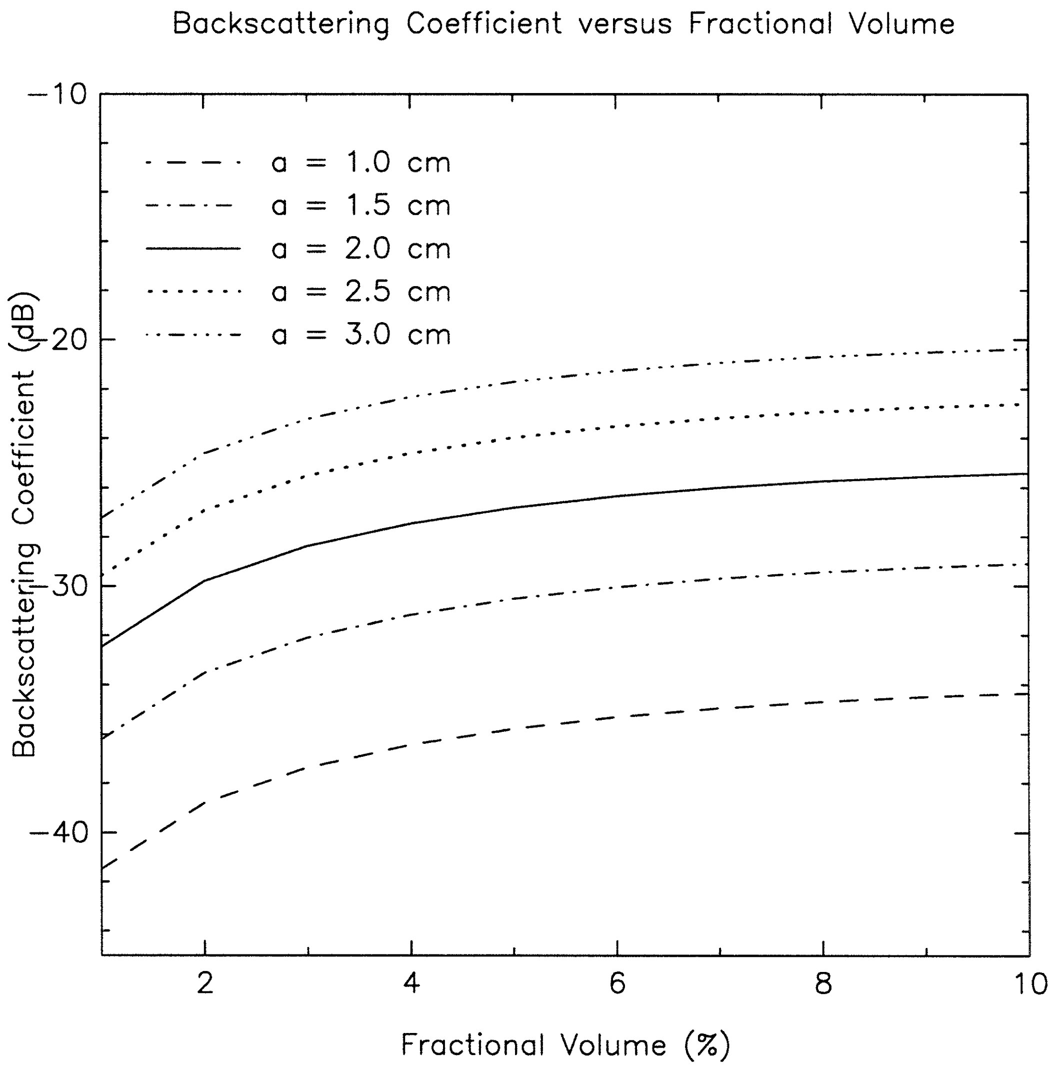

Figure 5-12: Backscattering coefficient of medium with size distribution versus total fractional volume.

Chapter 6

Summary

In June 1993, MIT Lincoln Laboratory conducted a ground penetration radar (GPR) experiment in Yuma, Arizona. During the experiment, extensive clutter data were collected for the desert terrain. These clutter data show that, even in an area where the surface is relatively flat and with no visible vegetation, the backscatter is significantly higher than the noise level. For GPR configuration, a possible explanation for this finding is volume scattering. Volume scattering is caused by inhomogeneity in the medium, such as rocks beneath the desert surface, heterogeneous soil types, and subsurface features. This thesis investigates the volume scattering arisen from the rocks.

For the ease of modeling, the desert is replaced by a lossy half–space medium, and the rocks are replaced by dielectric spherical particles embedded in the half–space. The radar backscatter were calculated as a function of incident angle, frequency, dielectric constant of the particles, dielectric constant of the half–space, conductivity of the half–space, size of the particles, and the fractional volume of the particles. (The fractional volume of particles in the medium is the ratio of the sum of the volume of all the particles to the bulk volume of the medium.) Three approaches are used to analyze this volume scattering problem: (1) the Transition Matrix with Monte Carlo simulation (T-matrix-Monte Carlo simulation), (2) the Radiative Transfer theory (RT) based on the eigenanalysis numerical solution, and (3) the Zeroth Order Analytical solution.

The Transition matrix (T-matrix) is derived from Maxwell's equations and is used to calculate the scattered field. The Monte Carlo simulation technique is applied to approximate the backscattering coefficient. In other words, the T-matrix-Monte Carlo simulation is based on solving the wave equation and averaging over many realizations of randomly generated particle positions. For accurate results, many realizations are needed, thus it means longer computation time. The appropriate number of realizations depends mainly on the configuration of the problem and the required accuracy. This approach is usually less efficient in terms of computational resources, but it has an advantage that it includes multiple scattering and coherent wave interaction among the particles.

The RT approach is based on the energy transportation concept and is used to calculate the intensity of the scattered power. The characteristics of the medium in the RT approach is described by two constituents, the phase matrix and the extinction matrix, which are calculated from the averaged particle configuration. Since the RT is based on intensities, it does not include coherent wave interaction, which may give appreciable contribution to the scattered power when the size of the problem is comparable to wavelength of the incident wave. However, the geometrical model used in the RT approach consists of infinitely extended particle layers, thus the use of the RT approach is already limited to infinite medium. In fact, this limitation does not restrain the use of RT approach to this study since the real physical problem itself can be modeled using an infinite medium. A major advantage of the RT approach is that it includes multiple interaction between particles. And since the constituents in the RT equation are calculated based on the already averaged quantities, there is no need to average over many realizations, which means shorter computation time and is another advantage of the RT approach.

The First Order Analytical solution is another approach derived from the Maxwell's equations by assuming single scattering and independent particle positions. Like the T-matrix-Monte Carlo technique, it accounts for coherent wave interaction. Unlike the T-matrix-Monte Carlo technique which requires calculation for many realizations, the averaging process in this approach is taken care of by assuming the particle's position to be a uniformly distributed random variable and by integrating over the whole medium. The integration is carried out once and the solution is in a compact form; the calculation in this approach is relatively simple comparing to the above two methods By its simplicity, this First Order Analytical Approximation gives better understanding of the behavior of the backscatter when the configuration of the medium is changed in various ways. However, the accuracy of this solution degraded when the fractional volume of the particles increases, owing to the assumption of single scattering and independent particle positions.

These three approaches were used to calculate the backscatters. Numerical calculations show that results of the three approaches agree well. The result of the First Order Analytical Approximation becomes inaccurate as compared the other two approaches when the fractional volume of particles is large. This is due mainly to the independent particle position assumption. Considering the accuracy and the computational efficiency, the RT approach appears to be the best method for this study. Note, again, the RT approach does not include coherent wave interaction and it may produce insufficient accurate result for an application where the coherent wave interaction is significant.

The observed total backscatter of a desert terrain consists of components due to various surface and subsurface features. Parametric study, in which backscatter is calculated as functions of frequencies, incident angles, fractional volumes, etc., shows that the backscatter of rocks beneath the surface can be a significant component of the total backscatter. This is expected, since, in the GPR applications, significant amount of electromagnetic energy penetrates into the ground. Dependence on the chosen parameters in the backscatter simulations, backscatter of rocks can be a principle factor that contributes to the observed high backscatter in the 1993 GPR experiment. To confirm this, however, the parameter used in the simulations must be verified and it requires ground truth.

The three developed volume scattering models are by no mean completed. A number of improvements to capture a more realistic geometrical configuration can be made. The particle size distribution may be added to represent the various sizes of rocks. The surface and subsurface contributions may also be incorporated in the model. The First Order Analytical solution can be improved and used for higher fractional volume problems. The improvements can come from a better approximation of the pair distribution function, which describes the dependency of the particles' positions in the medium.

Appendix A

Transmission Coefficient for a Dipole Field

In this appendix, we shall derive the transmission coefficient for a dipole field. The dipole is in the lower half–space (region 1). Transmission coefficient for this dipole field at the upper half–space (region 0) is calculated.

A.1 Integral Representation of Free–space Dyadic Green's Function

$$\nabla \times \nabla \times \overline{\overline{G}}(\overline{r}, \overline{r}') - k_0^2 \overline{\overline{G}}(\overline{r}, \overline{r}') = \overline{\overline{I}} \delta(\overline{r} - \overline{r}') \tag{A.1}$$

or

$$\overline{\overline{G}}(\overline{r}, \overline{r}') = [\overline{\overline{I}} - \frac{1}{k_0^2} \nabla\nabla] \, g(\overline{r}, \overline{r}') \tag{A.2}$$

where

$$g(\overline{r}, \overline{r}') = g(\overline{r} - \overline{r}') = \frac{e^{ik_0|\overline{r} - \overline{r}'|}}{4\pi |\overline{r} - \overline{r}'|} \tag{A.3}$$

$$(\nabla^2 + k_0^2) g(\overline{r}, \overline{r}') = -\delta(\overline{r} - \overline{r}') \tag{A.4}$$

Let $\overline{r}' = 0$. Fourier Transform gives:

$$g(\overline{r}) = \frac{1}{(2\pi)^3} \iiint d^3\overline{k}\, e^{i\overline{k}\cdot\overline{r}} g(\overline{k}) \tag{A.5}$$

$$\delta(\overline{r}) = \frac{1}{(2\pi)^3} \iiint d^3\overline{k}\, e^{i\overline{k}\cdot\overline{r}} \tag{A.6}$$

Substitute into (A.4)

$$(\nabla^2 + k_0^2)\frac{1}{(2\pi)^3} \iiint d^3\overline{k}\, e^{i\overline{k}\cdot\overline{r}} g(\overline{k}) = -\frac{1}{(2\pi)^3} \iiint d^3\overline{k} e^{i\overline{k}\cdot\overline{r}} \tag{A.7}$$

Since the integral sign operates on $\overline{k}$ and the ∇^2 operates on $\overline{r}$, we can swap the integral sign and the ∇^2 operator.

$$e^{i\overline{k}\cdot\overline{r}} = e^{i(k_x x + k_y y + k_z z)} \tag{A.8}$$

$$\nabla^2 e^{i\overline{k}\cdot\overline{r}} = -k^2 e^{i\overline{k}\cdot\overline{r}} \tag{A.9}$$

Thus

$$\frac{1}{(2\pi)^3} \iiint d^3\overline{k}\, (-k^2 + k_0^2) e^{i\overline{k}\cdot\overline{r}} g(\overline{k}) = -\frac{1}{(2\pi)^3} \iiint d^3\overline{k}\, e^{i\overline{k}\cdot\overline{r}} \tag{A.10}$$

$$(-k^2 + k_0^2) g(\overline{k}) = -1 \tag{A.11}$$

$$g(\overline{k}) = \frac{1}{(k^2 - k_0^2)} \tag{A.12}$$

From (A.5)

$$g(\overline{r}) = \frac{1}{(2\pi)^3} \int d^3\overline{k}\, e^{i\overline{k}\cdot\overline{r}} \frac{1}{(k^2 - k_0^2)} \tag{A.13}$$

Let $k_p^2 = k_x^2 + k_y^2$ then

$$\frac{1}{k^2 - k_0^2} = \frac{1}{k_x^2 + k_y^2 + k_z^2 - k_0^2} = \frac{1}{k_z^2 + k_p^2 - k_0^2} = \frac{1}{k_z^2 - (k_0^2 - k_p^2)} \tag{A.14}$$

$$g(\bar{r}) = \frac{1}{(2\pi)^3} \iiint \frac{e^{i(k_x x + k_y y + k_z z}}{k_z^2 - (k_0^2 - k_p^2)} dk_z \, dk_y \, dk_z \tag{A.15}$$

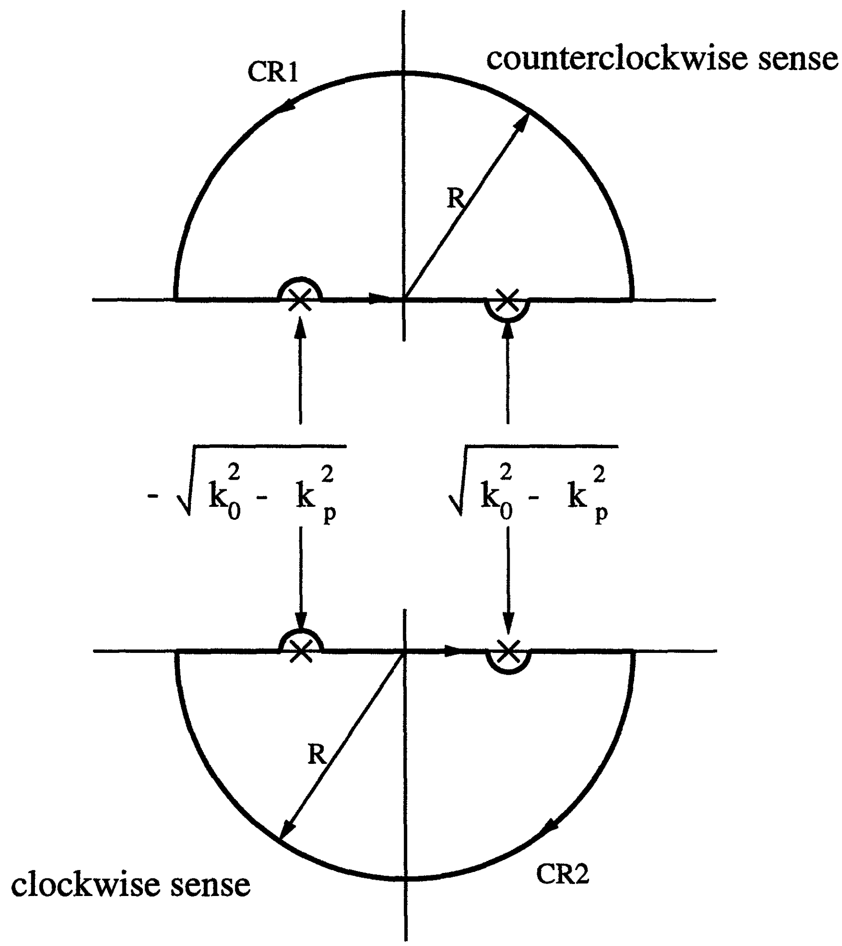

Figure A-1: Contours of Integration

Integrate with respect to k_z.

- Singular points are at $k_z = \pm\sqrt{k_0^2 - k_p^2}$.

- Notice that $k_z > 0$ is for $z > 0$ and $k_z < 0$ is for $z < 0$ and that $\sqrt{k_0^2 - k_p^2}$ is always larger than 0.

- Deform the contour upwards and pick the contribution from the singular point $+\sqrt{k_0^2 - k_p^2}$. And deform the contour downwards and pick the contribution from the singular point $-\sqrt{k_0^2 - k_p^2}$ (Figure A-1).

Then

$$\int \frac{e^{i(k_x x+k_y y+k_z z)}dk_z}{(k_z-\sqrt{k_0^2-k_p^2})(k_z+\sqrt{k_0^2-k_p^2})} = \begin{cases} 2\pi i \frac{e^{i(k_x x+k_y y+z\sqrt{k_0^2-k_p^2})}}{2\sqrt{k_0^2-k_p^2}} + \int_{CR_1} \frac{e^{i\bar{k}\cdot\bar{r}}}{(k^2-k_0^2)}dk_z \\ -2\pi i \frac{e^{i(k_x x+k_y y-z\sqrt{k_0^2-k_p^2})}}{-2\sqrt{k_0^2-k_p^2}} + \int_{CR_2} \frac{e^{i\bar{k}\cdot\bar{r}}}{(k^2-k_0^2)}dk_z \end{cases} \tag{A.16}$$

for $z > 0$ and $z < 0$ respectively. The second terms on the right-hand side of (A.16) are zero for both $z > 0$ and $z < 0$ cases.

In free space we have

$$k_x^2 + k_y^2 + k_z^2 = k_0^2 \quad \Rightarrow \quad k_p^2 + k_z^2 = k_0^2 \quad \Rightarrow \quad \sqrt{k_0^2 - k_p^2} = k_z \tag{A.17}$$

Then the right-hand side of Equation (A.16) is reduced to

$$2\pi i \frac{e^{i(k_x x+k_y y+k_z|z|)}}{2k_z} \tag{A.18}$$

Using (A.18 in (A.15),thus

$$g(\bar{r}) = \frac{i}{(2\pi^2)} \iint d^2\bar{k}_\perp \, e^{i(\bar{k}_\perp\cdot\bar{r}_\perp + k_z|z|)} \tag{A.19}$$

where

$$\bar{k}_\perp = \hat{x}k_x + \hat{y}k_y, \quad \bar{r}_\perp = \hat{x}r_x + \hat{y}r_y$$

To find $\overline{\overline{G}}(\bar{r})$ we have to find $\nabla\nabla g(\bar{r})$. We then first consider $\frac{\partial^2 g(\bar{r})}{\partial z^2}$

$$\frac{\partial}{\partial z} g(\bar{r}) = \frac{i}{(2\pi)^2} \iint d^2\bar{k}_\perp \, \frac{\partial}{\partial z} \frac{e^{i(\bar{k}_\perp\cdot\bar{r}_\perp + k_z|z|)}}{2k_z} \tag{A.20}$$

Note that

$$\frac{d|z|}{dz} = \left\{ \begin{array}{cc} 1 & z > 0 \\ -1 & z < 0 \end{array} \right\} = \frac{z}{|z|}$$

, thus

$$\frac{\partial}{\partial z} g(\bar{r}) = -\frac{1}{(2\pi)^2} \iint d^2\bar{k}_\perp \, \frac{e^{i(\bar{k}_\perp\cdot\bar{r}_\perp + k_z|z|)}}{2} \frac{z}{|z|} \tag{A.21}$$

$$\frac{\partial^2}{\partial z^2} g(\overline{r}) = -\frac{1}{(2\pi)^2} \iint d^2\overline{k}_\perp \, \frac{e^{i\overline{k}_\perp \cdot \overline{r}_\perp}}{2} \left[\frac{z}{|z|} \frac{de^{ik_z|z|}}{dz} + e^{ik_z|z|} \frac{d}{dz} \frac{z}{|z|} \right]$$

$$= -\frac{1}{(2\pi)^2} \iint d^2\overline{k}_\perp \, \frac{e^{i\overline{k}_\perp \cdot \overline{r}_\perp}}{2} \left[\frac{z}{|z|} \frac{z}{|z|} ik_z e^{ik_z|z|} + \delta(z) e^{ik_z(z)} \right]$$

$$= -\frac{i}{8\pi^2} \iint d^2\overline{k}_\perp \, k_z e^{i(\overline{k}_\perp \cdot \overline{r}_\perp + k_z|z|)} - \frac{1}{8\pi^2} \iint d^2\overline{k}_\perp \, \delta(z) e^{i(\overline{k}_\perp \cdot \overline{r}_\perp + k_z|z|)} \tag{A.22}$$

But from Equation (A.4) we have

$$(\nabla^2 + k_0^2) g(\overline{r}) = -\delta(\overline{r})$$

and

$$\frac{\partial}{\partial x} g(\overline{r}) = -\frac{1}{(2\pi)^2} \int d^2\overline{k}_\perp \, k_x \frac{e^{i(\overline{k}_\perp \cdot \overline{r}_\perp + k_z|z|)}}{2k_z}$$

$$= -\frac{i}{8\pi^2} \int d^2\overline{k}_\perp \, \frac{k_x}{k_z} e^{i(\overline{k}_\perp \cdot \overline{r}_\perp + k_z|z|)} \tag{A.23}$$

$$\frac{\partial^2}{\partial x^2} g(\overline{r}) = -\frac{i}{8\pi^2} \int d^2\overline{k}_\perp \, \frac{k_x^2}{k_z} e^{i(\overline{k}_\perp \cdot \overline{r}_\perp + k_z|z|)} \tag{A.24}$$

$$\frac{\partial^2}{\partial y^2} g(\overline{r}) = -\frac{i}{8\pi^2} \int d^2\overline{k}_\perp \, \frac{k_y^2}{k_z} e^{i(\overline{k}_\perp \cdot \overline{r}_\perp + k_z|z|)} \tag{A.25}$$

Upon balancing Equation (A.4), it is necessary that the second term on the right-hand side of Equation (A.22) equals $-\delta(\overline{r})$.

$$-\frac{1}{8\pi^2} \iint d^2\overline{k}_\perp \, \delta(z) e^{i(\overline{k}_\perp \cdot \overline{r}_\perp + k_z|z|)} = -\delta(\overline{r}) \tag{A.26}$$

From Equation (A.2)

$$\overline{\overline{G}}(\overline{r}) = \left[\overline{\overline{I}} + \frac{1}{k_0^2} \nabla\nabla \right] g(\overline{r}) \tag{A.27}$$

$$\overline{\overline{G}}(\overline{r}) = \left[\overline{\overline{I}} + \frac{1}{k_0^2} \nabla\nabla \right] \frac{i}{8\pi^2} \int d^2\overline{k}_\perp \, \frac{e^{i(\overline{k}_\perp \cdot \overline{r}_\perp + k_z|z|)}}{k_z} \tag{A.28}$$

But

$$\nabla\nabla g(\overline{r}) = \begin{bmatrix} \frac{\partial^2}{\partial x^2}\hat{x}\hat{x} & \frac{\partial^2}{\partial x\partial y}\hat{x}\hat{y} & \frac{\partial^2}{\partial x\partial z}\hat{x}\hat{z} \\ \frac{\partial^2}{\partial y\partial x}\hat{y}\hat{x} & \frac{\partial^2}{\partial y^2}\hat{y}\hat{y} & \frac{\partial^2}{\partial y\partial z}\hat{y}\hat{z} \\ \frac{\partial^2}{\partial z\partial x}\hat{z}\hat{x} & \frac{\partial^2}{\partial z\partial y}\hat{z}\hat{y} & \frac{\partial^2}{\partial z^2}\hat{z}\hat{z} \end{bmatrix} \begin{bmatrix} g(\overline{r}) & 0 & 0 \\ 0 & g(\overline{r}) & 0 \\ 0 & 0 & g(\overline{r}) \end{bmatrix} \tag{A.29}$$

for $z > 0$

$$g(\overline{r}) = \frac{i}{8\pi^2}\int d^2\overline{k}_\perp \frac{e^{i(\overline{k}_\perp\cdot\overline{r}_\perp + k_z z)}}{k_z} \tag{A.30}$$

Thus the $\left[\overline{\overline{I}} + \frac{1}{k_0^2}\nabla\nabla\right] g(\overline{r})$ can be written in the form

$$\left[\overline{\overline{I}} + \frac{1}{k_0^2}\nabla\nabla\right] g(\overline{r}) = -\hat{z}\hat{z}\frac{\delta(\overline{r})}{k_0^2} + \frac{i}{8\pi^2}\int d^2\overline{k}_\perp \frac{1}{k_z}\left[\overline{\overline{I}} - \frac{\overline{kk}}{k_0^2}\right] e^{i(\overline{k}_\perp\cdot\overline{r}_\perp + k_z z)} \tag{A.31}$$

,where $\overline{k} = k_x\hat{x} + k_y\hat{y} + k_z\hat{z}$ and the term $-\hat{z}\hat{z}\frac{\delta(\overline{r})}{k_0^2}$ comes from $\frac{\partial^2}{\partial z^2}$ term

for $z < 0$

$$g(\overline{r}) = \frac{i}{8\pi^2}\int d^2\overline{k}_\perp \frac{e^{i(\overline{k}_\perp\cdot\overline{r}_\perp - k_z z)}}{k_z} \tag{A.32}$$

Thus

$$\left[\overline{\overline{I}} + \frac{1}{k_0^2}\nabla\nabla\right] g(\overline{r}) = -\hat{z}\hat{z}\frac{\delta(\overline{r})}{k_0^2} + \frac{i}{8\pi^2}\int d^2\overline{k}_\perp \frac{1}{k_z}\left[\overline{\overline{I}} - \frac{\overline{k}^-\overline{k}^-}{k_0^2}\right] e^{i(\overline{k}_\perp\cdot\overline{r}_\perp - k_z z)} \tag{A.33}$$

where $\overline{k} = k_x\hat{x} + k_y\hat{y} + k_z\hat{z}$

Then

$$\overline{\overline{G}}(\overline{r}) = -\hat{z}\hat{z}\frac{\delta(\overline{r})}{k_0^2} + \begin{cases} \frac{i}{8\pi^2}\int d^2\overline{k}_\perp \frac{1}{k_z}\left[\overline{\overline{I}} - \frac{\overline{kk}}{k_0^2}\right] e^{i\overline{k}\cdot\overline{r}} \\ \frac{i}{8\pi^2}\int d^2\overline{k}_\perp \frac{1}{k_z}\left[\overline{\overline{I}} - \frac{\overline{k}^-\overline{k}^-}{k_0^2}\right] e^{i\overline{k}^-\cdot\overline{r}} \end{cases} \tag{A.34}$$

But

$$\frac{\overline{kk}}{k_0^2} = \frac{\overline{k}}{k_0}\frac{\overline{k}}{k_0} = \hat{k}\hat{k} \tag{A.35}$$

We define unit vectors:

$$\hat{e}(k_z) = \frac{\hat{k}\times\hat{z}}{|\hat{k}\times\hat{z}|} \tag{A.36}$$

$$\hat{h}(k_z) = \frac{1}{k_0}\hat{e} \times \hat{z} \tag{A.37}$$

Then

$$\overline{\overline{I}} = \hat{e}\hat{e} + \hat{h}\hat{h} + \hat{k}\hat{k} \tag{A.38}$$

,or

$$\overline{\overline{I}} - \hat{k}\hat{k} = \hat{e}\hat{e} + \hat{h}\hat{h} \tag{A.39}$$

for $z < 0$, $\quad \overline{k}^- = \hat{x}k_x + \hat{y}k_y - \hat{z}k_z$

$$\hat{e}(-k_z) = \frac{\hat{k}^- \times \hat{z}}{|\hat{k}^- \times \hat{z}|} = \hat{e}(k_z) \tag{A.40}$$

$$\hat{h}(-k_z) = \frac{1}{k_0}\hat{e}(k_z) \times \overline{k}^- \tag{A.41}$$

Then

$$\overline{\overline{G}}(\overline{r}, \overline{r}') = -\hat{z}\hat{z}\frac{\delta(\overline{r}, \overline{r}')}{k_0^2}$$

$$+ \begin{cases} \frac{i}{8\pi^2} \int d^2\overline{k}_\perp \frac{1}{k_z} \left[\hat{e}(k_z)\hat{e}(k_z) + \hat{h}(k_z)\hat{h}(k_z)\right] e^{i\overline{k}\cdot(\overline{r}-\overline{r}')} & for \quad z > 0 \\ \frac{i}{8\pi^2} \int d^2\overline{k}_\perp \frac{1}{k_z} \left[\hat{e}(-k_z)\hat{e}(-k_z) + \hat{h}(-k_z)\hat{h}(-k_z)\right] e^{i\overline{k}^-\cdot(\overline{r}-\overline{r}')} & for \quad z < 0 \end{cases} \tag{A.42}$$

Notice that the $\hat{e}(-k_z), \hat{h}(-k_z), \overline{k}^-$ are for down-going wave and $\hat{e}(k_z), \hat{h}(k_z), \overline{k}$ are for up-going wave. By starting with the dyadic Green's function in a homogeneous medium, the boundary can be added later, which gives rise to reflected wave terms in the dyadic Green's function.

A.2 Half–space Dyadic Green's Function

Consider the case where a point source is located at far zone in region 1 such that $z > z'$. Then $\overline{\overline{G}}(\overline{r}, \overline{r}')$ to be used will be the one for $z > z'$.

$$\overline{\overline{G}}(\overline{r},\overline{r}') = -\hat{z}\hat{z}\frac{\delta(\overline{r},\overline{r}')}{k_0^2} + \frac{i}{8\pi^2}\iint d^2\overline{k}_\perp \frac{1}{k_z}\left[\hat{e}(k_z)\hat{e}(k_z) + \hat{h}(k_z)\hat{h}(k_z)\right] e^{i\overline{k}\cdot(\overline{r}-\overline{r}')} \quad \text{(A.43)}$$

for $z > z'$

$$\left[\hat{e}(k_z)\hat{e}(k_z) + \hat{h}(k_z)\hat{h}(k_z)\right] e^{i\overline{k}\cdot(\overline{r}-\overline{r}')}$$

$$= \hat{e}(k_z)e^{i\overline{k}\cdot\overline{r}}\hat{e}(k_z)e^{-i\overline{k}\cdot\overline{r}'} + \hat{h}(k_z)e^{i\overline{k}\cdot\overline{r}}\hat{h}(k_z)e^{-i\overline{k}\cdot\overline{r}'} \quad \text{(A.44)}$$

Upon realizing that $\hat{e}(k_z)e^{i\overline{k}\cdot\overline{r}}$ is a up-going wave in TE mode and $\hat{h}(k_z)e^{i\overline{k}\cdot\overline{r}}$ is a up-going wave in TM mode for free–space dyadic Green's function, then, for half–space Green's function, we add $R^{TE}\hat{e}(-k_z)e^{i\overline{k}^-\cdot\overline{r}}$, a reflected down-going wave, in TE mode and $R^{TE}\hat{h}(-k_z)e^{i\overline{k}^-\cdot\overline{r}}$, a reflected down-going wave in TM mode into Equation (A.44).

$$\left[\hat{e}(k_z)\hat{e}(k_z) + \hat{h}(k_z)\hat{h}(k_z)\right] e^{i\overline{k}\cdot(\overline{r}-\overline{r}')}$$

$$\Longrightarrow \left[R^{TE}\hat{e}(-k_z)e^{i\overline{k}^-\cdot\overline{r}} + \hat{e}(k_z)e^{i\overline{k}\cdot\overline{r}}\right]\hat{e}(k_z)e^{-i\overline{k}\cdot\overline{r}'} + \left[R^{TM}\hat{h}(-k_z)e^{i\overline{k}^-\cdot\overline{r}} + \hat{h}(k_z)e^{i\overline{k}\cdot\overline{r}}\right]\hat{h}(k_z)e^{-i\overline{k}\cdot\overline{r}'} \quad \text{(A.45)}$$

Since $\overline{r}' \to \infty$, then $\delta(\overline{r},\overline{r}') = 0$ unless $\overline{r} \to \infty$. Thus

$$\overline{\overline{G}}_{11}(\overline{r},\overline{r}') = \frac{i}{8\pi^2}\iint d^2\overline{k}_\perp \frac{1}{k_{1z}}\Big\{[R_{10}^{TE}\hat{e}_1(-k_{1z})e^{i\overline{k}_1^-\cdot\overline{r}} + \hat{e}_1(k_{1z})e^{i\overline{k}_1\cdot\overline{r}}]\hat{e}_1(k_{1z})e^{-i\overline{k}_1\cdot\overline{r}'}$$

$$+[R_{10}^{TM}\hat{h}_1(-k_{1z})e^{i\overline{k}_1^-\cdot\overline{r}} + \hat{h}_1(k_{1z})e^{i\overline{k}_1\cdot\overline{r}}]\hat{h}_1(k_{1z})e^{-i\overline{k}_1\cdot\overline{r}'}\Big\} \quad \text{(A.46)}$$

Similarly,

$$\overline{\overline{G}}_{01}(\overline{r},\overline{r}') = \frac{i}{8\pi^2}\iint d^2\overline{k}_\perp \frac{1}{k_{1z}}\Big[T_{10}^{TE}\hat{e}(k_z)e^{i\overline{k}\cdot\overline{r}} + \hat{e}_1(k_{1z})e^{-i\overline{k}_1\cdot\overline{r}'}$$

$$+T_{10}^{TM}\hat{h}(k_z)e^{i\overline{k}\cdot\overline{r}} + \hat{h}_1(k_{1z})e^{-i\overline{k}_1\cdot\overline{r}'}\Big] \quad \text{(A.47)}$$

where

$$\overline{k}_1 = k_x\hat{x} + k_y\hat{y} + k_{1z}\hat{z}$$

$$\overline{k_1^-} = k_x\hat{x} + k_y\hat{y} - k_{1z}\hat{z}$$

$$k_{1z} = \sqrt{k_1^2 - k_x^2 - k_y^2}$$

$$\hat{e}(k_z) = \frac{\hat{k} \times \hat{z}}{|\hat{k} \times \hat{z}|} = \frac{1}{k_p}(\hat{x}k_y - \hat{y}k_x)$$

$$\hat{h}(k_z) = \frac{1}{k_0}\hat{e}_x\overline{k} = -\frac{k_z}{k_0 k_p}(\hat{x}k_x - \hat{y}k_y) + \frac{k_p}{k_0}\hat{z}$$

Note that $k_x = k_{1x}$ and $k_y = k_{1y}$ from phase matching.

We can find $R^{TM}, R^{TE}, T^{TM}, T^{TE}$ by matching boundary conditions at $z = 0$. At $z = 0$ tangential components are continuous.

$$\hat{z} \times \overline{\overline{G}}_{11}(\overline{r}, \overline{r}') = \hat{z} \times \overline{\overline{G}}_{01}(\overline{r}, \overline{r}'), \quad z = 0 \tag{A.48}$$

$$\hat{z} \times [\nabla \times \overline{\overline{G}}_{11}(\overline{r}, \overline{r}')] = \hat{z} \times [\nabla \times \overline{\overline{G}}_{01}(\overline{r}, \overline{r}')], \quad z = 0 \tag{A.49}$$

Note that the cross products operate on the first vectors of dyads, then from Equation (A.48), we have:

$$\hat{z} \times [R_{10}^{TE}\hat{e}_1(-k_{1z})e^{i\overline{k_1^-}\cdot\overline{r}} + \hat{e}_1(k_{1z})e^{i\overline{k}_1\cdot\overline{r}}] = \hat{z} \times T_{10}^{TE}\hat{e}(k_z)e^{i\overline{k}\cdot\overline{r}} \tag{A.50}$$

$$\hat{z} \times [R_{10}^{TM}\hat{h}_1(-k_{1z})e^{i\overline{k_1^-}\cdot\overline{r}} + \hat{h}_1(k_{1z})e^{i\overline{k}_1\cdot\overline{r}}] = \hat{z} \times T_{10}^{TM}\hat{h}(k_z)e^{i\overline{k}\cdot\overline{r}} \tag{A.51}$$

at $z = 0$ then $\overline{k_1^-} \cdot \overline{r} = \overline{k} \cdot \overline{r} = \overline{k}^- \cdot \overline{r}$, then

$$\hat{z} \times [R_{10}^{TE}\hat{e}_1(-k_{1z}) + \hat{e}_1(k_{1z})] = \hat{z} \times T_{10}^{TE}\hat{e}(k_z) \tag{A.52}$$

$$\hat{z} \times [R_{10}^{TM}\hat{h}_1(-k_{1z}) + \hat{h}_1(k_{1z})] = \hat{z} \times T_{10}^{TM}\hat{h}(k_z) \tag{A.53}$$

But $\hat{e}_1(k_{1z}) = \hat{e}_1(-k_{1z}) = \hat{e}(k_z)$, thus, from Equation (A.52)

$$R_{10}^{TE} + 1 = T_{10}^{TE} \tag{A.54}$$

And

$$\hat{z} \times \hat{h}_1(-k_{1z}) = \begin{vmatrix} \hat{x} & \hat{y} & \hat{z} \\ 0 & 0 & 1 \\ \frac{k_x k_{1z}}{k_1 k_p} & \frac{k_y k_{1z}}{k_1 k_p} & \frac{k_p}{k_1} \end{vmatrix}$$

$$= -\frac{k_y k_{1z}}{k_1 k_p}\hat{x} + \frac{k_x k_{1z}}{k_1 k_p}\hat{y} = \frac{k_{1z}}{k_1}\left[\frac{1}{k_p}(-k_y\hat{x} + k_x\hat{y})\right]$$

$$= \frac{k_{1z}}{k_1}\hat{e}_1(-k_{1z}) \tag{A.55}$$

Similarly,

$$\hat{z} \times \hat{h}_1(k_{1z}) = \frac{k_{1z}}{k_1}\hat{e}_1(k_{1z}) \tag{A.56}$$

and

$$\hat{z} \times \hat{h}(k_z) = \frac{k_z}{k_0}\hat{e}(k_z) \tag{A.57}$$

Then from Equation (A.53)

$$[1 - R_{10}^{TM}]\frac{k_{1z}}{k_1} = \frac{k_z}{k_0}T_{10}^{TM} \tag{A.58}$$

From Equation (A.49), we replace ∇ with $i\overline{k}$ then

$$\hat{z} \times [R_{10}^{TE} i\overline{k}_1^- \times \hat{e}_1(-k_{1z}) + i\overline{k}_1 \times \hat{e}_1(k_{1z})] = \hat{z} \times T_{10}^{TE} i\overline{k} \times \hat{e}(k_z) \tag{A.59}$$

$$\hat{z} \times [R_{10}^{TM} i\overline{k}_1^- \times \hat{h}_1(-k_{1z}) + i\overline{k}_1 \times \hat{h}_1(k_{1z})] = \hat{z} \times T_{10}^{TM} i\overline{k} \times \hat{h}(k_z) \tag{A.60}$$

But we know that

$$\hat{h}_1(k_{1z}) = \frac{1}{k_1}\hat{e}_1 \times \overline{k}_1$$

$$\overline{k}_1 \times \hat{e}_1 = -k_1\hat{h}_1(k_{1z}) \tag{A.61}$$

and

$$\overline{k}_1 \times \hat{h}_1(k_{1z}) = \overline{k}_1 \times \frac{1}{k_1}\hat{e}_1 \times \overline{k}_1 = \frac{\hat{e}_1}{k_1}(\overline{k}_1 \cdot \overline{k}_1) - \overline{k}_1(\overline{k}_1 \cdot \frac{\hat{e}_1}{k_1})$$

as $\overline{k}_1 \cdot \overline{k}_1 = k_1^2$ and $\overline{k}_1 \cdot \hat{e}_1 = 0$, thus

$$\overline{k}_1 \times \hat{h}_1(k_{1z}) = k_1 \hat{e}_1 \tag{A.62}$$

Using (A.61) in (A.59) , then

$$\hat{z} \times [R_{10}^{TE} k_1 \hat{h}_1(-k_{1z}) + k_1 \hat{h}_1(k_{1z})] = \hat{z} \times T_{10}^{TE} k_0 \hat{h}(k_z) \tag{A.63}$$

$$k_{1z}[1 - R_{10}^{TE}] = T_{10}^{TE} k_z \tag{A.64}$$

and using (A.62) in (A.60),then

$$\hat{z} \times [R_{10}^{TM} k_1 \hat{e}_1(-k_{1z}) + k_1 \hat{e}_1(k_{1z})] = \hat{z} \times T_{10}^{TM} k_0 \hat{e}(k_z) \tag{A.65}$$

$$k_1[1 + R_{10}^{TM}] = T_{10}^{TM} k_0 \tag{A.66}$$

Combining (A.54), (A.58), (A.64) and, (A.66), we can solve this set of equations for the four unknowns. The solution is

$$T_{10}^{TM} = \frac{k_1}{k_0}\left[\frac{2\epsilon_0 k_{1z}}{\epsilon_1 k_z + \epsilon_0 k_{1z}}\right] = \sqrt{\frac{\epsilon_1}{\epsilon_0}}\left[\frac{2\epsilon_0 k_{1z}}{\epsilon_1 k_z + \epsilon_0 k_{1z}}\right] \tag{A.67}$$

$$T_{10}^{TE} = \frac{2k_{1z}}{k_z + k_{1z}} \tag{A.68}$$

$$R_{10}^{TM} = \frac{\epsilon_0 k_{1z} - \epsilon_1 k_z}{\epsilon_0 k_{1z} + \epsilon_1 k_z} \tag{A.69}$$

$$R_{10}^{TE} = \frac{k_{1z} - k_z}{k_{1z} + k_z} \tag{A.70}$$

Then

$$\begin{aligned}\overline{\overline{G}}_{11}(\overline{r}, \overline{r}') = \frac{i}{8\pi^2} \iint d^2\overline{k}_\perp \frac{1}{k_{1z}} \Big\{ &[R_{10}^{TE} \hat{e}_1(-k_{1z}) e^{i\overline{k_1^-}\cdot\overline{r}} + \hat{e}_1(k_{1z}) e^{i\overline{k}_1\cdot\overline{r}}]\hat{e}_1(k_{1z}) e^{-i\overline{k}_1\cdot\overline{r}'} \\ &+ [R_{10}^{TM} \hat{h}_1(-k_{1z}) e^{i\overline{k_1^-}\cdot\overline{r}} + \hat{h}_1(k_{1z}) e^{i\overline{k}_1\cdot\overline{r}}]\hat{h}_1(k_{1z}) e^{-i\overline{k}_1\cdot\overline{r}'} \Big\}\end{aligned} \tag{A.71}$$

$$\overline{\overline{G}}_{01}(\bar{r},\bar{r}') = \frac{i}{8\pi^2}\iint d^2\bar{k}_\perp \frac{1}{k_{1z}}\left[T_{10}^{TE}\hat{e}(k_z)e^{i\bar{k}\cdot\bar{r}}\hat{e}_1(k_{1z})e^{-i\bar{k}_1\cdot\bar{r}'}\right.$$
$$\left. +T_{10}^{TM}\hat{h}(k_z)e^{i\bar{k}\cdot\bar{r}}\hat{h}_1(k_{1z})e^{-i\bar{k}_1\cdot\bar{r}'}\right] \tag{A.72}$$

or

$$\overline{\overline{G}}_{01}(\bar{r},\bar{r}') = \frac{i}{8\pi^2}\int d^2\bar{k}_\perp \frac{1}{k_{1z}}\left[\frac{2k_{1z}}{k_z+k_{1z}}\hat{e}(k_z)e^{i\bar{k}_1\cdot\bar{r}}\hat{e}_1(k_{1z})e^{-i\bar{k}_1\cdot\bar{r}'}\right.$$
$$\left.+\sqrt{\frac{\epsilon_1}{\epsilon_0}}\left(\frac{2\epsilon_0 k_{1z}}{\epsilon_1 k_z+\epsilon_0 k_{1z}}\right)\hat{h}(k_z)e^{i\bar{k}_1\cdot\bar{r}}\hat{h}_1(k_{1z})e^{-i\bar{k}_1\cdot\bar{r}'}\right] \tag{A.73}$$

A.3 Stationary Phase Approximation Method for Double Integrals

Consider

$$I = \iint_S f(x,y)e^{ikg(x,y)}\,dx\,dy \tag{A.74}$$

,where s contains the sources. The stationary Phase point is at x_0, y_0 where

$$\nabla g(x_0,y_0) = 0 \tag{A.75}$$

or

$$\frac{\partial g}{\partial x}(x_0,y_0) = \frac{\partial g}{\partial y}(x_0,y_0) = 0 \tag{A.76}$$

Let $s_1 = x - x_0$ and $s_2 = y - y_0$

We define the notation to represent the partial differential operation as follows:

$$g'''_{xyz} = \frac{\partial^3 g}{\partial x\partial y\partial z} \qquad g''_{s_1,s_2} = \frac{\partial^2 g}{\partial s_1\partial s_2}$$

Taylor series expansion of $g(s_1,s_2)$ around stationary point $s_1 = 0, s_2 = 0$ becomes

$$g(s_1,s_2) = \Big\{g(0,0) + \frac{1}{2!}[s_1^2 g''_{s_1s_1}(0,0) + s_2^2 g''_{s_2s_2}(0,0) + 2s_1s_2 g''_{s_1s_2}(0,0)]$$

$$+\frac{1}{3!}[s_1^3 g'''_{s_1s_1s_1}(0,0) + s_2^3 g'''_{s_2s_2s_2}(0,0) + 3s_1^2 s_2 g'''_{s_1s_1s_2}(0,0) + 3s_1 s_2^2 g'''_{s_1s_2s_2}(0,0)] + ...\}$$

(A.77)

For the first order approximation, we keep only the first two terms.

We use matrix notation to represent

$$s_1^2 g''_{s_1s_2} + s_2^2 g''_{s_2s_2} + 2s_1s_2 g''_{s_1s_2} = \overline{s}^T \overline{\overline{G}}_s \overline{s} \tag{A.78}$$

where

$$\overline{s} = \begin{bmatrix} s_1 \\ s_2 \end{bmatrix} \quad \overline{\overline{G}}_s = \begin{bmatrix} g''_{s_1s_1} & g''_{s_1s_2} \\ g''_{s_1s_2} & g''_{s_2s_2} \end{bmatrix} \quad \overline{s}^T = [s_1 \quad s_2]$$

We introduce a coordinate rotation such that s_1, s_2 change to u_1, u_2 and make $g''_{u_1u_2} = 0$. This allows us to treat each integration independently.

The relation between s and u can be written as

$$\overline{s} = \overline{\overline{J}}\,\overline{u} \tag{A.79}$$

where

$$\overline{\overline{J}} = \begin{bmatrix} \cos\theta & \sin\theta \\ -\sin\theta & \cos\theta \end{bmatrix} \quad \overline{u} = \begin{bmatrix} u_1 \\ u_2 \end{bmatrix} \tag{A.80}$$

then we have

$$\overline{\overline{G}}_u = \begin{bmatrix} g''_{u_1u_1} & 0 \\ 0 & g''_{u_2u_2} \end{bmatrix} \tag{A.81}$$

and

$$\overline{s}^T\, \overline{\overline{G}}_s\, \overline{s} = \overline{u}^T\, \overline{\overline{G}}_u\, \overline{u} \tag{A.82}$$

But $\overline{s} = \overline{\overline{J}}\overline{u}$ and $(AB)^T = B^T A^T$ then

$$\overline{u}^T\, \overline{\overline{J}}^T\, \overline{\overline{G}}_s\, \overline{s} = \overline{u}^T\, \overline{\overline{G}}_u\, \overline{u} \tag{A.83}$$

Note that $det\,\overline{\overline{J}} = 1$ then we have

$$det\,\overline{\overline{G}}_s = det\,\overline{\overline{G}}_u \tag{A.84}$$

Since $\frac{\partial}{\partial s_1} = \frac{\partial}{\partial x}, \quad \frac{\partial}{\partial s_2} = \frac{\partial}{\partial y}$ then

$$g''_{xx}\, g''_{yy} - \; g''_{xy} g''_{xy} = det\, \overline{\overline{G}}_u \tag{A.85}$$

In order to make $g''_{u_1u_2} = 0, \quad \theta$ in $\overline{\overline{J}}$ must be (from Equation (A.83))

$$\theta = \frac{1}{2}\tan^{-1}\left[\frac{2g''_{xy}}{g''_{yy} - g''_{xx}}\right]\Bigg|_{\substack{x=x_0\\y=y_0}} \tag{A.86}$$

Then we have

$$I = \iint_S f(\overline{u}) e^{ikg(\overline{u})} d\overline{u} \tag{A.87}$$

And we have the first order approximation of I as:

$$I \approx f(0,0)e^{ikg(0,0)} P_{u_1}(0,0) P_{u_s}(0,0) \tag{A.88}$$

where

$$P_{u_n}(\overline{u}) = \int_{-\infty}^{\infty} e^{\left[\frac{iku_n^2}{2} g''_{u_nu_n}(\overline{u})\right]} d\, u_n \tag{A.89}$$

$$P_{u_n}(\overline{u}) = \left[\frac{k}{2\pi}\left|g''_{u_nu_n}(\overline{u})\right|\right]^{-\frac{1}{2}} e^{\left[\frac{i\pi}{4} sign\left(g''_{u_nu_n}(\overline{u})\right)\right]} \tag{A.90}$$

$$I \approx \frac{2\pi f}{k}\frac{1}{\sqrt{\left|det\, \overline{\overline{G}}_u\right|}} e^{i\left[kg + \frac{\pi}{4}\left\{\mathrm{sign}(g''_{u_1u_1}) + \mathrm{sign}(g''_{u_2u_2})\right\}\right]}\Bigg|_{\substack{u_1=0\\u_2=0}} \tag{A.91}$$

A.4 Far–Field Half–space Green's Function

We can rewrite (A.72) into:

$$\overline{\overline{G}}_{01}(\overline{r},\overline{r}') = \frac{i}{8\pi^2}\iint dk_x dk_y \, \frac{1}{k_{1z}}\left[T_{10}^{TE}\hat{e}(k_z)\hat{e}_1(k_{1z})e^{-i\overline{k}_1\cdot\overline{r}'}\right.$$

$$\left. + T_{10}^{TM}\hat{h}(k_z)\hat{h}_1(k_{1z})e^{-i\overline{k}_1\cdot\overline{r}'}\right] e^{i\overline{k}\cdot\overline{r}} \tag{A.92}$$

, where the exponent term is

$$e^{i\bar{k}\cdot\bar{r}} = e^{k_x x + k_y y + \left(\sqrt{k_0^2 - k_x^2 - k_y^2}\right) z} \tag{A.93}$$

By assuming the observation point is in the far field zone, $kr \to \infty$, the significant contribution of this integral comes from the stationary phase point. Then, we can use the two dimensional stationary phase approximation method given in the previous section to find the far-field $\overline{\overline{G}}_{01}$.

Comparing (A.74) with (A.92), we have

$$g(k_x, k_y) = k_x x + k_y y + \left(\sqrt{k_0^2 - k_x^2 - k_y^2}\right) z \tag{A.94}$$

Finding the stationary phase point,k_{x0}, k_{y0}, we set

$$\left.\frac{\partial \bar{k}\cdot\bar{r}}{\partial k_x}\right|_{\substack{k_x = k_{x0}\\ k_y = k_{y0}}} = \left.\frac{\partial \bar{k}\cdot\bar{r}}{\partial k_y}\right|_{\substack{k_x = k_{x0}\\ k_y = k_{y0}}} = 0 \tag{A.95}$$

Solving for k_{x0} and k_{y0}, we have

$$k_{x0} = k_0 \sin\theta\cos\phi, \quad k_{y0} = k_0 \sin\theta\sin\phi \tag{A.96}$$

, where we make use of the relations

$$x = r\sin\theta\cos\phi, \quad y = r\sin\theta\sin\phi, \quad z = r\cos\theta \tag{A.97}$$

Next, we find the angle in Jacobian matrix, denoted by θ' to avoid confusing with the angle θ in spherical coordinate. Using (A.86), we find

$$\theta' = \phi \tag{A.98}$$

Thus the Jacobian matrix is

$$\overline{\overline{J}} = \begin{bmatrix} \cos\phi & \sin\phi \\ -\sin\phi & \cos\phi \end{bmatrix} \tag{A.99}$$

Let $s_1 = k_x - k_{x0}$ and $s_2 = k_y - k_{y0}$, then

$$g(s_1, s_2) = x(s_1 + k_0 \sin\theta\cos\phi) + y(s_2 + k_0\sin\theta\sin\phi) +$$

$$z\sqrt{k_0^2 - (s_1 + k_0\sin\theta\cos\phi)^2 - (s_2 + k_0\sin\theta\sin\phi)^2} \tag{A.100}$$

Using the relation (A.79)

$$s_1 = \cos\phi\, u_1 + \sin\phi\, u_2$$

$$s_2 = -\sin\phi\, u_1 + \cos\phi\, u_2 \tag{A.101}$$

Substitute (A.101) in (A.100)

$$g(u_1, u_2) = x(u_1\cos\phi + u_2\sin\phi + k_0\sin\theta\cos\phi) + y(-u_1\sin\phi + u_2\cos\phi + k_0\sin\theta\sin\phi)$$

$$+z\sqrt{k_0^2 - (u_1\cos\phi + u_2\sin\phi + k_0\sin\theta\cos\phi)^2 - (-u_1\sin\phi + u_2\cos\phi + k_0\sin\theta\sin\phi)^2} \tag{A.102}$$

One can find that

$$\frac{\partial^2 g(0,0)}{\partial u_1^2} = \frac{\partial^2 g(0,0)}{\partial u_2^2} = -\frac{r}{k_0} - \frac{r}{k_0}\tan^2\theta\cos^2(2\phi) < 0 \tag{A.103}$$

Then the $\left\{\mathrm{sign}(g''_{u_1,u_2}) + \mathrm{sign}(g''_{u_1,u_2})\right\}$ gives -2.
Using (A.85), one can find

$$det\overline{\overline{G}}_u = \frac{r^2}{k_z^2} \tag{A.104}$$

Then we write (A.92) in the form of (A.74) as

$$I \approx 2\pi f \frac{1}{\sqrt{|det\overline{\overline{G}}_u|}} e^{i\left[kr - \frac{\pi}{2}\right]} \tag{A.105}$$

where

$$f = \frac{i}{8\pi^2}\frac{1}{k_{1z}}\left[T_{10}^{TE}\hat{e}(k_z)\hat{e}_1(k_{1z})e^{-i\bar{k}_1\cdot\bar{r}'} + T_{10}^{TM}\hat{h}(k_z)\hat{h}_1(k_{1z})e^{-i\bar{k}_1\cdot\bar{r}'}\right] \tag{A.106}$$

Then the far–field half–space Green's function is

$$\overline{\overline{G}}_{01}(\bar{r},\bar{r}') = I = \frac{e^{ikr}}{4\pi r}\frac{k_z}{k_{1z}}\left[T_{10}^{TE}\hat{e}(k_z)\hat{e}_1(k_{1z}) + T_{10}^{TM}\hat{h}(k_z)\hat{h}_1(k_{1z})\right]e^{-i\bar{k}_1\cdot\bar{r}'} \tag{A.107}$$

or

$$\overline{\overline{G}}_{01}(\bar{r},\bar{r}') = \frac{e^{ikr}}{4\pi r}\left[\frac{2k_z}{k_z+k_{1z}}\hat{e}(k_z)\hat{e}_1(k_{1z}) + \sqrt{\frac{\epsilon_1}{\epsilon_0}}\left(\frac{2\epsilon_0 k_z}{\epsilon_1 k_z + \epsilon_0 k_{1z}}\right)\hat{h}(k_z)\hat{h}_1(k_{1z})\right]e^{-i\bar{k}_1\cdot\bar{r}'} \tag{A.108}$$

Thus we can see from the far–field half–space Green's function that, in the cases of a dipole source with the observation point in the far field zone, the transmission coefficients T_{10}^{TM}, T_{10}^{TE} are multipled by k_z/k_{1z}, which is equivalent to T_{01}^{TM}, T_{01}^{TE} for plan wave.

Appendix B

Typical Properties of Sand and Rocks

B.1 Electrical Properties of Sand: A sample from Al Labbah Plateau

Site	Sample Depth (cm)	Moisture (wt. %)	Dielectric Constant	Loss Tangent
28-1A	0-5	0.054	2.466	0.0054
28-1B	27-32	0.148	2.490	0.0054
28-1C	50-55	0.361	2.490	0.0067
28-2A	0-5	0.077	2.386	0.0038
28-2B	20-25	0.148	2.475	0.0065
28-2C	38-43	0.183	2.515	0.0075
6-A	0-5	0.057	2.585	0.0057
6-B	20-25	0.248	2.515	0.0084
6-C	45-50	0.578	2.605	0.0086
$\bar{X}$		0.206	2.503	0.0066

Table B.1: Moisture and electrical properties of Al Labbah Plateau Sand samples

Reference:[3], p 325 - 336.

(a) Electrical-property measurements were made at a frequency of 1.3 GHz by the resonant-cavity technique. Uncertainty in absolute values of measured dielectric and loss tangent properties is less than 2 percent.

(b) 1 standard deviation uncertainty of the dielectric constant = 0.018 (average).

(c) 1 standard deviation uncertainty of the loss tangent = 0.00016 (average).

(d) Sampling sites 28-1 and 28-2 were 106-meter apart.

B.2 Electrical Property of Rocks

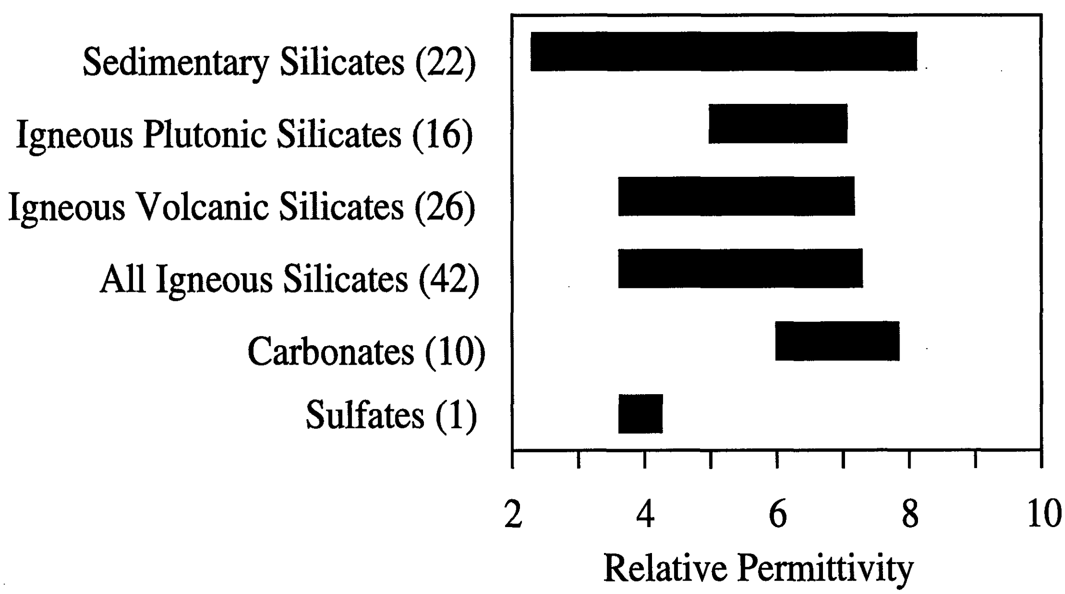

Figure B-1: Electrical properties of rocks

Reference:[32], p 595 - 602.

- The real part of the relative dielectric constant ϵ was measured in 0.1-GHz step from 0.5 to 18 GHz.

Bibliography

[1] M. Abramowitz and J. A. Stegun. *Handbook of Mathematical Functions.* Dover Publications, New York, 1965.

[2] P. W. Barber and S. C. Hill. *Light Scattering by Particles: Computational Methods.* World Scientific, NJ, 1990.

[3] Graydon L. Berlin, Mohammed A. Tarabzouni, Abdullah H. Al-Naser, Kamel M. Sheikho, and Richard W. Larson. Sir-b subsurface imaging of a sand-buried landscape: Al labbah plateau, saudi arabia. *IEEE Transactions on Geoscience and Remote Sensing*, GE-24(4):595+, 7 1986.

[4] O. R. Cruzan. Translational addtion theorems for spherical vector wave functions. Technical report, Diamond Ordinance Fuse Laboratories, Department of the Army, Washington DC, 1961.

[5] O. R. Cruzan. Translational addition theorems for spherical vector wave functions. *Quart. J. Appl. Math.*, 20:33–40, 1962.

[6] A. R. Edmonds. *Angular Momentum in Quantum Mechanics.* Princeton University, Princeton, NJ, 1957.

[7] A. K. Fung. Application of a combined rough surface and volume scattering theory to sea ice and snow backscatter. *IEEE Trans. Geosci. Remote Sensing*, GE-20(4):528–536, 1982.

[8] A. K. Fung, M. Dawson, and S. Tjuatja. An analysis of scattering from a thin saline ice layer. In *IGARSS'92 Conf. Proc.*, pages 1262–1264, 1992.

[9] A. K. Fung and H. S. Fung. Application of first order renormalization method to scattering from a vegetated-like half space. *IEEE Trans. Geosci. Electron.*, GE-15:189–195, 1977.

[10] H. C. Han. *Electromagnetic Wave Phenomena in Inhomogeneous and Anisotropic Media.* PhD thesis, Massachusetts Institute of Technology, 1992.

[11] A. Ishimaru, D. Lesselier, and C. Yeh. Multiple scattering calculations for non-spherical particles based on the vector radiative transfer theory. *Radio Science*, 19-5:1356–1366, 1984.

[12] J. D. Jackson. *Classical Electrodynamics.* John & Sons, New York, 1975.

[13] J. A. Kong. *Electromagnetic Wave Theory.* John Wiley & Sons Inc., 1990.

[14] J. C. Leader. Polarization dependence in em scattering from rayleigh scatterers embedded in a a dielectric slab. i. theory. *J. Appl. Phys.*, 46:4371–4385, 1970.

[15] C. F. Lee. Ground penetration radar phenomenology investigations. Project Report GPR-2, Lincoln Laboratory, Lexington, Massachusetts, September 1994.

[16] M. I. Mirkin, T. O. Grosch, T. J. Murphy, S. Ayasli, H. Hellsten, R. S. Vickers, and J. M. Ralston. Results of the june 1993 yuma ground penetration experiment. In *SPIE's international symposium on optical engineering and photonics in aerospace sensing*, Orlando, Florida, April 1994.

[17] B. Peterson and S. Strom. T matrix for electromagnetic scattering from an arbitrary number of scatterers and representation of. *Phy. Rev. D*, E(3)(8):3661–3678, 1973.

[18] M. Rotenberg, R. Bivins, N. Metroplis, and Jr. J. K. Wooten. *The 3-j and 6-j Symbols.* Technology Press, Cambridge, MA, 1959.

[19] R. T. Shin. Radiative transfer theory for active remote sensing of layered homogeneous media containing spherical scatterers. Master's thesis, Massachusetts Institute of Technology, 1980.

[20] R. T. Shin. *Theoretical Models for Microwave Remote Sensing of Earth Terrain.* PhD thesis, Massachusetts Institute of Technology, 1984.

[21] R. T. Shin and J. A. Kong. Radiative transfer theory for active remote sensing of a homogeneous layer containing spherical scatterers. *Journal of Applied Physics*, 6:4221–4230, 1981.

[22] R. T. Shin and J. A. Kong. Theory for thermal microwave emission from a homogeneous layer with rough surfaces containing spherical scatterers. *Journal of Geophysical Research*, 87-B7:5566–5576, 1981.

[23] R. T. Shin and J. A. Kong. Radiative transfer theory for active remote sensing of two-layer random media. In *PIER1, Progress in Electromagnetics Research*, pages 359–417, Elsevier, New York, 1989.

[24] Maxim Shoshany. Roughness - reflectance relationship of bare desert terrain: An empirical study. *Remote Sens. Environ.*, 45:15–27, 1993.

[25] A. Stogryn. Electromagnetic scattering by random dielectric dielectric constant fluctuations in a bounded medium. *Radio Science*, 9:509–518, 1970.

[26] L. Tsang and J. A. Kong. Emissivity of half-space random media. *Radio Science*, 11:593–598, 1976a.

[27] L. Tsang and J. A. Kong. Thermal microwave emission from a random homogeneous layer over a homogeneous medium using the method invariant embeeding. *Radio Science*, 12:185–195, 1977.

[28] L. Tsang and J. A. Kong. Radiative transfer theory for active remote sensing of half space random media. *Radio Science*, 13:763–774, 1978.

[29] L. Tsang, J. A. Kong, and R. T. Shin. Radiative transfer theory for active sensing of a layer of nonspherical scatterers. *Journal of Applied Physics*, 19:629–642, 1980.

[30] L. Tsang, J. A. Kong, and R. T. Shin. *Theory of Microwave Remote Sensing.* John Wiley & Sons Inc., 1985.

[31] L. Tsang, M. C. Kubacsi, and J. A. Kong. Radiative transfer theory for active remote sensing of a layer of small ellipsoidal scatterers. *Radio Science*, 16-3:321–329, 1981.

[32] Fawwaz T. Ulaby, Thomas H. Bengal, Myron C. Dobson, Jack R. East, James B. Garvin, and Diane L. Evans. Microwave dielectric properties of dry rocks. *IEEE Transactions on Geoscience and Remote Sensing*, 28(3):325+, 5 1990.

[33] P. C. Waterman. Matrix formulation of electromagnetic scattering. *Proc. IEEE*, 53:805–811, 1965.

[34] P. C. Waterman. New formulation of acoustic scatttering. *J. Acoustic Soc. Am.*, 45:1417–1429, 1968.

[35] P. C. Waterman. Symmetry, unitarity and geometry in electromagnetic scattering. *Phys. Rev.D*, 3:825–839, 1971.

[36] D. P. Winebrenner, T. C. Grenfell, and L.Tsang. On microwave sea ice signature modeling : Connecting models to the real world. In *IGARSS'92 Conf. Proc.*, pages 1268–1270, 1992.

2307-17